MECANISMOS NEURONALES DE LA SELECCIÓN DE ESTÍMULOS VISUALES EN EL CIRCUITO ISTMO-TECTAL

Tesis entregada a la Universidad de Chile en cumplimiento parcial de los requisitos para optar al grado de Doctor en Ciencias con Mención en Biología Molecular, Celular y Neurociencias

BRYAN REYNAERT GODEFROY

Facultad De Ciencias Universidad de Chile

Tutor de Tesis: Dr. Juan Carlos Letelier

Co-Tutor de Tesis: Gonzalo Marín G.

Diciembre 2023

Santiago - Chile

FACULTAD DE CIENCIAS

UNIVERSIDAD DE CHILE

INFORME DE APROBACION

TESIS DE MAGÍSTER

Se informa a la Escuela de Postgrado de la Facultad de Ciencias que la Tesis de Doctorado presentada por el candidato.

Bryan Reynaert Godefroy

Ha sido aprobada por la comisión de Evaluación de la tesis como requisito para optar al grado de Doctor en Ciencias con Mención en Biología Molecular, Celular y Neurociencias, en el examen de Defensa Privada de Tesis rendido el día 6 de Noviembre de 2023.

Director de Tesis:
Dr. Juan Carlos Letelier .....

Co-Director de Tesis
Gonzalo Marín
.....

Comisión de Evaluación de la Tesis

Dr. Jorge Mpodozis (Presidente) .....

Dra. Alexia Núñez .....

Dr. Julio Alcayaga .....

Dr. Pedro Maldonado .....

There is no real ending. It's just the place where you stop the story.

-Frank Herbert

Cuando estaba iniciando este doctorado, tenía una empresa de acompañamiento científico para colegios que me llevó a medir el radio de la Tierra desde el sur de Chile así como también acompañar el primer congreso científico de colegios de Cerro Navia. También era CTO de una start-up de ingeniería de software que al día de hoy sigue funcionando. Hacía clases de ciencias, electrónica y matemáticas. Estaba saliendo con quien se casaría conmigo y participando de un programa piloto en Japón. Hoy estoy en Canadá, mucho más viejo ya buscando la calma. Los últimos 20 años de mi vida han estado ligados a la Universidad de Chile, y han sido legendarios. Lo haría mil veces de nuevo. El Bryan que empezó el doctorado es distinto del que lo terminó, pero continúo feliz.

Agradecimientos

Realmente no me es posible enumerar las personas a las que les estaré eternamente agradecido por permitir que a los 37 años de edad me esté graduando de doctor en ciencias, por lo tanto espero que todas las omisiones de esta sección sean comprendidas por lo que son, una incapacidad en la compresión de información, más no de mi memoria. Dicho esto, aquí va mi mejor intento.

Primero, debo agradecer a mi compañera del alma, quien ha puesto tanto esfuerzo en este trabajo como yo.Gracias por apoyarme en cada una de estas alocadas aventuras. No puedo esperar para ver qué es lo que sigue.

Por supuesto, a continuación debo mencionar a mis padres, Eugene y Claudia. Yo soy un constante mal agradecido, pero en mis momentos de lucidez espero que sepan que los pienso con amor infinito. Siempre los siento cerca.

Luego están mis madres adoptivas, quienes me han acogido a lo largo de esta travesía. Luise, Maria de las Nieves, Sra. Maritza, Pingrid, Sra. Raquel, Ani, Bárbara, Pony, y Ceci. Gracias por reservar un rincón en su corazón para mí y tratarme como uno de los suyos.

No puede faltar mi hermanita, quien siempre me recuerda como es mi mejor versión.

Agradezco a mis amigos, mis más temibles enemigos y fuertes detractores, que por más lejos que nos encontremos, no permiten que haya distancia. El que yo termine esta tesis es una tragedia para muchos, tendrán que encontrar una nueva forma de molestarme. Sé que estarán a la altura. En un tono más serio, la felicidad solo es real cuando es compartida, así que agradezco su sincera e incondicional compañía todos estos años.

También debo nombrar al excelente grupo humano del Rayo, laboratorio mundial. Este laboratorio, que me ha acogido en mis mejores y peores momentos, es único, y le estaré siempre en deuda a todos sus miembros.

He dejado a mis tutores para el final, para distinguirlos pues el esfuerzo que han hecho, durante incontables horas de discusión, experimentación y riguroso análisis ha sido sobrehumano. Lete y Marín, gracias por no rendirse nunca, por dar siempre lo mejor de ustedes y nunca escatimar en sacrificios.

Resumen

El tectum óptico (TeO) es un componente principal de la vía visual tectofugal del cerebro, encontrándose entre la retina y el tálamo. Ha sido estudiado en múltiples especies de vertebrados; sin embargo, aún quedan muchas interrogantes sin respuesta sobre sus mecanismos y función conductual asociada. Recientemente, investigaciones realizadas en este laboratorio han encontrado evidencia que sugiere que el tectum, junto con el complejo del istmo, podría implementar un circuito recursivo que actúa como un filtro de selección de estímulos. El modelo postula que la influencia excitatoria localizada del núcleo istmo parvocelular (Ipc) en el tectum, junto con las proyecciones inhibitorias de campo amplio del núcleo istmo magnocelular (Imc), dan lugar a un "punto focal" local que regula la entrada visual desde la retina que se transmite río arriba hacia el núcleo talámico rotundus (Rt) y el pallium. Sin embargo, la evaluación experimental de las características espaciotemporales de la retroalimentación istmotectal todavía está pendiente.

Para obtener una comprensión más completa del funcionamiento del circuito istmotectal, esta investigación utilizó arreglos de múltiples electrodos para investigar la respuesta visual en el tectum óptico de *Columbia livia*. El estudio se centró en los patrones espaciotemporales de las ráfagas oscilatorias tectales (OBs), que sirven como una indicación distintiva de la retroalimentación del Ipc al tectum.

Aunque las OBs tectales son respuestas características, son altamente variables y su detección automática ha sido un desafío. En este estudio, utilizamos una técnica de descomposición en matrices llamada Factorización en Matrices Semipositivas Invariantes al Desplazamiento (SSNMF, por sus siglas en inglés). Los resultados de la anotación automática demostraron un nivel significativo de concordancia con las anotaciones realizadas por un experto humano, lo que nos brinda confianza en los resultados obtenidos. Utilizando este método pudimos caracterizar la respuesta de retroalimentación del Ipc a un nivel de detalle y escala sin precedentes.

Durante nuestra examinación de las OBs registradas, observamos un patrón distintivo de expansión radial en la superficie del tectum, donde las OBs se manifestaban inicialmente en una localización fuente singular y posteriormente se propagaban horizontalmente en todas las direcciones. Llamamos a cada uno de estos eventos de expansión una "onda-ráfaga". Luego estudiamos la distribución de los puntos fuente de las ondas-ráfaga individuales en respuesta a diferentes patrones de estimulación. Encontramos que la presentación de un círculo pequeño de luz estático produce una serie de ondas-ráfaga, cada una de las cuales se expande aún más desde su centro. Las fuentes de cada onda-ráfaga aparecen en las cercanías de la ubicación del estímulo visual en el mapa tectal, y para estímulos en movimiento, las fuentes de los onda-ráfaga sucesivas siguen la representación tectal de la trayectoria de los estímulos en movimiento. En todos los casos, las ondas ocurren de manera iterativa y secuencial, abarcando los lugares estimulados y sus alrededores. La presentación de dos estímulos en movimiento resulta en que los puntos fuente siguen ambas trayectorias en alternancia consecutiva. Hasta la escala determinada por el arreglo de electrodos, observamos sólo una onda-ráfaga en un momento dado.

Replicamos los experimentos en palomas despiertas y obtuvimos resultados similares. Esta observación crucial elimina la posibilidad de atribuir las onda-ráfaga tectales a los efectos de la anestesia, lo que refuerza nuestra confianza en su relevancia biológica.

Estos hallazgos contribuyen a nuestra comprensión de un circuito neural que parece implementar un mecanismo de selección de estímulos en el TeO. El patrón espacio-temporal exhibido por la actividad del Ipc en el tectum se puede describir como un foco de excitabilidad que recorre el TeO y realza las características visuales en la región que abarca, mientras que el resto de la escena visual se inhibe. Los conocimientos obtenidos en este estudio con respecto a las propiedades del foco, como su tamaño, velocidad y frecuencia de parpadeo, nos permiten establecer conexiones entre estudios fisiológicos y conductuales. Además, la dinámica de este sistema potencialmente nos brinda una idea de cómo podría funcionar un mecanismo de atención en el cerebro, ya que varios estudios han llevado a la noción de que la atención espacial es comparable a un foco perceptual que escanea representaciones internas de la escena visual. En definitiva, hasta donde sabemos, un correlato neural real de un foco parpadeante como el que describimos en el tectum aviar nunca se ha informado en otras áreas cerebrales de ninguna especie de vertebrados, lo que convierte nuestro hallazgo en una contribución muy significativa al campo.

Abstract

The optic tectum (TeO) is a main component of the brain's tectofugal visual pathway, found between the retina and the thalamus. It has been studied in multiple vertebrate species, yet how it operates and many associated questions related to its neural mechanisms and behavioral function remain unanswered. Recently, research conducted at this laboratory has found evidence suggesting that the tectum, along with the isthmic complex, may implement a recursive circuit acting like a stimulus selection filter. The model posits that the localized excitatory influence of the parvocellular isthmic nucleus (Ipc) on the tectum, along with the wide-field inhibitory projections of the magnocellular isthmic nucleus (Imc) give rise to a local "spotlight" that gates the visual input from the retina en route to the thalamic nucleus rotundus (Rt) and the pallium. However, the experimental assessment of the spatio-temporal characteristics of the isthmotectal feedback is still pending.

To gain a comprehensive understanding of the isthmotectal circuit's operation, this research employed multi-electrode arrays to investigate the visual response in the optic tectum of *Columbia livia*. The study focused on the spatio-temporal patterns of the tectal oscillatory bursts (OBs), which serve as a distinctive indication of Ipc feedback to the tectum.

Although the tectal OBs are characteristic responses, they are highly variable and their automatic detection has been a challenge. In this study, we utilized a matrix decomposition technique called Shift-invariant Semi Non-negative Matrix Factorization (SSNMF). The results of the automatic annotation demonstrated a significant level of

concordance with annotations conducted by a human expert, giving us confidence on the obtained results. Using this method we were able to characterize the Ipc feedback response to an unprecedented level of detail and scale.

During our examination of the recorded OBs, we observed a distinct pattern of radial expansion on the surface of the tectum, whereby the OBs initially manifested at a singular point source and subsequently propagated horizontally in all directions. We called each of these expanding events a burst-wave.

We found that the presentation of a static spot of light produced a series of burst-waves each of which expanded further away from their center. The sources of each burst-wave appeared in close vicinity of the visual stimulus location on the tectal map and for moving stimuli the sources of the successive burst-waves tracked the tectal representation of the trajectory of the moving stimuli. In every case, the waves occurred in an iterative, sequential fashion, encompassing the stimulated loci and their surroundings. The presentation of two moving stimuli resulted in source points tracking both trajectories in consecutive alternation. Up to the scale determined by the array of electrodes, we observed only a single burst-wave at any given time.

We replicated the experiments in awake pigeons and obtained comparable results. This crucial observation eliminates the potential for tectal burst-waves to be attributed to the effects of anesthesia, thereby bolstering our confidence in their biological relevance.

These findings contribute to our understanding of a neural circuit that seems to implement a mechanism of stimulus selection in the TeO. The spatio-temporal pattern exhibited by Ipc activity on the tectum can be described as an spotlight of excitability

traversing the TeO which would enhance visual features in the region it comprises, while the rest of the visual scene would be inhibited. The insights obtained in this study relative to the properties of the spotlight, such as its size, speed and blinking frequency allow us to draw bridges between physiological and behavioral studies. Moreover, the dynamics of this system potentially provide a glimpse into how an attention mechanism might operate in the brain as several studies have led to the notion that spatial attention is comparable to a perceptual spotlight that scans internal representations of the visual scene. All in all, to our knowledge, a true neural correlate of a blinking spotlight such as the one we describe in the avian tectum has never been reported in other brain areas in any vertebrate species, making our finding a highly significant contribution to the field.

Table of Contents

List of Figures

List of Tables

List of Abbreviations

AP	Action potential
Pulc	Caudal pulvinar
ChAT	Choline acetyltransferase
GLM	General linear model
ISI	Inter-source interval
ION	Istmo-optic complex
LFP	Local field potential
MEA	Multi-electrode Array
NMF	Non-negative Matrix Factorization
Imc	Nucleus isthmi pars magnocellularis
Ipc	Nucleus isthmi pars parvocellularis
SLu	Nucleus isthmi pars semilunaris
OPT	Nucleus opticus principalis thalami
Rt	Nucleus rotundus
TeO	Optic tectum
OB	Oscillatory burst
PB	Paintbrush axon
RF	Receptive field
Shcs	Shepherd's crooks
SSNMF	Shift-Invariant Semi-non-negative Matrix Factorization
SNR	Signal to noise ratio
SC	Superior colliculus
TGC	Tectal ganglion cell

Introduction

The tectofugal pathway is one of the main routes through which vertebrates perform visual processing. The isthmo-tectal system, a component of this neural pathway, has been suggested to perform stimulus selection through the establishment of an excitatory spotlight mediated by the interaction between wide-range inhibitory projections and a confined excitatory loop. This spotlight gates the visual flow between the optic tectum and the thalamic nucleus rotundus and might be a part of the process of selective spatial attention. In this work we performed multi-electrode recordings of the visual tectal responses to characterize the spatio-temporal patterns of the isthmo-tectal feedback and increase our understanding of a highly organized recurrent circuit in the tectofugal visual pathway of vertebrates.

Stimulus Selection and the tectofugal Pathway

In order to behave in correspondence with a dynamic environment, animals must constantly interact with their surroundings, strategically prioritizing and selecting a subset of objects to direct their behavior. This selection process is essential, considering the abundance of objects that are presented to their sensory organs. Organisms possess neural mechanisms which filter their sensory flow such that the processing of selected stimuli takes precedence over others with less relevant content. This phenomenon of stimulus selection is thus fundamental to survival and an integral part of perception, yet, how the brain selects a specific stimulus is still a matter of intense research. Extensive efforts have been devoted to investigating the role of the optic tectum in visual processing, particularly regarding its contribution to generating head

movements, orienting behavior, and escape responses. All these functions require the engagement of stimulus selection circuits to single out a stimulus to react to.

In vertebrates, the thalamofugal and tectofugal pathways are the two principal routes through which visual input is transmitted from the retina to the telencephalon. In birds, the thalamofugal pathway originates in the nucleus opticus principalis thalami (OPT) (lateral geniculate nucleus in mammals) and reaches the visual Wulst, the primary visual area of the pallium (striated cortex of mammals). The tectofugal pathway, on the other hand, originates in the optic tectum (or superior colliculus in mammals), makes a relay in the nucleus rotundus (Rt) in the thalamus (caudal pulvinar in most mammals), and reaches the entopallium (extrastriate cortex in mammals). See figure 1.

Figure 1. Diagram of the two visual pathways in vertebrates.

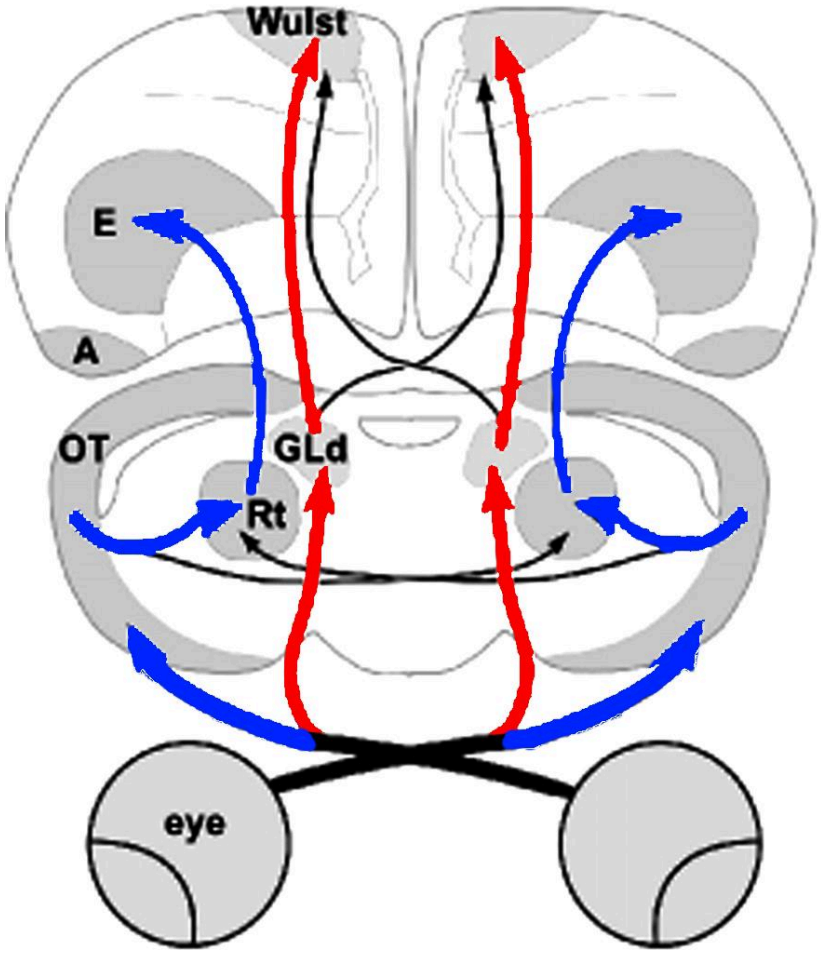

The ascending tectofugal (blue) pathway has the tectum as its first relay and then follows to the thalamic nucleus rotundus, while the thalamofugal (red) visual pathway has the dorsal nucleus of the lateral geniculate body as its direct target. **OT**: optic tectum, **Rt**: rotundus, **GLd**: dorsal nucleus of the lateral geniculate body, **E**: entopallium, **A**: arcopallium. Adapted from Folta et al. (2004)[1].

The optic tectum of birds is a prominent, laminated midbrain structure that integrates visual, auditory and somatosensory information and plays a crucial role in generating

sensory-guided behavior such as orienting movements, prey capture and predator avoidance[2,3]. In all vertebrate lineages, including birds, the retinal fibers carrying visual input innervate the uppermost layers while other sensory modalities occupy intermediate layers. The superposition of multiple sensory maps across tectal layers in register with a motor map in deeper layers allows the TeO to perform a relatively straightforward sensory-motor transformation to locate and respond to objects in a unified behavioral space. In birds, the TeO, its associated nuclei and projections have been extensively studied from an anatomical, immunohistochemical, developmental, and electrophysiological standpoint, becoming a model system for systems neuroscience.

In this context, the isthmotectal system, constituted by a reciprocal projection between the tectum and nuclei from the isthmic region[4], has been signaled as a neural mechanism for stimulus selection in sauropsids (the clade including birds and reptiles) as the Ipc activity on the tectum gates the transference of neural activity between the tectum and its main ascending target, the thalamic nucleus rotundus [5,6]. Several studies have pointed to this stimulus selection mechanism as a neural substrate of spatial attention. The study of this system provides a unique opportunity to understand the underlying neural mechanisms involved in this filtering process, specifically the physiological basis of stimulus selection in the tectofugal visual pathway.

Over the last four decades, the putative role of the tectum has shifted from being a reflex center towards it being involved in higher cognitive functions. Evidence has accumulated that the tectum plays a role in learning, decision making and attention[7–10]. The tectal ascending outputs to thalamic nuclei are indicative of this, as they ultimately

reach cerebral regions removed from the generation of motor responses and rather involved in higher visual processing such as the entopallium and the caudolateral nidopallium, a putative analog of the prefrontal cortex. Visual spatial attention is a process by which specific spatial locations are selected for further perceptual processing or as targets of orienting behavior, enhancing the neural representations of the objects at such locations. Two main theories about attention are worth mentioning: the premotor theory of attention which characterizes it as facilitating the generation of a motor response to the attended stimulus, and the spotlight theory of attention which involves the enhancement or boosting of certain sensory signals while suppressing others. In this regard, the tectum sits in a privileged position as it might play a part in both: the deeper layers of the tectum are involved in the development of saccades and orienting movements related to attention, while the superficial layers form microcircuits containing excitation-inhibition networks which could give rise to an attentional spotlight. Moreover, such a saliency or priority map has been observed in the tectum, but the mechanisms behind its establishment remain to be elucidated.

The isthmotectal circuit

In birds, retinal ganglion cells innervate the contralateral tectum in a topographic fashion, providing a high fidelity map of the visual space on the tectal surface. The tectum has efferent and afferent connections to and from multiple regions in the brain, most of which are retinotopically organized. The ascending projection to the nucleus rotundus, on the other hand, the main tectal output, is not retinotopic, but displays an interdigitated topography, coined "field-to-locus" by Marin et al., (2003)[11]. In this topographic arrangement, tectal ganglion neurons (TGCs), distributed in an interdigitated fashion across the entire tectal map, project to neighboring regions in the

nucleus rotundus. As a consequence of this, neurons in the Rt possess large receptive fields that cover most of the visual field, apparently losing the fine spatial information characteristic of the tectal organization. The optic tectum also displays a dense reciprocal projection to a group of nuclei in the isthmic region called the isthmic complex. It consists of four cytoarchitectonically distinct nuclei: the nucleus isthmi pars magnocellularis (Imc), pars parvocellularis (Ipc), pars semilunaris (SLu) and the nucleus isthmo-opticus (ION). The ION projects upon the retina and seems to play a different role from the other isthmic nuclei, which are more intimately connected to the tectum itself. The Imc, Ipc, and SLu all have reciprocal connections with the ipsilateral optic tectum. In the case of the Ipc and SLu, the topography is homotopic, that is, they project back to the same locus in the tectum from which they receive their input, whereas for the Imc, the efferences to the tectum are diffuse and heterotopic or more explicitly, anti-topographic, which means Imc neurons innervate most of the tectum (and the Ipc) except the region from which they receive tectal input.

Some cellular types identified by their morphology are particularly relevant for this thesis, namely the Shepherd's crook (Schs) cells located in the layer ten of the tectum, which through ramifying axons simultaneously innervate the three isthmic nuclei. And the paintbrush axon (PB) terminals which are the tectal axon terminals of the Ipc neurons. Both structures have peculiar morphologies from which they derive their name. Shepherd's crook neurons have a dense dendritic system in layers 10-13, and a curved axon in the form of a shepherd's crook. The paintbrush axon terminals, on the other hand, form densely packed columns of thin ramifications and synaptic buttons comprising layers 10 to 3 of the tectum (see figure 2). The spike firing of these axons produces oscillatory bursts, a typical tectal response which will be described below.

Figure 2. Reciprocal connectivity of the isthmotectal system.

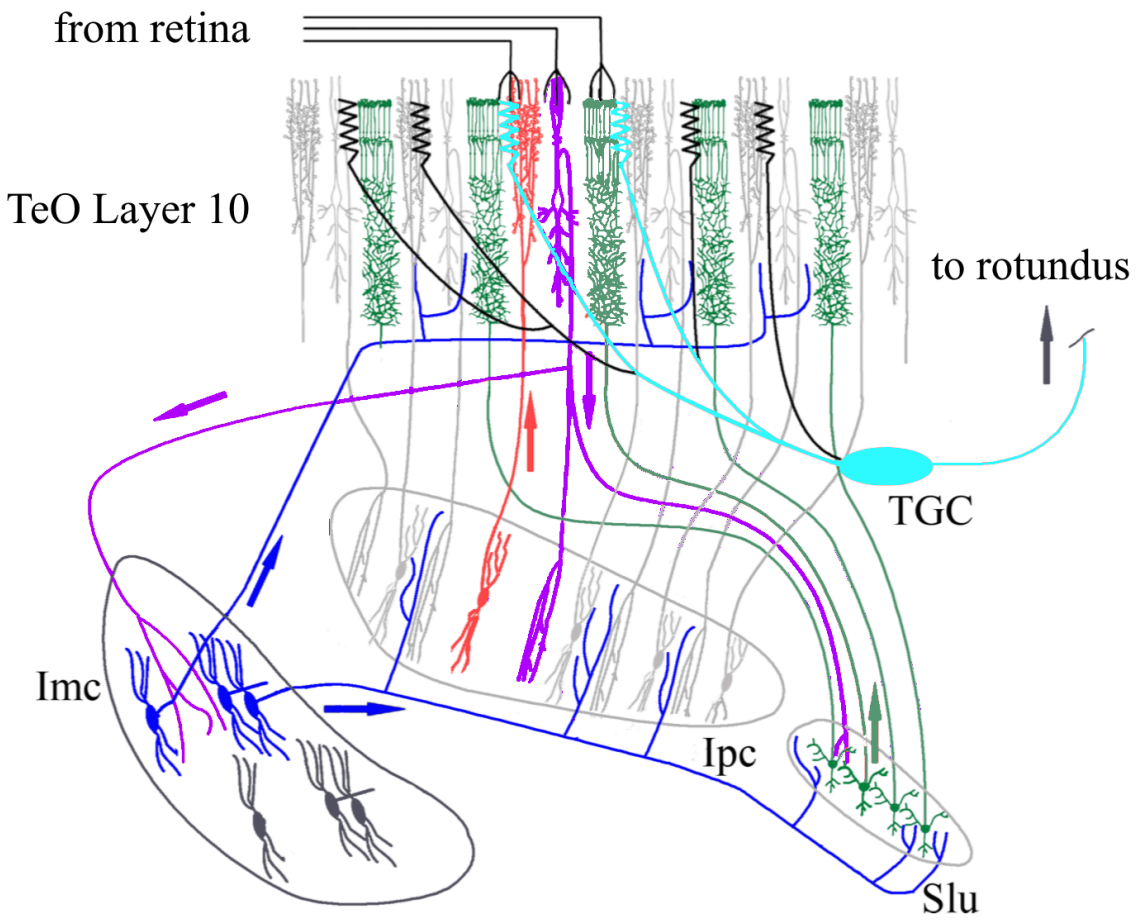

Schematic diagram showing the reciprocal connections between the optic tectum (TeO) and the isthmic nuclei. Retinotopy is maintained from the retina to the tectum, from the tectum to the nucleus isthmi pars parvocellularis (Ipc) through the Shepherd's Crook (SC) neurons (purple), and back into the tectum through the Ipc paintbrush axons (red), and the nucleus isthmi pars semilunaris (SLu) axons (green). The nucleus isthmi pars magnocelullaris (Imc) inhibitory feedback consists of heterotopic projections (blue) over the TeO, Ipc and SLu. The output of the tectum towards the nucleus rotundus is transmitted by the tectal ganglion cell neurons (TGC)(cyan). Adapted from Marin et al., (2005)[3].

This reciprocal connectivity is essential for the operation of the isthmotectal circuit. It suggests a model for understanding the physiological basis of visual stimulus selection in which afferent inputs from the Ipc and Imc have an antagonistic modulatory effect on retinal inputs to the TeO. This model posits that stimuli from different retinal regions activate neurons in the Ipc and Imc, which in turn emphasize the tectal location defining the strongest stimulus and inhibit the rest of the TeO, generating a spotlight supported by neuronal excitability. The reciprocal istmo-tectal circuit then functions as a relevance or salience filter through the recursive signals traveling between the TeO and isthmic nuclei, leading to a winner-takes-all dynamic, in which only one TeO region is effectively excited while the rest of the TeO is inhibited. This "spot-like" dynamics would be responsible for the final selection of the visual activity that will ascend through the tectofugal pathway to the rotundus and the entopallium, propagating also to other telencephalic regions involved in visual processing and the generation of the ongoing behavior. The mechanism through which visual processing proceeds in the absence of a clear topographic organization, as described in the tectofugal pathway, has been an unresolved question. However, the presence of a spotlight filter could offer a potential solution. By restricting the input to focal parts of the visual input, the convergence and potential confusion provoked by stimuli in different locations could be avoided. Although further investigation is required, the concept of a spotlight holds promise in addressing this challenge, and might become a model of a spatial attentional focal mechanism.

Oscillatory Bursts

The extracellular responses recorded in the optic tectum in response to visual stimuli are known as oscillatory bursts[12,13] (OB), and they occur at different depths in the TeO, ranging from layers 2 to 10. Recent research has shown that these responses

correspond to the reentrant activity of the paintbrush axons and thus their presence identifies the feedback activity from Ipc in the tectum[13,14]. In other words, OBs delineate the region in which the stimulus selection filter is open[5].

Oscillatory bursts have several striking characteristics. Their principal component contains a high frequency of around 600Hz, with a magnitude that can reach up to 600 μV, an amplitude larger than a typical extracellular action potential (AP). This magnitude might be the result of the extensive arborization of the PB or arise as a result of Ipc axon terminals firing in relative synchrony. Either way, the result is that OBs tend to mask responses generated by other cell types. However, despite the general similarity between any two OBs, they are highly variable, making it challenging to automate the annotation of recordings. In particular, since OBs cannot be easily identified either by their shape (highly variable structure) or their frequency (broad spectrum composition), most filters, transforms, decompositions and other algorithms like template matching are rendered ineffective, and those which look promising for a given recording fail in the next one. See figure 3.

Figure 3. Oscillatory bursts are a prominent tectal response

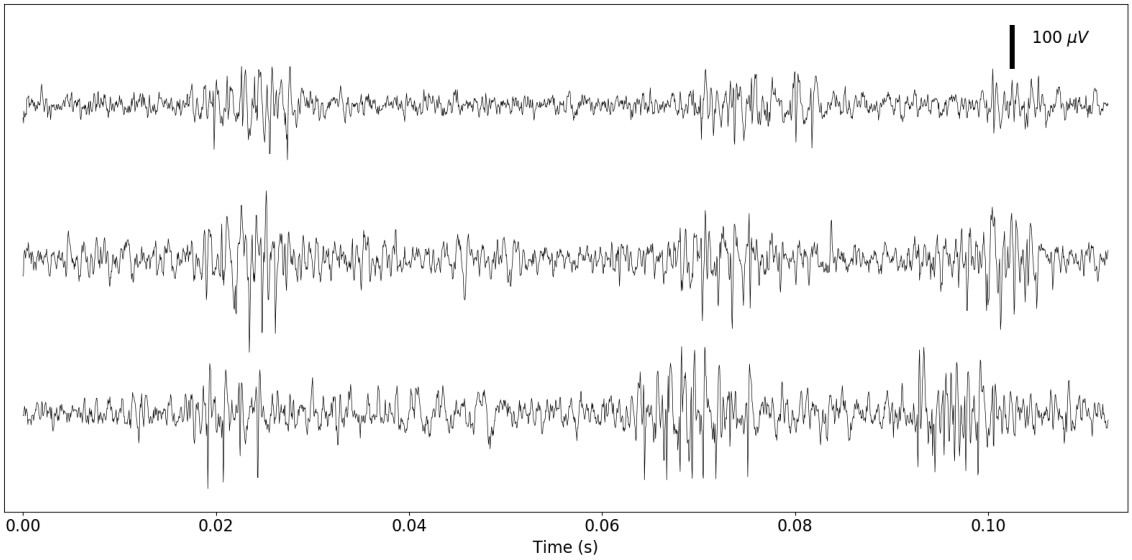

Three multi-electrode array (MEA) recordings of the tectum containing oscillatory bursts. These responses exhibit high variability, no oscillatory burst (OB) is identical to any other, even when recorded within the same second with the same electrode. Their envelope has a gaussian modulation and their spectrum contains high frequencies (from hundreds of Hz up to 3 kHz). The high amplitude of OBs makes them stand out compared to other signals in the tectum.

Another conspicuous feature of this tectal response is that oscillatory bursts occur in bouts: once the first burst is triggered, it is followed by multiple repetitions lasting about 300ms after the first response is elicited. This recursive dynamic may be produced by the recurrent feedback interactions between the optic tectum and the isthmic nuclei. Despite this complexity, the presence of oscillatory bursts allows one to univocally track the Ipc activity in the tectum. In the present context, given that Ipc activity gates the visual flow of ascending to the rotundus nucleus, the study of oscillatory bursts and their spatio-temporal patterns would allow us to visualize the dynamics of a stimulus selection mechanism directly.

In this thesis we will search for a method which allows us to automatically and reliably isolate the OBs so that we can analyze significant amounts of data. This will be of particular importance since we will be performing recordings with multiple electrodes, which multiplies the effort needed to annotate the recordings. Moreover, because we intend to capture a detailed correspondence between the visual space and the tectal surface, experiments will comprise several hours of random stimulation to establish the correct mapping between these two spaces, resulting in a vast amount of raw data that needs to be processed.

Multi-electrode Recordings

The pattern of oscillatory bursts in the tectum has previously been approximated with one or two electrodes, which allows the comparison of near and far recording sites relative to the site of stimulation. In other instances, simultaneous recordings of the TeO and Ipc have been performed, revealing the origin of the OBs[13]. But while there have been many studies investigating the anatomical and electrophysiological properties of the tectum and associated isthmic nuclei, many questions still linger. For example, it is unclear how the feedback is distributed in space and time in TeO, in response to moving objects or to more complex stimulation, like an expanding disc or multiple simultaneous stimuli. To address these questions, a new experimental approach is needed that allows for recordings of neural activity across multiple sites of the tectum. One such technique is the use of multi-electrode arrays, which allow directly surveying a large area of the tectum simultaneously. By using this technique, we aim to gain insights into the operation of the neural circuit underlying tectal processing and ultimately shed light on the underlying principles of stimulus selection. Specifically, our focus is on

characterizing the proposed focal spotlight defined by the feedback of the Ipc on the tectum through an examination of the spatio-temporal patterns of the oscillatory bursts.

Hypothesis

The main hypothesis of this work is that at any given moment, in the visual tectal map there is a single gating spotlight defined by the facilitating activity of the Ipc feedback. This spotlight blinks from locus to locus discontinuously scanning visual stimuli.

Objectives

The general objective is to characterize the neurodynamics encompassing the establishment and movement of the gating spotlight generated by the istmo-tectal circuit.

The specific objectives are:

1. To create a computational platform to automatically deliver stimuli to both anesthetized and awake animals

2. To characterize the geometry and dynamics of the spotlight is response to simple stimuli

3. To capture the phenomenology of competing pairs of stimuli in the TeO

Chapter I

Automatic Detection of avian Bursts in the avian Optic Tectum using Shift-Invariant Semi-Nonnegative Matrix Factorization

Bryan Reynaert[1,3*], Juan Carlos Letelier[1] and Gonzalo J Marín[1,2]

[1]Departamento de Biología, Facultad de Ciencias, Universidad de Chile, Santiago, 7800003, Chile

[2]Facultad de Medicina, Universidad Finis Terrae, Santiago, 7501015, Chile.

[3] Lead Contact

*Correspondence: br@akori.cl

Abstract

Non-Negative Matrix Factorization (NMF) is a powerful signal decomposition technique widely used for dimensionality reduction and demultiplexing composite signals. In this study, we apply the Shift-Invariant Semi-nonnegative Matrix Factorization (SSNMF) approach to automatically detect burst discharges in the axon terminals of the nucleus isthmi pars parvocellularis (Ipc) of the avian optic tectum (TeO), a very characteristic but highly variable visually-evoked electrophysiological response. Our results demonstrate the efficiency of SSNMF in accurately identifying burst sequences, achieving performance comparable to human annotators.

The SSNMF method presents a combination of computational efficiency and flexibility. It enables the decomposition to be learned from a subset of the dataset, reducing computational burden, while also eliminating the need for extensive parameter tuning. Furthermore, the interpretability of the learned matrices empowers researchers to manually fine-tune the results, incorporate prior knowledge, and apply additional post-processing techniques, enhancing the overall versatility of the approach making it a suitable candidate for complex data processing pipelines.

With this analytical tool, we were able to obtain activation coefficients that accurately captured the precise timing of tectal bursts (OBs). Additionally, we extracted the constituent waveforms that form these bursts and made a significant discovery: the waveforms exhibit a remarkable similarity across electrodes and closely resemble the shape of extracellularly recorded action potentials. These findings provide compelling evidence that burst responses predominantly arise from the simultaneous propagation

of multiple action potentials through the complex arborization of Ipc axon terminals, resulting in a decoherent superposition.

In conclusion, SSNMF proves to be an effective and automated technique for detecting burst discharges in Ipc axon terminals. It provides directly interpretable results and accommodates the variability observed in burst responses. The technique holds promise for investigating neural activity and understanding the underlying mechanisms of a broad set of electrophysiological responses.

Introduction

The optic tectum (TeO) is a highly conserved region of the midbrain in vertebrates. In birds, its superficial layers receive topographic inputs from the contralateral retina, while its lower layers control orienting eye and head movements[1,2]. Over the years, the TeO has been subject to intensive research, and with the recent advancements in multi-electrode arrays (MEA), it is to be expected that the volume of electrophysiological data concerning this brain region will grow exponentially. However, despite decades of investigation, the automatic detection and classification of signals in the TeO remains challenging.

The most prominent signals recorded extracellularly in the superficial and intermediate layers of the avian TeO are sequences of large amplitude bursts of potentials called “tectal bursts” (or oscillatory bursts, OBs, in Marin et al, 2005[3]). These bursts arise from the bursting firing of action potentials of Ipc neurons as they propagate through the terminal arborization of the nucleus istmi pars parvocellularis (Ipc) axons, which extend in a columnar field from tectal layer 13 to tectal layer 2. Lesion studies and

simultaneous recordings have revealed that OBs play a fundamental role in visual processing by gating or boosting the ascending flow of visual activity from the tectum to the nucleus rotundus and the visual pallium[4]. Furthermore, the OBs represent the efferent limb of a winner-takes-all mechanism that points and selects the most salient retinal input arriving to the tectum[5]. Consequently, there is an increasing interest in studying the distribution of OBs under different visual stimulation contexts. These studies would benefit from an automatic method that can effectively detect and differentiate OBs from other tectal activity, especially if using MEA recordings to collect large amounts of data.

The dense field of Ipc axon terminals along with their intricate geometry, which includes multiple branching points, diverse axonal diameters and even en passant buttons[6], presumably results in action potentials mobilizing relatively strong but variable currents, leading to voltage signals of large amplitude but of considerable complexity, as typically recorded with extracellular electrodes. OBs, even those repeatedly recorded by the same electrode, can exhibit substantial variations in shape and duration, ranging from 5 to 30 milliseconds. Additionally, the voltage envelope of individual OBs, despite being described as gaussian, can also exhibit different profiles (see figure 1). These variations increase in MEA recordings, where electrode tips of different electrodes may be positioned at different proximities to the axon terminals and at various tectal depths, causing the burst's polarity recorded by different electrodes to change depending on the electrode.

Fourier transform analysis of tectal recordings reveal that OBs are broadband signals, with the main component ranging from 500 Hz to 1kHz, corresponding to the bursting

firing range of Ipc neurons[3,7–9]. However, they also exhibit a strong presence of higher frequencies (see figure 1). In addition, their mixing with spike signals from other sources, makes the OBs resistant to automatic detection and analysis using regular filtering procedures, including advanced techniques like the cepstral analysis, the Hilbert-Huang transform, wavelet analysis or principal component analysis. In this work we propose the utilization of Shift-Invariant Semi-Nonnegative Matrix Factorization (SSNMF), a matrix factorization approach, supplemented with additional post-processing, as a robust detector for OBs. Furthermore, we suggest that SSNMF may provide additional insights into the composition of the recorded tectal bursts. By extension we suggest that SSNMF might be an ideal technique for the detection, analysis and classification of complex bursting signals in other systems as well.

Materials and Methods

Extracellular Recordings

Extracellular recordings from the tectal visual response were obtained from anesthetized pigeons as described in Reynaert et al, 2023[10]. Extracellular recordings were performed on an exposed region of the tectum using two arrays of regularly spaced tungsten microelectrodes (1 MΩ, 300 µm separation). Neural signals were amplified, band-passed between 10 Hz and 10 KHz, sampled at 20 KHz, and digitized by an Intan RHD2000 board and stored in a personal computer for offline processing. Acquisition, display and analysis of neural data and presentation of visual stimuli were

controlled by custom software written in Presentation and Python v3.8.10 with the modules Numpy v1.17.4, Scipy v1.3.3 and Scikit-learn v0.20.2.

SSNMF in a nutshell

Non-Negative Matrix Factorization (NMF) is a family of signal decomposition techniques broadly used for clustering[11], dimensionality reduction[12], denoising[13] and demultiplexing composite signals[14]. After its formulation by Lee and Seung[15], it has gained popularity in many fields of science, such as chemometrics[16], pattern recognition[17], multimedia data analysis[18], text mining[19] and molecular biology[20,21]; with many specialized variants being developed within those fields. In neuroscience, its applications range from template matching[22] to calcium imaging analysis[23]. The core of these techniques is the approximate decomposition of a signal **S** (**n** segments x **t** samples) into the product of two matrices which represent the learned basis of components and their corresponding activation patterns:

$$S_{nt} = \sum_{k} A_{nk} B_{kt} + \varepsilon_{nt}$$

where **A** (**N** segments x **K** templates) is the activation matrix, **B** (**K** templates x **T** samples) is the dictionary or components matrix, and **ε** is an error term. Here **K** is the number of different templates contained in the signal, **N** is how many rows are present in **S** (channels, recordings, etc…) and **t** represents time. That is, the signal is modeled as the linear superposition of events of **K** different types occurring at scale dictated by matrix **A** and whose shape is captured in matrix **B**.

The non-negativity constraint in NMF ensures that the resulting components and activations are additive and non-negative, allowing for intuitive interpretations in many real-world applications. By capturing the underlying structure of the signal in terms of

these non-negative components and activations, NMF enables efficient representation, analysis, and manipulation of complex signals in various domains. Moreover, the inherent sparsity and parts-based nature of NMF make it particularly suited for tasks where the signals of interest are characterized by localized and non-overlapping patterns.

In this work, **S** corresponds to the extracellular electrical potential recorded by electrodes in the tectum in response to visual stimulation. **S** can contain one or multiple channels, or even multiple recordings under different stimulation protocols. The only condition on the signal is that the base waveforms remain constant so they can be learned.

Depending on the nature of the signal and the assumptions made on the templates, a wide range of factorizations can be achieved within the framework of NMF. In the case of SSNMF, introduced by Le Roux[22], the non-negativity constraint on the dictionary matrix is removed, allowing the learning of bipolar templates. The shift invariance comes from redefining the **B** matrix as holding templates for events that could happen at any time in the signal and with arbitrary duration **L**, so it becomes **B** (**K** templates x **L** samples). Consequently, a redefinition of **A** is needed, which must now include the sample index **d** at which events of type **k** occur. To combine the effects of **A** and **B** and reconstruct the signal, we must convolve **A** with **B** so that a single event contributes with the whole event template. For a 1-dimensional signal, this can be expressed by the formula:

$$S_t = \sum_d \sum_l \sum_k A_{dk} \delta_{d\,t-l} B_{kl}$$

While the equation may seem complex, the interpretation of **A** and **B** remains straightforward. If **S** is composed by the summation of stereotypical, time-discrete

events, **A** indicates when these events happen and with which amplitude, while **B** contains the waveforms of these events. The shift-invariance property allows the events to happen at any time in the signal, removing the need for alignment to a specific cue or reference point (see figure 2).

A remarkable property of this decomposition is that it is unsupervised, meaning that no user input is required to obtain **A** and **B**. The learning process for **A** and **B** involves an optimization procedure, initialized with a random solution that already satisfies the constraints. The goal is to minimize the error term iterating through alternating updates to the current solutions for **A** and **B**. In general, there exist multiplicative update formulas for the coefficients of the matrices, ensuring that the minimization adheres to the non-negativity constraints. However, in the case of semi-NMF, a different approach can be taken by directly using the optimal least-squares solution.

To obtain robust and more interpretable results, it is often desirable to impose additional constraints on **A** and **B**. These constraints can include sparsity, orthogonality and normalization conditions among others. They are incorporated as additional terms to the objective function; it is often possible to incorporate them into the update formulas.
Despite the relative popularity of NMF techniques, SSNMF has not been broadly used, possibly because of the initially striking complexity of its update formulas. They are included here to illustrate this point:

$$B^{n+1} = \left(\tilde{A}^{t}_{kl}\tilde{A}^{t}_{tk'l'} + \Lambda_{kl,k'l'}\right)^{-1}\tilde{A}^{k'l'}_{t}X^{t}$$

$$A^{n+1} = A^{n}\sqrt{\frac{\left(X^{l}_{n}B_{kl}\right)^{+} + A^{n'k'}\left(B^{t}_{n'k'}B_{nkt}\right)^{-}}{\left(X^{l}_{n}B_{kl}\right)^{-} + A^{n'k'}\left(B^{t}_{n'k'}B_{nkt}\right)^{+} + \alpha\beta A^{\alpha-1}_{nk}}}$$

It must be noted that even when the algorithm converges, it does not ensure a global minimum, nor are there guarantees that such a minimum would be unique. For this reason multiple solutions should be obtained by randomizing the initial conditions and assessed later on, dropping the ones that diverge. The degree of agreement between the solutions will depend strongly on the signal to noise ratio (SNR) of the data.

Three characteristics of SSNMF make this technique particularly well suited for the detection of tectal bursts:

1. It learns the signal, not the noise. Given enough samples of the desired signal, this technique can learn the waveforms independently of the nature of noise, be it dynamic or static, broadband or narrowband, even under circumstances of a low signal-to-noise ratio; as long as the desired signal is repeated/present enough times, it can be extracted by SSNMF. This also means that as an optimization, a recording can be filtered to include only signal containing segments to accelerate the learning of the signals.

2. It is an unsupervised technique, requiring no parameter tuning other than the selection of the number k of templates to learn.

3. It decomposes the signal into isolated waveforms which can provide information on the underlying mechanism generating the signal and it also provides timing and magnitude information, which again, can be further analyzed.

Post-processing

After the reconstruction, the signal S = AB, contained enhanced burst signals and reduced noise. This signal was then rectified and smoothed over 2 ms, and then thresholded to their 90th percentile value. Thresholded segments were further filtered using either one of two criteria: the segment was at least 5 ms long, or more than one segment was detected within a millisecond, in which case they were fused, as was frequent with some bursts which contained very demarcated spikes.

These segments provided a good indicator of the presence of bursts; however, as bursts co-occurred in neighboring electrodes, we used this property to further refine the burst selection by defining concurrence windows. These windows are periods in which at least the majority of a set of 5 neighboring electrodes detected bursting responses simultaneously. Gaps smaller than 4 ms were filled, and windows shorter than 3 ms were removed. Concurrence windows were then used to further filter and refine the initial segments by selecting segments intersecting with the concurrence window and lowering the threshold of detection. This procedure improved the recognition of the bursts' onset.

Results

We analyzed extracellular recordings of 4 specimens obtained from MEA. Since the tectum is mostly silent under experimental conditions, we increased the information density of the training dataset by selecting recording segments which exhibited tectal activity. No other selection criteria were applied.

Utilizing **K**=1, a consistent waveform was obtained from most electrodes. For each electrode we ran the optimization procedure until convergence 10 times employing a different bootstrap solution each time and selected the most representative solution as the one exhibiting the lowest intra-solution root mean square (RMS). Multiple such optimization trials yielded very similar results, indicating the reliability of the solution, as seen in figure 3. Moreover, the different electrodes also yielded a similar solution, specially those in close proximity again confirming the robustness of the learned waveform. This result also indicates that variation between electrodes is likely due to each electrode's particular circumstances.

The recovered waveform has the profile of a stereotypical extracellular action potential (EAP), exhibiting all 3 phases: 1) a brief, positive peak; 2) a much larger negative peak; and 3) a positive period of longer duration and slowly decaying amplitude as described in Gold et al., (2006)[25]. Although a couple of the waveforms exhibit some variation, for example no initial peak, this is expected due changes in the relative position of the electrode with respect to the Ipc axon.

When higher values for **K** were tested, the additional learned waveforms had high variability between optimization trials and accounted for a very small percentage of the signal, indicating that a single template was enough to recreate the signal with high fidelity (see figure 4). Moreover, we explored the **K**x**L** space and found that there was always an EAP-like waveform and that increasing the time window (L) had the effect of introducing small amplitude artifacts at the border, adding no value (data not shown). This indicates that the fundamental atom behind the complex tectal bursts are extracellular action potentials which superimpose densely.

We observed similar results in all datasets. For each specimen, we employed multiple stimulation protocols, including a spot of light flashed during 16ms, a moving spot of light, a moving bar and a looming stimulus, again obtaining a similar decomposition each time.

SSNMF correctly captured and recreated the MEA recordings, effectively denoising the tectal bursts (see figure 4). The activity coefficients obtained from the decomposition are informative, but precise event timing is obscured due to the bursting nature of the signal. To derive a more meaningful indicator of burst presence, we turned to post-processing the denoised signal. Exploiting the discovery that tectal bursts propagate horizontally through the tectal surface and thus are often recorded by multiple nearby electrodes, we defined concurrence windows as an additional filter. This post-processing cleaned the signal further, providing very similar results to a human annotator.

The final automatic detection of tectal bursts was compared to a human expert annotator in 968 runs (see table 1). The matching matrix shows that the method accuracy is as high as 94%, which is more than enough for most studies requiring automatic signal detection.

Figures

Figure 1. Tectal bursts as recorded by MEA are high amplitude, high frequency responses in the tectum

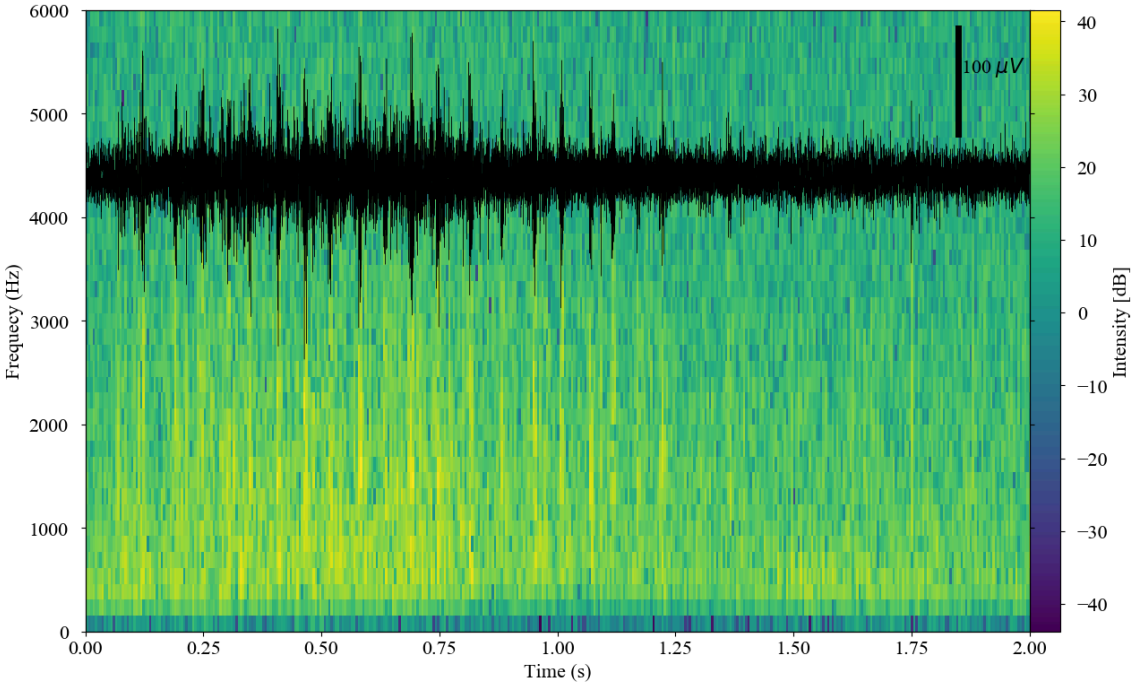

Extracellular recording (black) and its spectrogram containing oscillatory bursts. Burst events in the first second of the recording are easily detectable due to their amplitude. During the bursts, a broad range of frequencies can be observed, up to 3kHz (yellow stripes).

Figure 2. The SSNM factorization decomposes the signal in an activation matrix and a waveform matrix

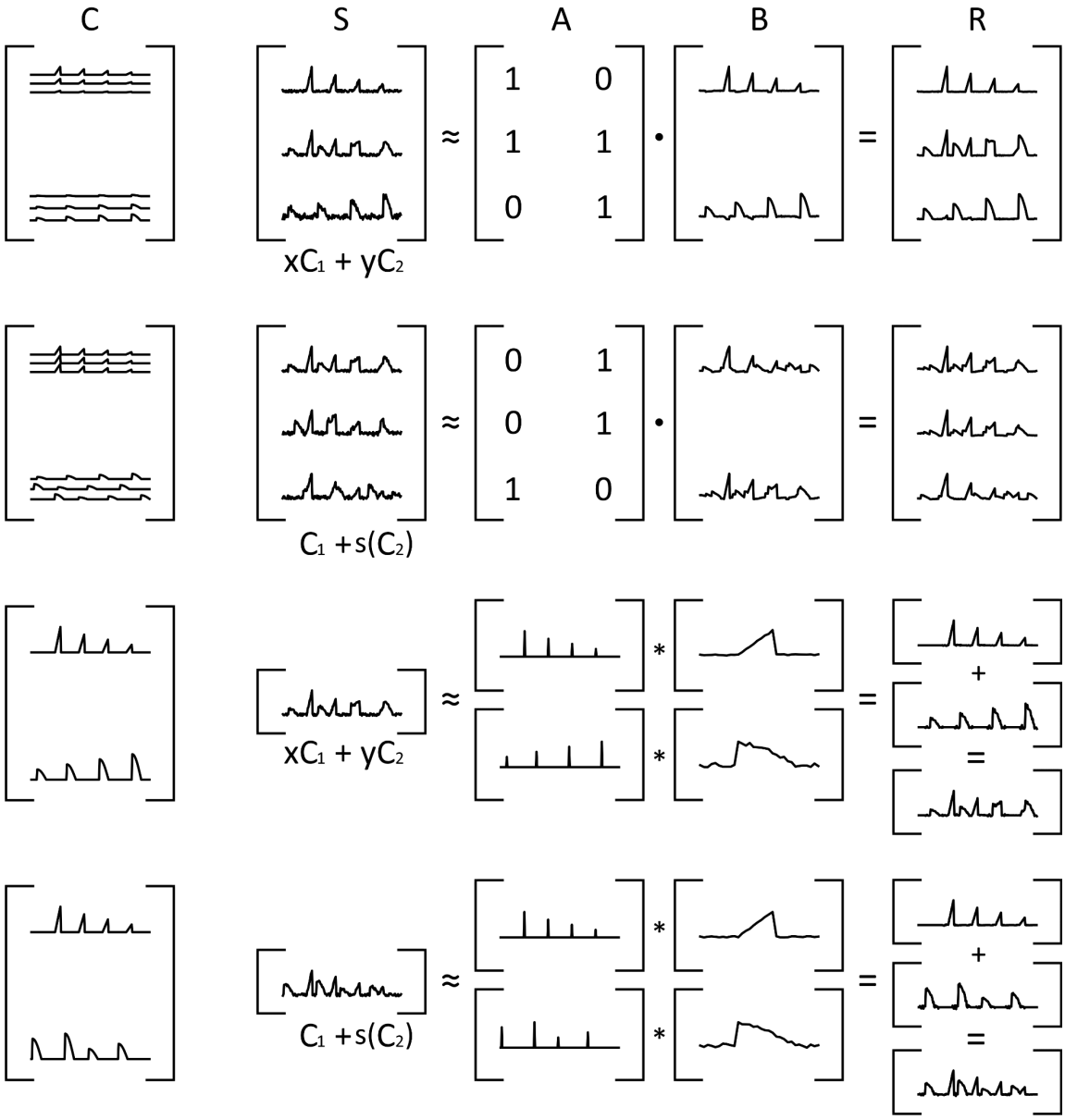

Example of decompositions with NMF (top rows) and SSNMF (bottom rows). We combined components **C** through a linear mix (rows 1 and 3) or by adding one component with a shifted version of another (rows 2 and 4) to obtain signals **S**. The signal **S** is then decomposed in a product of **A**, the activation matrix and **B**, the dictionary matrix. From **A** and **B**, a reconstruction **R** of the signal can be obtained. NMF

(top rows) can decompose a time series into separate signals (top) as long as the signals are time-aligned. If this is not the case, then a correct decomposition can not be obtained (second row) and artifacts appear in the results. SSNMF decomposition (bottom rows) finds the constituent waveforms (B matrix) and thus is resistant to phase shifts, correctly reconstructing the signal and effectively denoising it. A and B matrices are very informative in the case of SSNMF, as they contain the precise timing of the events and their waveforms. • indicates matrix multiplication, * indicates convolution.

Figure 3. Waveforms learned from 48 different recording electrodes

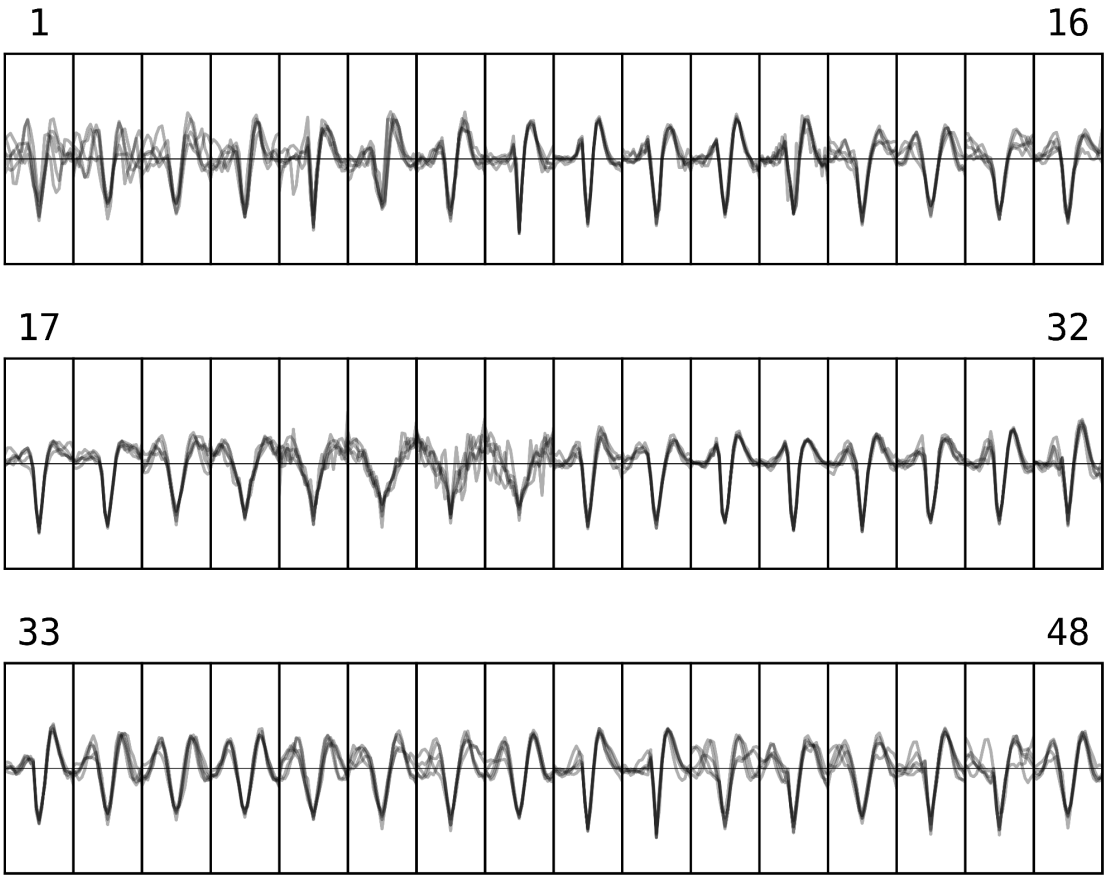

Applying SSNMF to recordings from 48 electrodes. Each window displays waveforms obtained from 5 independent recordings obtained during the same experiment, average shown in darker traces. Although each electrode yields slightly different waveforms, all of them share a similar shape, easily recognizable as the profile of an action potential recorded extracellularly. Differences between channels are probably due to differences in tectal depth, electrode state and local environment. Channels in which the signal was not strong show a higher variability, that is, do not converge to the same waveform. Each window represents 1 ms. For waveforms the vertical axis does not have a scale, points are measured relative to each other.

Figure 4. Signal reconstruction and burst detection

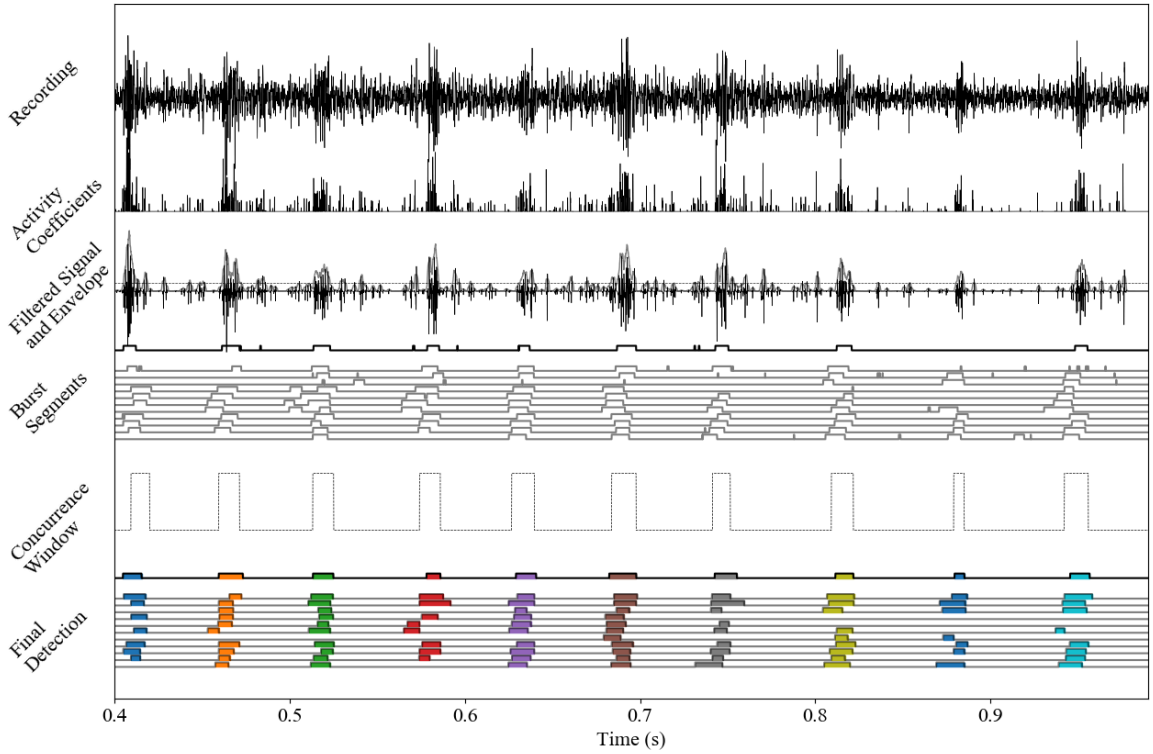

The different stages of burst detection. **Activity coefficients** are extracted from the **original recording** through SSNMF and the signal is reconstructed, removing most of the noise. Then, the **envelope** of the detected bursts is calculated by rectifying and smoothing. The envelope is then thresholded, yielding **burst segments**. Segments of near channels are pooled together to define **concurrence windows**, which are employed to filter out spurious burst segments.

Table 1. Matching matrix between SSNMF and human annotator

		Human annotator	
		Oscillatory burst	No burst
Detection by SSNMF	No burst	0.3 %	90.9 %
	Oscillatory burst	2.9 %	5.9 %

Matching matrix comparing our proposed algorithm vs. a human annotator (considered ground truth). Analysis of 968 runs encompassing a total of 1h15m of recordings at 20kHz total. The automatic detection of oscillatory bursts has an accuracy of 94%. 96.8% of samples are deemed non-bursting, while the remaining 3.2% of the recordings contain oscillatory bursts. From this fraction, 91% (2.9% of total) is detected by SSNMF.

Discussion

Our results demonstrate the efficiency of SSNMF as a method for automated detection of burst discharges in the Ipc axon terminals recorded in the avian TeO, achieving comparable performance to that of a human annotator. The SSNMF pass is capable of detecting 91% of oscillatory burst-containing samples and it only generates a 6% of false positives. Depending on the goal of the detection, the trade-off between false positives and false negatives can be tuned, for example, by modifying SSNMF parameters like the a priori description of the SNR or increasing the detection threshold. In our case, later filtering stages, like the concurrency windows we implemented, drop most of these spurious detections. Given the nature of our analysis, we deemed it far more important to detect as many true positives as possible, while accepting some false positives.

We observed that complete sequences of bursts, recorded by a single electrode, could be accurately reconstructed by multiplying a single constituent waveform with varying amplitude coefficients. Remarkably, this characteristic held consistently across bursts elicited by different visual stimuli presented during the recording session, indicating the robustness and stability of the approach.

The constituent waveforms obtained for each recording electrode had distinct shapes and temporal profiles, yet all presented typical characteristics of extracellularly recorded spikes. These results are significant, as they suggest that each OB primarily arises from extracellular currents that, despite variations in magnitude, maintain a constituent waveform of constant spatiotemporal profile. This phenomenon may arise from the

superposition of action potentials propagating through individual axon terminal branches, where successive impulses invade different proportions of the terminal arborization. Additionally, the contribution of a varying number of axon terminals firing synchronously at any given time cannot be ruled out. Overall, these findings support the notion that burst responses predominantly represent the propagation of action potentials through the branches of the Ipc axon terminals.

An additional advantage of SSNMF is its computational efficiency. The dictionary matrix can be learned from a representative but relatively small data set; which then enables efficient activation matrix calculation for large volumes of data. Moreover, this computation can be trivially distributed. Furthermore, the interpretability of both matrices allows for manual curation if necessary. Strategies such as pruning small activity coefficients to steer towards sparse activation matrices or incorporating prior knowledge through initial solutions derived from the original signal (e.g., peak detection schemes) can be implemented during the learning phase. The dictionary matrix can also be edited to fine-tune or expedite the learning process if previous knowledge exists regarding the contributors to the signal. Overall, multiple strategies can be implemented to guide and augment the algorithm by incorporating prior knowledge[22,24].

To gain further insights and accurately investigate the varying profiles of the recorded bursts, future studies could employ 3D reconstructions of Ipc axon terminals. Such reconstructions would enable the modeling of spike propagation through individual branches, facilitating a more precise examination of the OB characteristics. The intricate morphology of the terminal, with synaptic buttons segregated in different tectal layers, aligns with the idea of action potentials not uniformly invading the entire arborization but

rather selectively targeting specific regions. This process may be under local modulatory control. Considering this perspective, the activity coefficients derived from recorded bursts could serve as diagnostic indicators of partial invasion, offering a powerful tool to investigate this phenomenon more comprehensively. Moreover, activity coefficients and their distribution might be an interesting basis for a spike sorting strategy.

Conclusions

In this study, we have demonstrated the effectiveness of SSNMF in automatically detecting neural signals, even in the presence of high variability and unknown underlying components. Notably, this technique eliminates the need for manual parameter tuning and yields directly interpretable results. Both the activation and template matrices obtained from the decomposition of the original signal contain valuable and readily interpretable data that can be further leveraged.

The template matrix provides insights into the underlying waveforms present in the neural signals, revealing information that may not be immediately evident from the raw recordings. Meanwhile, the activation coefficients, in combination with additional ad-hoc post-processing methods, can be utilized for denoising purposes and recovering precise timing information of neural activity. Remarkably, the accuracy achieved by this automated approach matches that of a trained technician, highlighting its potential for efficient and reliable analysis in situations where the sheer volume of available data surpasses our capacity for manual inspection and analysis.

Our findings shed light on the nature of tectal bursts, which occur in response to visual stimuli. The factorization indicates that OBs are composed of a series of consecutive spikes in partial overlap. These spikes exhibit the typical waveform of extracellular action potentials and maintain consistent characteristics across large portions of the tectum, even under different stimulation protocols. While the cellular mechanism underlying tectal bursts is yet to be fully elucidated, previous studies have demonstrated that they originate from the Ipc nucleus in the paintbrush neurons, which possess highly ramified axons. It is plausible that as paintbrush neurons burst, the consecutive action potentials decohere as they propagate through the branching axon structure and might even undergo dynamic selective propagation, giving rise to the complexity of tectal bursts.

These results provide valuable insights into the complex dynamics and mechanisms underlying tectal bursts and highlight the potential of SSNMF as a powerful tool for unraveling intricate neural activity patterns. The automatic and efficient extraction of such information is of paramount importance in the current era, where the availability of data far exceeds our human capacity to comprehensively analyze it. SSNMF opens up new avenues for understanding neural processes and holds promise for broader applications in the analysis of complex signals in other systems as well.

References

1. Luksch, H. 2003. Cytoarchitecture of the Avian Optic Tectum: Neuronal Substrate for Cellular Computation. Rev. Neurosci. 14: 85–106

2. Wylie, D., Gutiérrez-Ibáñez, C., Pakan, J. & Iwaniuk, A. 2009. The optic tectum of birds: Mapping our way to understanding visual processing. Can. J. Exp. Psychol. 63: 328–338.

3. Marín, G., Mpdozis, J., Sentis, E., Ossandón, T., & Letelier, J. C. 2005. Oscillatory Bursts in the Optic Tectum of Birds Represent Re-Entrant Signals from the Nucleus Isthmi Pars Parvocellularis. J. Neurosci. 25: 7081–7089

4. González-Cabrera, C., Garrido Charad, F., Mpodozis, J., Bolam, J. & Marín, G. 2015. Axon terminals from the nucleus isthmi pars parvocellularis control the ascending retinotectofugal output through direct synaptic contact with tectal ganglion cell dendrites. J. Comp. Neurol. 524: 362–379

5. Marín, G. Durán, E., Morales, C., Gonzáles'Cabrera, C., Sentis, E., Mpodozis, J., Letelier, J.C. 2012. Attentional Capture? Synchronized Feedback Signals from the Isthmi Boost Retinal Signals to Higher Visual Areas. J. Neurosci. Off. J. Soc. Neurosci. 32: 1110–1122

6. Wang, Y., Major, D. & Karten, H. 2004. Morphology and Connections of Nucleus Isthmi Pars Magnocellularis in Chicks (Gallus gallus). J. Comp. Neurol. 469: 275–297

7. Marín, G., Salas, C., Sentis, E., Rojas, X., Letelier, J.C. & Mpodozis, J. 2007. A Cholinergic Gating Mechanism Controlled by Competitive Interactions in the Optic Tectum of the Pigeon. J. Neurosci. 27: 8112–8121

8. Goddard, C., Sridharan, D., Huguenard, J. & Knudsen, E. 2012. Gamma Oscillations Are Generated Locally in an Attention-Related Midbrain Network. Neuron 73: 567–580

9. Goddard, C.A., Huguenard, J., & Knudsen, E. 2014. Parallel Midbrain Microcircuits Perform Independent Temporal Transformations. J. Neurosci. 34, 8130–8138

10. Reynaert, B., Morales, C., Mpodozis, J., Letelier, J. C. & Marín, G. J. 2023. A blinking focal pattern of re-entrant activity in the avian tectum. Curr. Biol. 33, 1-14

11. T. Li & C. Ding. 2006. The Relationships Among Various Nonnegative Matrix Factorization Methods for Clustering. in Sixth International Conference on Data Mining (ICDM'06) 362–371

12. S. Tsuge, M. Shishibori, S. Kuroiwa, & K. Kita. Dimensionality reduction using non-negative matrix factorization for information retrieval. 2001. IEEE International Conference on Systems, Man and Cybernetics. e-Systems and e-Man for Cybernetics in Cyberspace vol. 2: 960–965.

13. Jeng, F.-C., Lin, T.-H., Hart, B. N., Montgomery-Reagan, K. & McDonald, K. 2022. Non-negative matrix factorization improves the efficiency of recording frequency-following responses in normal-hearing adults and neonates. Int. J. Audiol. 1–11

14. M. Morup, K. H. Madsen, & L. K. Hansen. 2007. Shifted Non-Negative Matrix Factorization. in 2007 IEEE Workshop on Machine Learning for Signal Processing 139–144

15. Lee, D. D. & Seung, H. S. 1999. Learning the parts of objects by non-negative matrix factorization. Nature 401: 788–791

16. Xie, Y.-L., Hopke, P. K. & Paatero, P. 1998. Positive matrix factorization applied to a curve resolution problem. J. Chemom. 12: 357–364

17. S. Z. Li, Xin Wen Hou, Hong Jiang Zhang, & Qian Sheng Cheng. 2001. Learning spatially localized, parts-based representation. in Proceedings of the 2001 IEEE Computer Society Conference on Computer Vision and Pattern Recognition. 1: 1–1

18. M. Cooper & J. Foote. 2002. Summarizing video using non-negative similarity matrix factorization. in 2002 IEEE Workshop on Multimedia Signal Processing. 25–28

19. Wei, X., Xin, L. & Yihong, G. Document Clustering Based on Non-Negative Matrix Factorization. 2003. Proc. 26th Annu. Int. ACM SIGIR Conf. Res. Dev. Inf. Retr. 267–273

20. Brunet, J.-P., Tamayo, P., Golub, T. R. & Mesirov, J. P. 2004. Metagenes and molecular pattern discovery using matrix factorization. Proc. Natl. Acad. Sci. 101, 4164–4169

21. Greene, D., Cagney, G., Krogan, N. & Cunningham, P. 2008. Ensemble non-negative matrix factorization methods for clustering protein-protein interactions. Bioinformatics 24: 1722–1728

22. Le Roux, J., de Cheveigne, A. & Parra, L. C. 2009. Adaptive Template Matching with Shift-Invariant Semi-NMF. Adv. Neural Inf. Process. Syst. 21: 921–928

23. Saxena S., Kinsella I., Musall S., Kim S.H., Meszaros J., Thibodeaux D.N., Kim C., Cunningham J., Hillman E.M.C., Churchland A., Paninski L. 2020. Localized semi-nonnegative matrix factorization (LocaNMF) of widefield calcium imaging data. PLoS Comput Biol.16:e1007791

24. Li P., Tseng C., Zheng Y., Chew J.A., Huang L., Jarman B., Needell D. 2022. Guided Semi-Supervised Non-Negative Matrix Factorization. Algorithms. 15: 136

25. Gold, C., Henze, D. A., Koch, C. & Buzsáki, G. 2006. On the Origin of the Extracellular Action Potential Waveform: A Modeling Study. Journal of Neurophysiology 95: 3113–3128

Chapter II

A blinking focal pattern of re-entrant activity in the avian tectum

Bryan Reynaert[1], Cristian Morales[1], Jorge Mpodozis[1], Juan Carlos Letelier[1] and Gonzalo J Marín[1,2,3*]

[1]Departamento de Biología, Facultad de Ciencias, Universidad de Chile, Santiago, 7800003, Chile

[2]Facultad de Medicina, Universidad Finis Terrae, Santiago, 7501015, Chile.

[3] Lead Contact

*Correspondence: gmarin@uchile.cl

Curr. Biol. 33 (2023): 1-14.e4

doi: 10.1016/j.cub.2022.10.070

Summary

Re-entrant connections are inherent to nervous system organization; however, a comprehensive understanding of their operation is still lacking. In birds, topographically organized re-entrant signals, carried by axons from the nucleus-isthmi-parvocellularis (Ipc), are distinctly recorded as bursting discharges across the optic tectum (TeO). Here, we used up to 48 microelectrodes regularly spaced on the superficial tectal layers of anesthetized pigeons to characterize the spatial-temporal pattern of this axonal re-entrant activity in response to different visual stimulation. We found that a brief luminous spot triggered repetitive waves of bursting discharges that, appearing from initial sources, propagated horizontally to areas representing up to 28 deg of visual space, widely exceeding the area activated by the retinal fibers. In response to visual motion, successive burst-waves started along and around the stimulated tectal path, tracking the stimulus in discontinuous steps. When two stimuli were presented, the burst-wave sources alternated between the activated tectal loci, as if only one source could be active at any given time. Because these re-entrant signals boost the retinal input to higher visual areas, their peculiar dynamics mimics a blinking "spotlight", just as the classic metaphor alluded to explain spatial attention. Tectal re-entry from Ipc is thus highly structured and intrinsically discontinuous, and higher tectofugal areas, which lack retinotopic organization, will thus receive incoming visual activity in a sequential and piecemeal fashion. We anticipate that analogous re-entrant patterns, perhaps hidden in less bi-dimensionally organized topographies, may organize the flow of neural activity in other parts of the brain as well.

KEYWORDS: re-entrant connections, attention spotlight, spatial attention, optic tectum, superior colliculus, vision, neural processing.

Introduction

Perception is invariably associated with the interplay of stimulus-elicited feed-forward activity and state-dependent processing contributed by the brain[1-3]. Internal processing largely relies on re-entrant connections occurring at all scales in the nervous system[4-7], as Lorente de Nó observed in his description of the intrinsic and extrinsic connections of the "modules" in the mammalian cortex[8,9]. Re-entrant connections are also prominent in sensory surfaces and subcortical structures and in the way these structures interact between themselves and with the cortex[10-13]. Through this connectivity, neurons receive multiple modulations from large parts of the brain, adding context to peripheral inputs and multiplexing their information content[14-16].

As carriers of internal signals, less governed by the periphery, re-entrant axons presumably display complex patterns of activity closely related to the mechanisms by which the brain reads, gates and transforms incoming sensory information. However, the spatial-temporal patterns taken by those signals are far from clear in any brain structure. This situation limits, on the one hand, our understanding of the "brain code" and, on the other, the design of realistic neural networks that incorporate recurrent architectures.

The massive recurrent connectivity between the optic tectum (TeO) and the parvocellular isthmic nucleus (Ipc) of birds possesses several characteristics that makes it an outstanding system for the analysis of re-entry[17-26]. It is composed of a laminar

array of tectal neurons, called shepherd's crooks (Shcs)[27], that topographically transmits the retinal input to the Ipc neurons, which project back to TeO via an equivalent array of columnar axons terminals that maintains the same topographic arrangement. Thus, retinal inputs to the TeO elicit a homotopic re-entrant response in TeO via the Ipc columnar axons (Figure 1A)[28]. The simultaneous activation of GABAergic neurons of the magnocellular isthmic nucleus that project diffusely to either TeO or Ipc opposes the activation of the Ipc axons at other tectal locations, promoting competition between simultaneous re-entrant signals[20,29,30]. Furthermore, input connections from the motor pallium modulate this competition in a top-down fashion[31] connecting this circuit operation to global states of the brain. Because the Ipc columnar axons have hundreds of branches and buttons concentrated in a restricted tectal volume, their characteristic bursting firing is manifested as repetitive bursting responses that are prominently recorded throughout the superficial and intermediate tectal layers, down to about 800 µms in depth (Figure 1B). The Ipc's axonal origin of these tectal responses has been demonstrated in intracellular and dual recordings performed both *in vivo* [19,20] and in brain slices [32]. These studies also showed that these stereotyped tectal bursts locally disappear after inactivation of the corresponding locus in the Ipc. In this study, we used the bursting signature of these re-entrant signals to record their spatial-temporal distribution in the tectum of anesthetized pigeons in response to simple and complex visual stimulation.

Results

Ipc re-entrant signals propagate as horizontal radial waves of burst activity on the tectal visual map.

The bursting discharges of Ipc axons were recorded using bi-dimensional arrays of tungsten microelectrodes regularly spaced in TeO. Experiments were carried out in seven anesthetized pigeons and in four of them we obtained enough recording data under different stimulus conditions to be used for quantitative analysis. Five types of visual stimuli were used: static spots, moving spots, moving bars, looming circles, and competing moving spots. Figure 2A depicts the typical distribution of 48 microelectrodes from a pair of 4x4 and 8x4 arrays inserted in the lateral part of the exposed tectum[33]. A bright spot (0.7 deg, 16-32 ms) flashed in different parts of the monitor elicited the characteristic bursting firing of Ipc axons (Figure 2C), defining for each electrode a receptive field (RF) ranging from 10 to 28 deg in diameter (18.6 +/- 3.8 deg, n=160) (Figure 2B). As expected from the homotopic TeO/Ipc reciprocal topography, the position of the RF center of the bursting response coincided in visual space with the RF of the retinal input, as estimated by the peak depolarization of the evoked LFP simultaneously recorded by the electrode (Figure S1A). As the microelectrodes were separated by about 300 μm, representing about 3 deg of visual space, the RF centers of neighboring electrodes were distinctly shifted, but their extended limits overlapped extensively (Figures 2B and S1A) (Note: As the relative RF center's separation between electrodes was similar in all experiments analyzed, visual space representation in the recorded area was near isotropic. However, for simplicity we will display responses and stimuli positions in visual space coordinates; transformation from one to the other can

be made assuming an approximate equivalence of 100-120 μm of tectal distance per 1 deg of visual angle[34]). The central response to the flashing spot had a relatively short delay (25-50 ms) and long duration (up to more than 200 ms) compared to the periphery, which triggered responses with increasing delays, up to more than 150 ms in the far periphery (Figures S1B and S1C).

The slow build-up of the peripheral response reveals a dual pattern of a horizontal propagation of activity that is manifested in the response pattern recorded by neighboring electrodes in the array. Figure 2C shows one recorded example in which the spot, presented near the center of the RF of electrode #12, triggers a sequence of bursts that lasts for nearly 300 ms. Recording sites nearby also recorded a sequence of bursting responses, each one aligned with those of the first site, but with increasing time lags and smaller amplitude the larger the recording distance. That is, each burst of the sequence seems to propagate radially as a horizontal wave, which we call a "burst-wave," that arises from a "source" at or near the electrode recording the burst with the shortest latency. Also, the first burst-wave only propagates to the nearby sites, but subsequent burst-waves propagate to longer distances, up to an area of about 20 deg in diameter, explaining the large size and long build up of the RFs mapped for each electrode (Figures 2B and S1B). A frame-by-frame representation of the horizontal propagation of two burst-waves (shown expanded in Figure 2D) is displayed in Figure 2E, and in a slow-motion video representing an entire recording (Video S1). This wave of expansion of bursting activity is clearly revealed by averaging frames across hundreds of bursts, after aligning their recording time-shifts from the beginning of each burst-wave (Figures 2F, 41 recordings as in Figure 2C from 4 pigeons).

When the burst delays of each burst-wave recorded by different electrodes were plotted as a function of the recording site distance from its estimated source (see

Methods), we found a linear relation (Figures 2G-2I), indicating that the burst-waves propagate at a near-constant, very fast speed (Average 1/speed ranging from 0.64 to 1.14 ms/deg in different pigeons (inset Figure 2I**)**, which corresponds to about 0.6 to 1.2 ms/100 μm of tectal surface). Burst-wave sources in response to a single flashing spot appeared at a regular pace, with a modal inter-source interval varying from 17 to 23 ms among 4 different pigeons (equivalent to 43 to 59 Hz). Although, on average, the position of the sources nearly coincided with the stimulus position, the sources usually started apart from the tectal site activated by the retinal input (Figure 2J). Part of this scattering is contributed by the discontinuous spatial sampling of the electrode array; however, numerous recordings distinctly showed burst-waves arising from electrodes away from the stimulated position (Note: The average values and ranges reported above for burst-wave spread, speed and source position were obtained across stimulus trials, and were statistically the same as those considering the trial as a factor; Wilcoxon Test, $p > 0.1$).

Ipc burst-waves track visual motion in a discontinuous fashion.

While a static spot produced a "blinking" pattern of burst-waves around the activated tectal site, a moving bright spot triggered a trail of burst-waves whose successive source positions shifted along and around the stimulated tectal path (Figures 3A and S2). A frame-by-frame representation of the burst-waves, marked with asterisks in Figure 3A, shows the expanding pattern of each burst-wave and the changing position of successive sources (Figures 3B and Video S2). From each source, burst-waves expanded at a constant speed with an average slope ranging from 0.7 - 1.8 ms/deg, (Figure 3C), slightly higher than that measured in the same pigeons using a

static spot (median: 0.99, IQR: 0.82 ms/deg for moving spot vs 0.84, IQR: 0.53 ms/deg for static spot, Wilcoxon Test, p = 0.0002). The tracking was discontinuous, as successive burst-wave sources appeared at a new place along the trail, after the previous burst-wave was completed. Therefore, with few possible exceptions, all bursts recorded at any given time appear to originate from a single source. This is shown in Figure 3D in which the normalized probability of recording simultaneous bursts (not source points to avoid any bias of the source's detection) by electrodes separated by more than 10 deg was near zero. The sources appear at a relatively constant pace, with modal intervals ranging from 35 to 50 ms (corresponding to 20 to 30 Hz) across trials (Inset Figure 3D), significantly lower than the "blinking" rate triggered by the static spot measured in the same pigeons (Kruskal Wallis, with pairwise post-hoc Wilcoxon test and Bonferroni correction, $P < e^{-16}$).

Burst-wave sources appear around the tectal representation of moving stimuli

The sources tended to appear along the moving spot path, but as in the case of static stimulation, the source position varied considerably with respect to the stimulus, especially in the axis orthogonal to the direction of motion (Figures 4A and 4B).

A moving bar elicited sources appearing across tectal positions activated by the bar's longer axis, thus distributing widely in the vertical axis compared to a moving spot (Fligner-Killeen Test for variance difference was significant in two pigeons tested, $P < 4.3 \times e^{-10,}$ and in all three pigeons after removing outliers, $P < 3.99 \times e^{-7}$)(Figures 4D and 4E; Video S3). Nonetheless, correlations of source position vs stimulus position in the movement direction axis (Figures 4C and 4F) showed that on average the sources

followed closely the stimulus movement, and, for both moving spots and bars, the sources kept a slight, but significant tendency to appear ahead of the stimulus position.

When a looming stimulus was presented, the evoked sources tended to occur within or near the edges of the expanding circle (Figure 4G; Video S4), although the position of successive sources could change in a seemingly random fashion to different locations of the expanding disk. Accordingly, the average radius of appearing sources increased as the disc expanded (Figure 4H). As in previous cases, only single sources of burst-waves occurred at any given time, and the probability of finding simultaneous sources or bursts beyond 10 deg tended to zero (Inset Figure 4H).

Burst-wave sources alternate positions during tracking of competing stimuli

To investigate the spatiotemporal re-entrant pattern under stimulus competition, two bright spots were presented sequentially in the visual field. The first bright spot elicited a series of burst-wave sources following the tectal stimulus path, but when the second spot was presented, sources shifted to the tectal location corresponding to the second stimulus, while disappearing at the first location. When the source positions were represented on a heat map two separate clusters could be observed, each one around the corresponding stimulus path (Figures 5A and 5B). Similarly, a hierarchical cluster analysis of the relative position of the sources with respect to the stimuli showed two separate clusters dispersed around the corresponding stimulus (Figure S3). There was no indication of merging of sources' locations, as sources elicited by the first stimulus before competition fall within the same cluster defined for this stimulus during competition.

Raster displays of the sources during competition showed that sources could appear around the second position for hundreds of ms before appearing back in the first position. Also, the sources could shift back and forth between the two stimulus paths in alternating fashion (Figures 5C and 5D). Sources did not sweep the space between stimuli nor cross the gap in small steps, but virtually jumped back and forth (Video S5). Despite the presence of two different stimuli, the probability of finding near-simultaneous sources (Figure 5E) or near-simultaneous bursts beyond 10 deg separation (Figure 5F), both tended to zero, verifying that a single source was present at any given time. Furthermore, the median of the inter-source interval during spot competition was similar to that obtained during stimulation with a single moving stimulus (spot, bar and looming; Pairwise Wilcoxon Test with Bonferroni correction, $P > 0.5$, except for one pigeon in which the median ISI for the moving spot stimulation was even larger during competition; Pairwise Wilcoxon Test with Bonferroni correction, $P < 9.8\ e^{-7}$), reinforcing the finding that despite the presence of two stimuli a single burst-wave scans the tectum at a high but fairly constant frequency. A shorter inter-source interval median (indicating higher blinking frequency) was observed only for static stimulation, compared to moving and competing stimulation (Pairwise Wilcoxon Test with Bonferroni correction, $P < 2e^{-16}$; Figure 5 F).

The blinking nature of the burst-waves and their fast scanning of the activated tectal region is best visualized when the process is displayed at its actual velocity. In video S6, burst-wave sources with circles representing the maximum wave expansion, both derived from sample records, are loop-played in real time. The spotlight representing the lpc re-entry keeps a nearly constant, very fast rhythm as it shifts around the stimulated tectal surface (Note that we are representing stimuli and responses in visual space coordinates, but both would be somewhat distorted if

represented in tectal coordinates).

Similar burst-wave responses are recorded in awake pigeons

Finally, to verify that the described phenomena were not the consequence of an abnormal condition produced by anesthesia, which may enhance synchrony and reverberant activity, we repeated these experiments in two head-fixed, awake pigeons. Although in this condition, increased spike activity and the presence of eye movements hampered a detailed analysis of stimulus-evoked bursting responses, in both birds we found a pattern similar to that observed in the anesthetized animal (Figures 6A and 6B). Specifically, identifiable bursts were organized in burst-waves spreading from one source (Figure 6C), which in cases of moving stimuli, shifted positions along the stimulus track (Figure 6D). As in the anesthetized condition, only single sources of burst seem to occur at any given time, and the probability of finding simultaneous bursts at distances longer than 10 deg tended to zero (Figure 6E).

Discussion

Recording the spatio-temporal activity pattern of re-entrant axons revealed new phenomena indiscernible with single recordings. We showed that the Ipc re-entry to TeO takes the form of fast, reverberant waves of bursting activity which, arising from single source locations, rapidly invade the stimulated tectal site. A moving target triggered source sequences that shifted around the stimulus position in the tectal representation of visual space, following its trajectory. In cases of large stimuli, the sources appeared, one at a time, at different positions within and near the borders of the stimulus, and during stimulus competition they alternated between stimulated locations. Altogether,

these phenomena seem to reveal at the first synaptic relay of the retino-tectal input a "blinking spotlight" which, operating at a frequency of 20-50 Hz, scans tectal locations stimulated by transient and moving visual features (Video S6).

Although most of the presented results were obtained in anesthetized animals, we showed that the same phenomenon is manifested in awake, head fixed pigeons. Nevertheless, a future challenge is to fully characterize the burst-wave dynamics in free behaving animals with an accurate control of gaze and stimulus positions, as the active searching behavior, including eyes and head saccades, is presumably coordinated with the Ipc re-entry.

The Ipc axon terminals are arranged in vertical columns that orderly tile the tectal surface (Figures 1A and 1B)[17]. Each expanding burst-wave must, therefore, be produced by axons that fire bursts with longer delays the further their location from the initial source[19]. This phenomenon presumably resulted from the recurrent activation of the shepherd crook-Ipc neuronal loops, which due to the horizontal dispersion of the recurrent connections, progressively invades neighboring loops[27].

Previous results from our lab have shown that the Ipc axons exert a gating/boosting effect on the tectofugal transmission by making synaptic contacts upon the "bottlebrush" dendritic specializations of the TGCs: the tectal neurons that project to the nucleus rotundus in the thalamus[20,28,35]. The bottlebrushes of different TGC types are bi-dimensionally distributed in a single tectal layer, specific for each type[17,35-39]; TGCs are only activated by transient visual stimulation especially object motion[40,41], and their responses cannot be transmitted to the thalamus if the Ipc re-entry is blocked[20,28]. This gating/boosting of the retinal input is fast to the extent that the visual responses at the rotundus and the pallium oscillate in synchrony with the Ipc re-entrant bursts[28]. By

sweeping a relatively large tectal area (2 mm in diameter), burst-waves might boost the transmission of retinal inputs at locations removed from the source loci.

It was frequently observed that the visually evoked sources appeared at considerable distances from the stimulus position, especially in the vertical axis in the case of horizontally moving spots and bars. In accordance with the restricted ramifications of the retinal axon terminals[42], retinal spike activity triggered by e.g. 1 deg spot is confined to tectal locations no wider than two hundred microns and could not directly activate Shc dendrites further away than a couple of deg. It is possible that tectal horizontal connections propagate retinal activity to ignite more distant Shc/Ipc loops. Additionally, top-down signals transmitted to the Shc, presumably from the motor pallium[31,43] and the basal ganglia[44], or the widespread GABAergic inhibition from Imc, could facilitate the feedback ignition at locations different from those receiving direct retinal stimulation. In any case, in order to have a deeper understanding of this phenomenon, it would be necessary to know the spatial-temporal profile of the incoming retinal spike activity during each stimulus condition.

It is noteworthy that a transient spot triggered a series of burst-waves from sources appearing at higher frequencies around the stimulus location, while a moving target elicited an orderly sequence of burst-wave sources that tracked the trajectory of the stimulus at a lower pace. This indicates that far from being the sequential addition of transiently elicited responses, the Ipc re-entry to moving targets is presumably shaped by substantial interactions between the activated tectal sites. Whether the higher scanning frequency triggered by a transient spot relates to assigning a high priority to suddenly appearing stimuli is an interesting possibility. Importantly, there was a single tracking source of burst-waves at any given time that shifted between the tectal area activated by larger stimuli, like the moving bar and the looming circle, and in cases in

which two stimuli were present, the source shifted between stimulus locations. By and large, this dynamic is the consequence of the neural architecture of the isthmo-tectal circuitry, which promotes antagonistic interactions between activated Ipc locations[18,20,28,30,45-47]. Previous studies have shown that the Imc mediates this mutual inhibition between simultaneously activated Ipc-tectal loci[20,30]. Ipc and Imc neurons are innervated by collaterals of the same Shc neurons, and Imc neurons could fire in alternating bursts or in a sustained fashion when activated by moving stimuli[27]. These two firing regimes would be related to the suppression patterns we observed during stimulus competition, in which at times one source completely suppressed the other, or both engaged in alternate suppression, presumably allowing asynchronous transmission of both inputs[27].

The optic tectum is homologous to the superior colliculus of mammals, a structure strongly involved in the control of spatial attention[48-52]. In all vertebrates, the TeO participates in orienting behaviors, either towards the stimulus, such in prey catching maneuvers, or away from it, in predator avoidance[53-55]. Stimulus selection is critical to both behaviors, and a spotlight mechanism to implement such selection may have co-evolved with the tectal control of spatial attention. The isthmotectal system is highly conserved in sauropsids, and the characteristics here described in the pigeon are presumably accurate for turtles, lizards and crocodiles[46,56].

TGC neurons are highly conserved also, as neurons with identical morphology, physiological properties and central projections are characteristic of the superficial layers of the SC of mammals[40,50,57]. It is unknown whether the mammalian TGCs receive the synaptic contact of parabigeminal axons, the presumptive homologue of the Ipc nucleus[58]. However, in the mouse, the TGCs are strongly modulated by direct synaptic input from V1 neurons[59-62]. They might also be modulated by re-entrant top-down

projections from the posterior temporal cortex, the specialized cortex that receives the TGC output via the caudal pulvinar (Pulc)[57,58,63-68].

In light of the present results, it is possible that re-entry either from the PBg, V1 or TP generates a blinking spotlight upon the TGC dendrites, provoking a discontinuous and selective transmission of the retinal input to the Pulc. Recent behavioral and chemo-lesion experiments in mice suggest that the TGCs are involved in both defensive and orienting behaviors, perhaps as carriers of fast attention signals[69]. Future studies in mammals should be directed to this highly conserved tectofugal pathway in comparison to birds.

Several studies have led to the notion that spatial attention is comparable to a perceptual spotlight that scans internal representations of the visual scene[70-74]. Current evidence in humans and other primates suggests that this perceptual spotlight is not continuous but seems to operate in a "blinking" fashion, even during sustained attention to a single stimulus[75-80]. Furthermore, it has been shown that perceptual sampling during attention is not restricted to the cued location but also spreads to other parts of the same object, much like a "propagating wave"[78]. Some of these properties have been sought in neural correlates of spatial attention, which are generally manifested as modulations of neural responses in multiple cortical and subcortical structures, such that attended stimuli acquire an increased neural representation[25,48,49,81]. In the cortex, some of these modulations are assumed to be effected by re-entrant projections that cascade from high cortical areas, especially frontal and parietal cortices, to earlier areas[82-84]. In addition, studies have shown that top-down modulations are phase-locked to brain rhythms, linking attention signals to the discrete parsing of perception[75,80,85-90]. All in all, to our knowledge, a true correlate of a blinking spotlight such as the one here described in the avian tectum has never been reported in other brain area in any vertebrate

species. As the Ipc re-entry gates/boosts the tectofugal transmission, the link between the blinking spotlight, the thalamo-telencephalic rhythms recorded in this pathway[28] and the parsing of perception is straightforward. The blinking burst-waves would transmit the incoming "visual image" in a sequential and piecemeal fashion to higher tectofugal areas, which lack retinotopic organization[39,43,66]. The induced rhythm might facilitate the propagation of the selected activity promoting large-scale neural interactions underlying an organized behavioral response. The single character of the blinking spotlight jumping across the borders of a moving object, without visiting a competing one, would help feature binding and the initial segmentation of the visual scene, which could be refined by recurrent top-down interactions governed by the executed behavior and the animal's previous experience. It is noteworthy that distributed thalamic and pallial rhythms might be so strongly associated with a highly structured re-entrant process operating at a sub-pallial level. In any case, whether the dynamics of this focal re-entry is part of a stimulus selection mechanism and the parsing of perception, or is indeed linked to how attention is deployed, should be investigated in animals behaving under controlled conditions.

The present findings benefitted from both the clear signature of the Ipc re-entrant signals, which permitted their selective recording, and the outstanding bi-dimensional array of the reentrant axons, which exposed the signals' stereotyped spatiotemporal pattern. Analogous re-entrant patterns might be hidden in less bi-dimensionally-organized topographies. Re-entry might not always take the form of rhythmic expanding waves of activity, but presumably is never chaotic or disorganized. Grasping the spatial-temporal characteristics in different neural structures is crucial to understand brain signal processing and will support further development of artificial neural networks with recurrent architectures.

ACKNOWLEDGEMENTS: We thank Diane Greenstein for editorial assistance, Zion Huidobro for the graphical abstract painting and Victoria Onate for valuable help with the data analysis. This work was funded by FONDECYT Grants: 1210169, 1151432 and 1210069.

AUTHOR CONTRIBUTIONS: B.R., J.C.L., J.M. and G.J.M designed the study. B.R, C.M. and G.J.M. conducted all the experiments. B.R analysed the data. C.M. performed the statistical tests. G.J.M and B.R. wrote the manuscript with contributions from all authors.

DECLARATION OF INTERESTS: The authors declare no competing interests.

INCLUSION AND DIVERSITY STATEMENT: We support diverse, inclusive and equitable conduct of research.

Figures

Figure 1. The isthmo-tectal circuit and the recording of bursting responses from Ipc axons

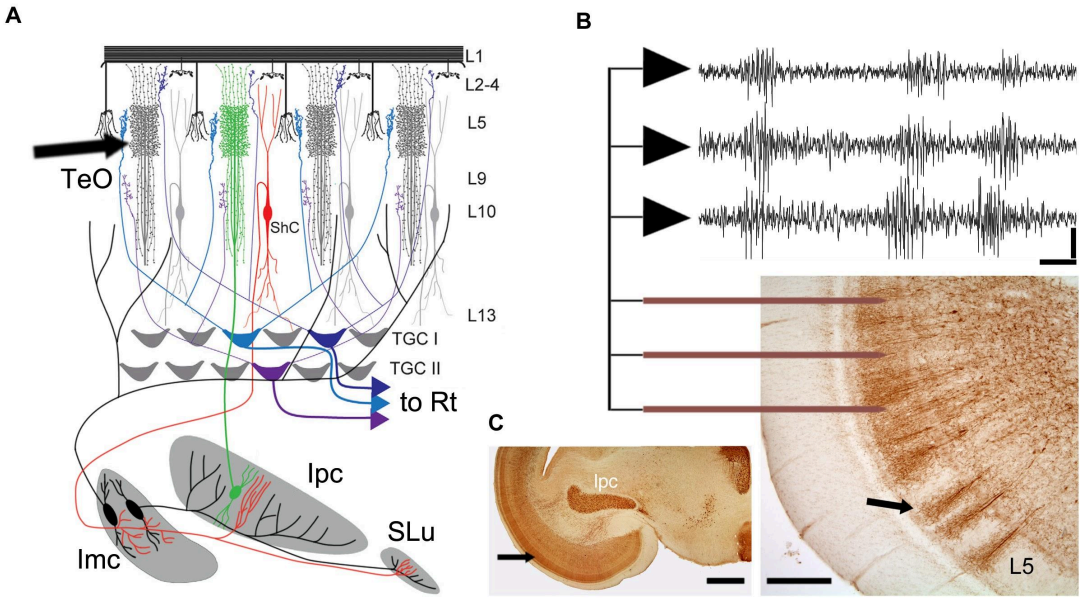

A, Schematic of the isthmotectal network representing a coronal view of the tectum (TeO, tectal layers from L1 to L13)) and the re-entrant axons from Ipc. A focal retinal input is transmitted by shepherd's crook neurons to the isthmic nuclei activating a zone (in red) in Ipc, Imc and SLu. The Ipc returns activity back to TeO via columnar axons (one marked in green) that terminate around the same locus that originates the input. Ipc axon terminal activity gates/boosts the retinal input to tectal ganglion cell (TGCs) dendrites (in blue) and thus the input transmission to the n. rotundus (Rt) in the thalamus. Imc neurons generate wide-field inhibition across complementary regions of the tectum, Ipc and SLu (Adapted from Garrido-Charad et al (2018)[27], based on Wang et al., 2006)[17]. **B,** Schematic of the recording method representing 3 microelectrodes inserted in the tectal layers where Ipc axons terminate, and a sample of multiunit

bursting responses recorded from these axons. The photomicrograph corresponds to part of a coronal tectal section immuno-reacted against choline acetyltransferase (ChAT), showing individual labeled Ipc axons (arrow). **C**, Similar immuno-reacted coronal section at lower magnification showing that the labeled Ipc axons form a continuous layer (arrow) across the entire tectum. Scale bars: **B**, 300 μm, 10 ms, 100 μV; **C**, 1mm. Imc, n. isthmi magnocelularis; Ipc, n. isthmi parvocelularis; TeO, optic tectum. SLu, n. isthmi semilunaris.

Figure 2. Ipc re-entrant signals propagate as horizontal radial waves of burst activity on the tectal visual map

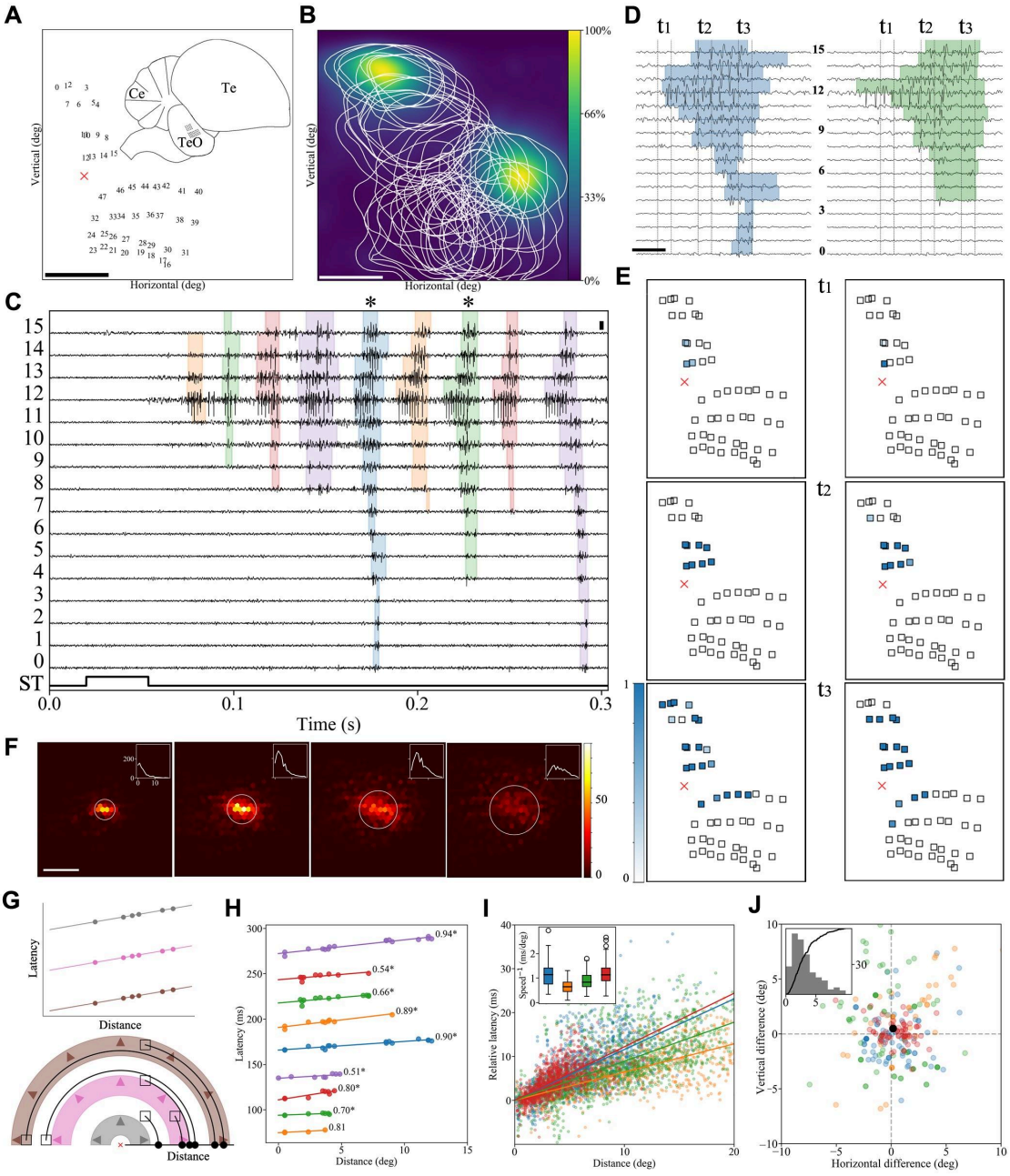

A, Schematic of the relative position of the RF centers of bursting responses recorded by two arrays of electrodes (4x4 and 4x8), numbered from 0 to 47, inserted in the optic

tectum as represented in the inset (scale bar, 10 deg). **B**, Heat map of the RFs of the bursting responses recorded by two of the electrodes and contour maps of all RFs recorded by the two arrays. **C**, Sequence of burst responses elicited by a bright spot (0.7 deg, 16-32 ms, bottom trace) flashed near the RF center of electrode 12 (marked with an x in **A**); burst responses recorded by contiguous electrodes in a near coincident time period (burst-waves) are colored equally (bursts recorded by electrodes of the bottom array were not included). **D**, Expanded view of recording traces of burst-waves 5 and 7 (*) of the sequence (scale bar: 5 ms). **E**, Frame by frame representation of the radial expansion of burst activity of burst-waves 5 (left column) and 7 (right column) recorded by each electrode in 2 ms frames separated by 6 ms (dotted lines in **D**). Blue scale: fraction of the 2 ms window containing a burst response; x: stimulation site. **F**, 2D histogram that pools the expanding activity of burst-waves aligned at the burst source (48 multi-electrode recordings in 4 pigeons (0.5 ms windows, separated by 2 ms; scale bar 10 deg). **F inset,** radial density of responses. **G**, Bottom: Schematic of a model predicting the burst latency vs recording distance relation of three successive burst-waves represented by colored semicircular arcs, which propagate linearly and radially from the origin of the wave; empty squares represent the position of the electrodes recording the successive burst-waves; Top: Model prediction of the relation between latency and distance to the source for the three burst-waves. **H**, Latency vs recording distance-to-the-source relation, with the linear regressions for each burst-wave recorded in (**C**) using the same color code (numbers and asterisks are R^2 and significance ($P < 0.05$) of linear regressions). **I,** Latency vs recording distance from source (1/speed) relation of 240 burst waves recorded in 4 pigeons (represented by different colors in this and the following figures). Lines represent the average slope of individual burst-wave linear regressions aligned at intercept zero; **I inset** displays the

slope's distribution of burst-waves for each pigeon (The median slope was significantly higher than zero in all pigeons, Wilconxon Test $p < 3.6 \times e^{-12}$). **J**, Scatter plot of the differences between the source location (defined as average position of the three electrodes with the shortest latencies) of the burst-waves and the location of the visual stimulus; Sources cluster around the stimulated position (x,y average difference marked by black dot = 0.17,0.49 deg), although the spread was considerable (σ_x=6.8 deg, σ_y=8.7 deg, data from 4 pigeons). **J inset,** radial distribution (bars) and cumulative density (curve) of the sources' distance in deg to the stimulus (P_{95} = 7.5 deg). See also Figure S1, Videos S1 and S6, and Table S1.

Figure 3. Ipc burst-waves track visual motion in a discontinuous fashion

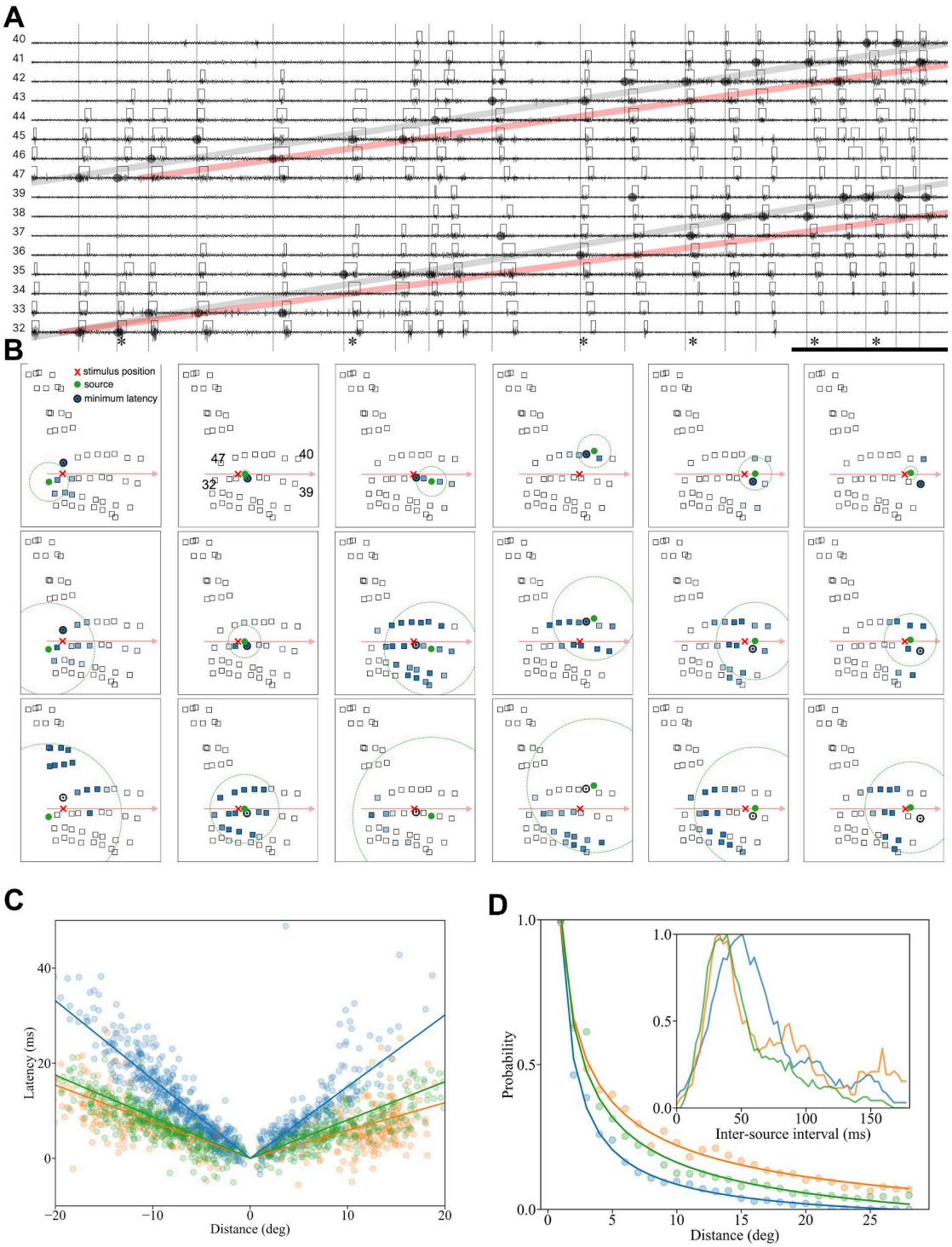

A, Burst responses recorded by 16 electrodes (same disposition as in Figure 2), in response to a bright spot (0.7 deg. 12 deg/sec) moving in the forward direction. The moving trajectory with respect to the RF center position of each electrode is represented in visual space coordinates as shown in **B** and Figure S2. The spot sweeps the screen passing between the RF centers rows of electrodes 32 to 39 and 47 to 40. Brackets mark the beginning and end of individual bursts; gray dots: beginning of the shortest latency burst recording (source) for each burst-wave; gray band: linear regression of the source locations vs time; orange band stimulus position vs time for each electrode row. Scale bar: 200 ms. **B,** Frame by frame representation of burst-waves, arranged vertically, to represent the horizontal expansion of individual burst-waves (marked with asterisks in **A**) in time windows as in Figure 2E; x: stimulus position in each frame**;** circles with black dot: minimum latency electrode; green dots: most probable origin of each burst-wave, (see Methods). The circle denotes the wave front according to the radial expansion speed of each burst. Note in the succession of top frames of each individual column that the burst sources shift their position towards the current position of the moving stimulus. **C,** Relation between burst latency and electrode distance to the source showing burst propagation in 3 pigeons (The linear model was significant and the average slope was higher than zero in all pigeons, $F = 186.7$, $P = 2{,}2 \times e^{-16}$); positive and negative distance values represent forward and backward propagation, respectively. **D**, Normalized probability of burst starting simultaneously, within a 5 ms window, vs distance in 3 pigeons. **D inset,** Inter-source interval distribution for three pigeons; the modal value ranges between 35 and 50 ms (corresponding to 20 to 30 Hz). See also Figure S2, Videos S2 and S6, and Table S1.

Figure 4. Burst-wave sources appear around the tectal representation of moving stimuli

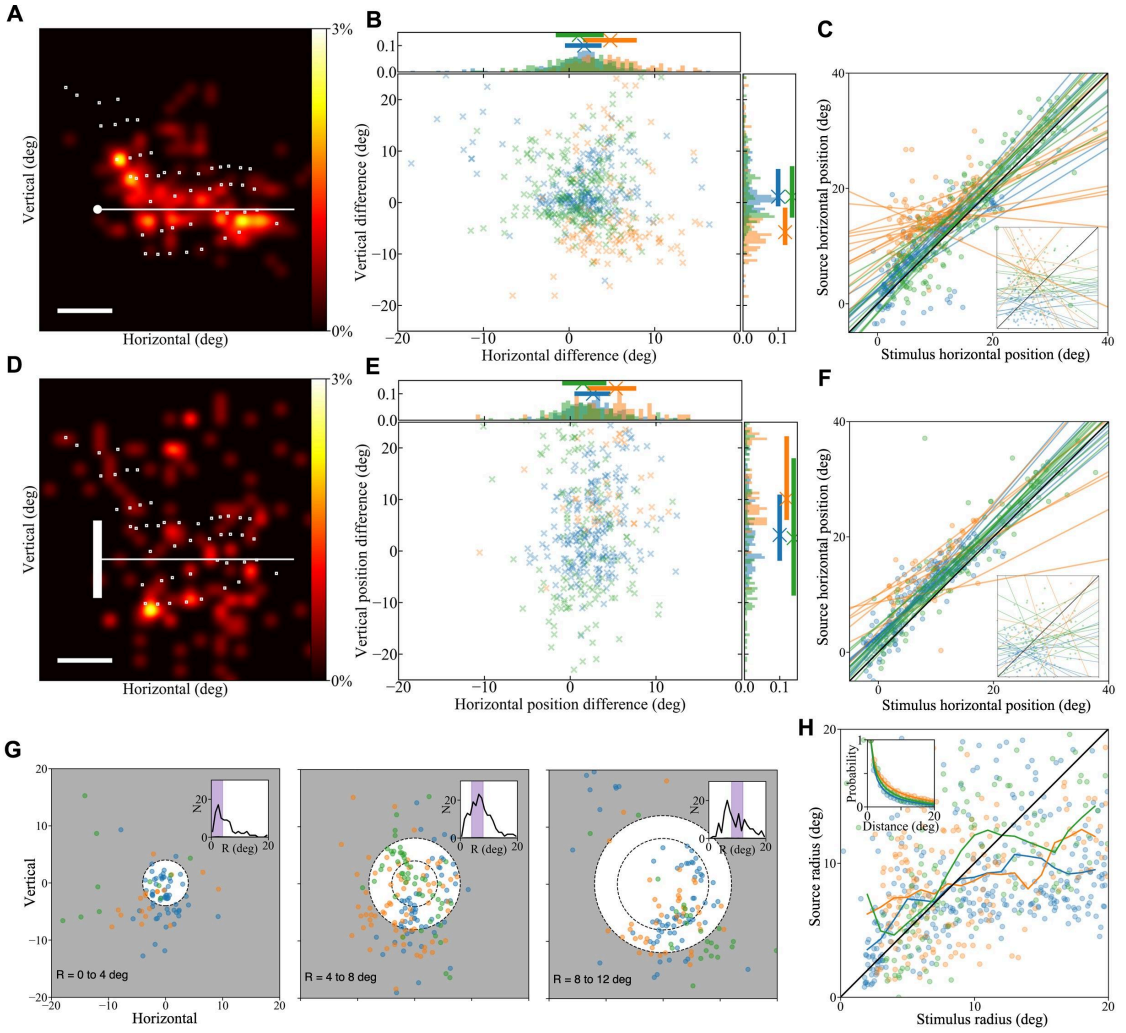

A,D, Heat map representations showing the accumulated burst-wave source density after 10 consecutive sweeps of a 1.5 deg bright spot (**A**) and a 15 deg-long bright bar (**D**) moved at 28 deg/sec in one pigeon; white dots: electrode grid; heat map scale normalized to the total response. **B,E,** scatter plot and histograms representing the spread of the sources with respect to the center of the spot (**B**) and the bar (**E**) along the moving axis (x) and across the moving axis (y) in three pigeons (different colors).

The distribution along the y axis is wider in the moving bar than in the moving spot (Fligner-Killen Test for variance was significant in two pigeons, $P < 4.3 \times e^{-10}$, and in all three pigeons after removing outliers, $P < 3.99 \times e^{-7}$), whereas the distribution along the x axis is not different in both stimulus (Fligner-Killen Test, $P > 0.1$). **C,F,** Scatter plots showing the correlation between the horizontal axes values of the burst-wave sources' position and the position of the moving spot and bar, respectively. Lines represent the linear regressions of individual trials (The median slope for each pigeon was significantly higher than zero, Wilcoxon Test, $p < 0.0016$ for both stimuli, and in two pigeons it was not significantly different from one, Wilcoxon Test, spot $p > 0.23$, bar $p > 0.63$). The insets in (**C**,**F)** correspond to the linear regressions of individual trials using sources calculated after shuffling the electrode numbers (Median not significantly different from zero in all conditions, Wilcoxon test, spot $p > 0.2$, bar $p> 0.77$). The intercept of the linear regressions reveals that the sources tend to appear slightly ahead of the stimulus for static and moving stimuli (median advance for spot: 1,4 - 11.2 and was significant larger than zero in two pigeons, Wilcoxon Test, $P < 0.006$; median advance for bar: 1.8 - 8.7 deg, Wilcoxon Test, $P < 0.02$ in the three pigeons). **G**, Distribution of the burst-wave sources in response to ten repetitions of a looming stimulus (bright disc, increasing radius from 0 to 12 deg in 0.5-1 sec) in 3 pigeons. The annulus on each panel indicates the interval covered by the stimulus expansion at which the wave sources were mapped. **G inset**, Radial distribution of the sources for each panel; the band represents the stimulus diameter interval. **H**, Scatter plot showing that the sources' radial position increases with the stimulus radius**.** Lines represent the average source radius vs stimulus radius in 3 deg windows. **H inset,** Normalized probability of burst starting simultaneously, within a 5 ms window, vs distance. See also Videos S3, S4 and S6 and Table S1.

Figure 5. Burst-wave sources alternate positions during tracking of competing stimuli

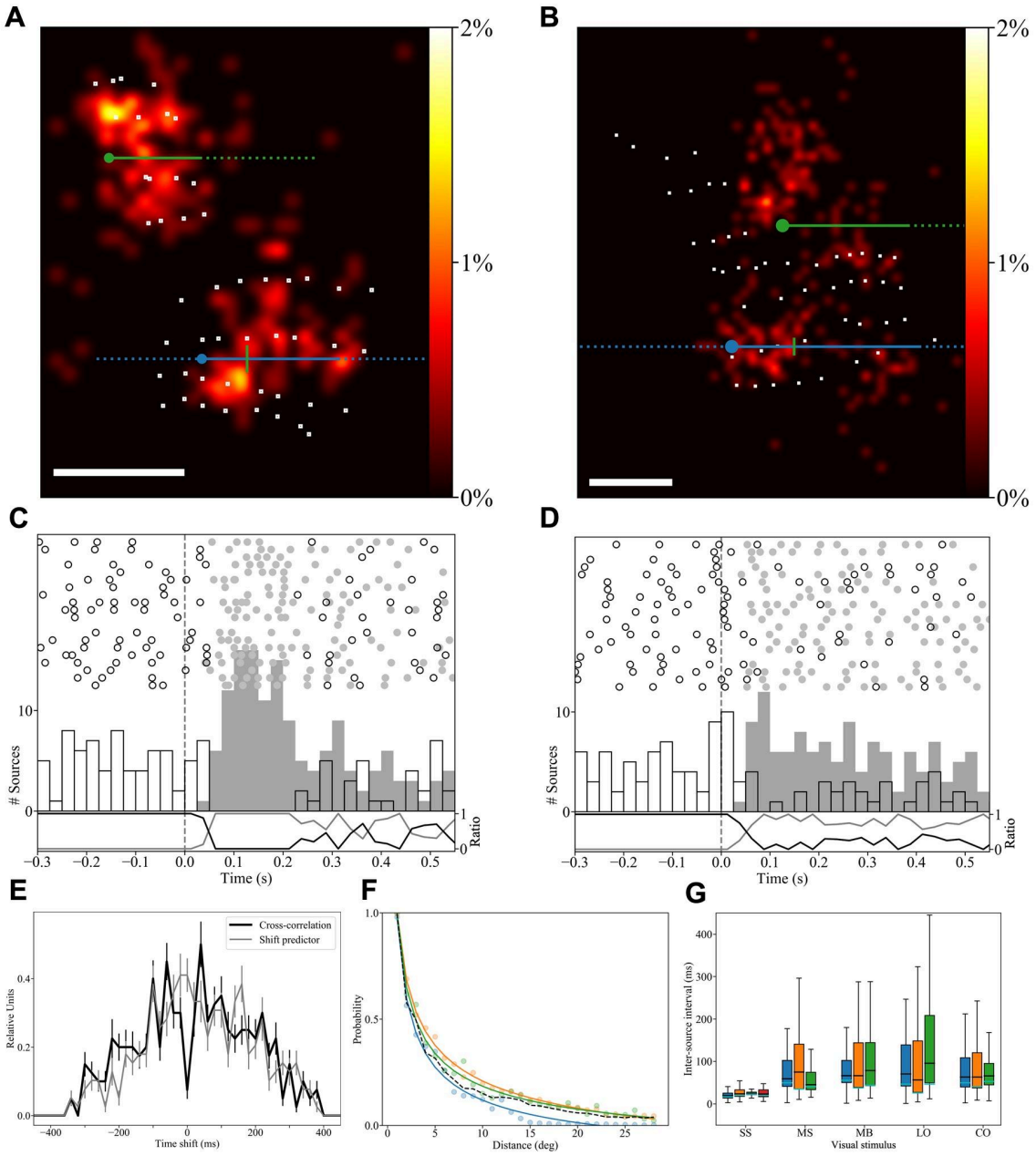

A,B, Heat maps representing the position in visual coordinates of burst-wave sources in

response to 2 bright spots (2 deg) moving sequentially on the visual monitor in two pigeons (white dots: electrodes grid, heat map scale normalized to the total response). The sources were computed in 20 trial repetitions when the stimuli swept the parts of the screen marked with continuous color lines; the marks on the lower stimulus tracks indicate the position of the lower stimuli when the upper stimuli appeared and started to move. **C,D**, Raster plots with cumulative histograms representing the sources' time for each stimulus repetition. The raster plots were aligned at the time of the second stimuli movement (dotted line). By means of a hierarchical cluster analysis using the relative distance between the source and the stimulus as a variable (**Figure S3**), sources were assigned to the respective top (empty dots) or bottom (gray dots) stimulus. Traces below each raster represent the reciprocal ratio of histogram bars' sizes across time. Note that the burst-wave sources alternate in slow (**C**) or rapid (**D**) succession between the two stimuli when both stimuli are present. **E**, Average cross-correlogram between sources' times of each stimulus during competition for three pigeons (error bars: standard error b; minimum value at zero delay non different from zero, Wilcoxon test, $p > 0.35$; gray trace, shift predictor correlogram, value at zero delay significantly higher than zero, Wilcoxon test, $p < 0.04$). **F**, Normalized probability of burst starting simultaneously during competition, within a 5 ms window, vs distance in 3 pigeons. Even when there were two stimuli present, the probability of finding simultaneous bursts has the same decay as when only one stimulus was present (dark line, average from single spot stimulation for the same pigeons). **G,** Box plot representing the distribution of inter-source intervals (ISI) for a static spot (SS), moving spot (MS), moving bar (MB), looming (LO) and competition (CO); black line: median, cyan line: mode. See also Figure S3, Videos S5 and S6, and Table S1.

Figure 6. Similar burst-wave responses are recorded in awake pigeons

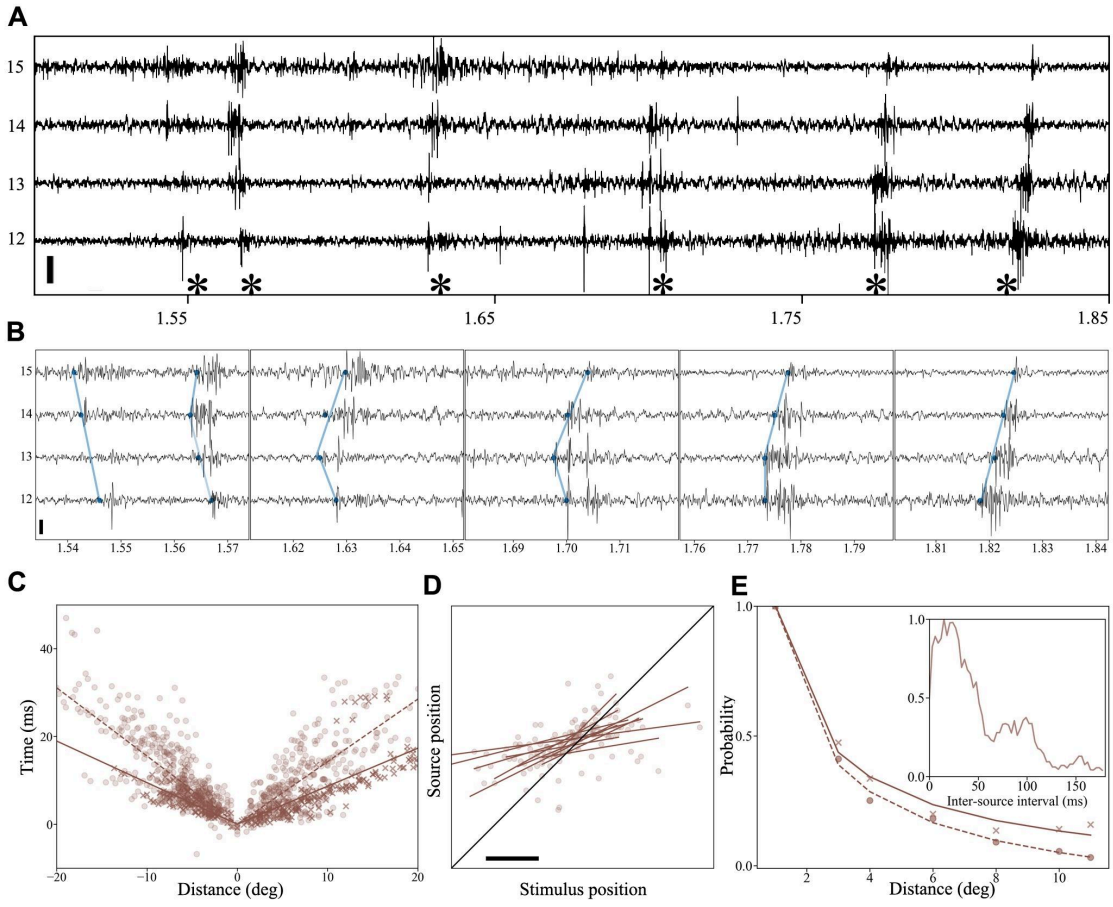

A, Sample recording of bursting responses to a moving bar, of four electrodes (numbered from 12 to 15) from a 16-electrode array in an awake pigeon. Bursting responses in neighboring electrodes follow similar burst-wave patterns as found in anesthetized pigeons. **B**, 40 ms recording expansions of the five bursts marked with asterisks in (**A**); Dots: beginning of bursts; lines: linear regression of position vs time of the marked dots using the shortest latency point as the first point. The shortest latency burst (signaling the source of the burst-wave) shifts position from the electrode #15 to

the electrode #12 as the bars move from left to right. **C**, Relation of burst latency vs electrode distance to the source, showing the burst-wave pattern after 10 stimulus repetitions of a 20 ms bright spot (crosses) and a moving bar (circles); slopes of individual burst-waves were all significantly higher than zero and the median slope for the moving bar was higher than for the static spot (1,5 vs 0.9 ms/deg, Kruskal Wallis test, $P < e^{-16}$. **D**, Correlation between the horizontal axes values of the burst-wave sources and of the moving bar for forward motion; Lines correspond to linear regressions of source positions vs stimulus position obtained in individual sweeps. Although eye movements impaired an accurate determination of both the RF center positions for each electrode and the relative trajectory of the stimulus, there is a clear tendency for the estimated burst-wave sources to follow the stimulus trajectory (Slope's median was significantly higher than zero, Wilcoxon test, P = 0.002). **E**, Normalized probability of bursts starting within a 5 ms window vs electrode distance, after a moving bar stimulation. Calibration bars: **A,B,** 100 μV; **D,** 10 deg.

Figure S1. Spatial-temporal characteristics of burst receptive fields.

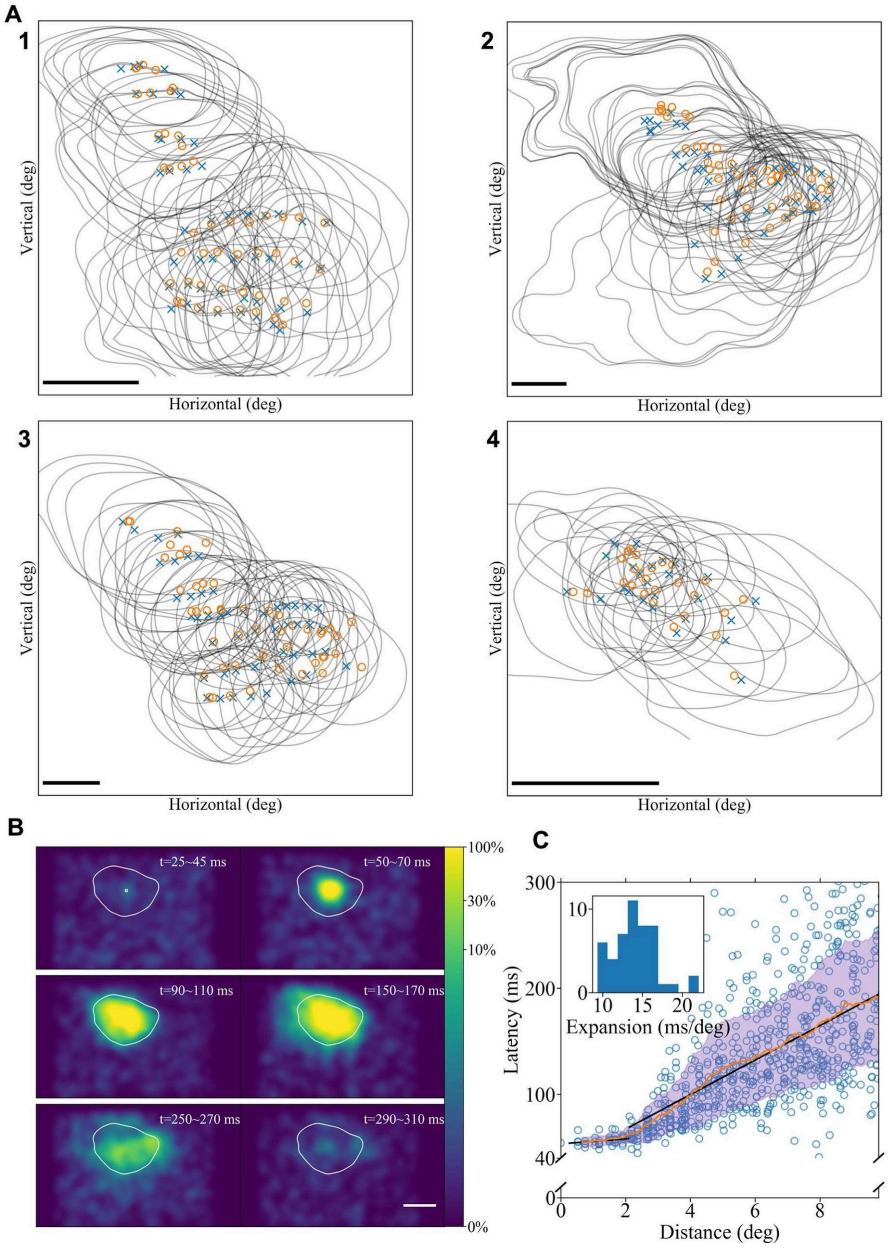

A1-A4, RF contour maps and defined center of the bursting-response RFs recorded by each electrode of the electrode arrays in four pigeons; The centers of the bursting RFs (x) tend to coincide with the centers of the retinal LFP (o) as expected by the homotopic reciprocal projection between Ipc and TeO. **B**, Heat map representing the bursting RF

recorded by one electrode, measured at different time frames from the stimulus onset presented at different positions. Responses from the periphery are recruited at increasing time-shifts with respect to the central responses, which also last longer. **C**, Latency of the bursting responses vs distance of the stimulus for one recording electrode. Responses from the RF center had a relatively short delay (40-50 ms) compared to the periphery, which triggered responses with increasing delays, up to more than 150 ms in the far periphery; **C inset,** distribution of slope values for the linear regression obtained for all electrodes in one experiment. Calibration bar: **A**, 10 deg.

Figure S2. Trace recording expansions of burst-waves tracking a moving stimulus.

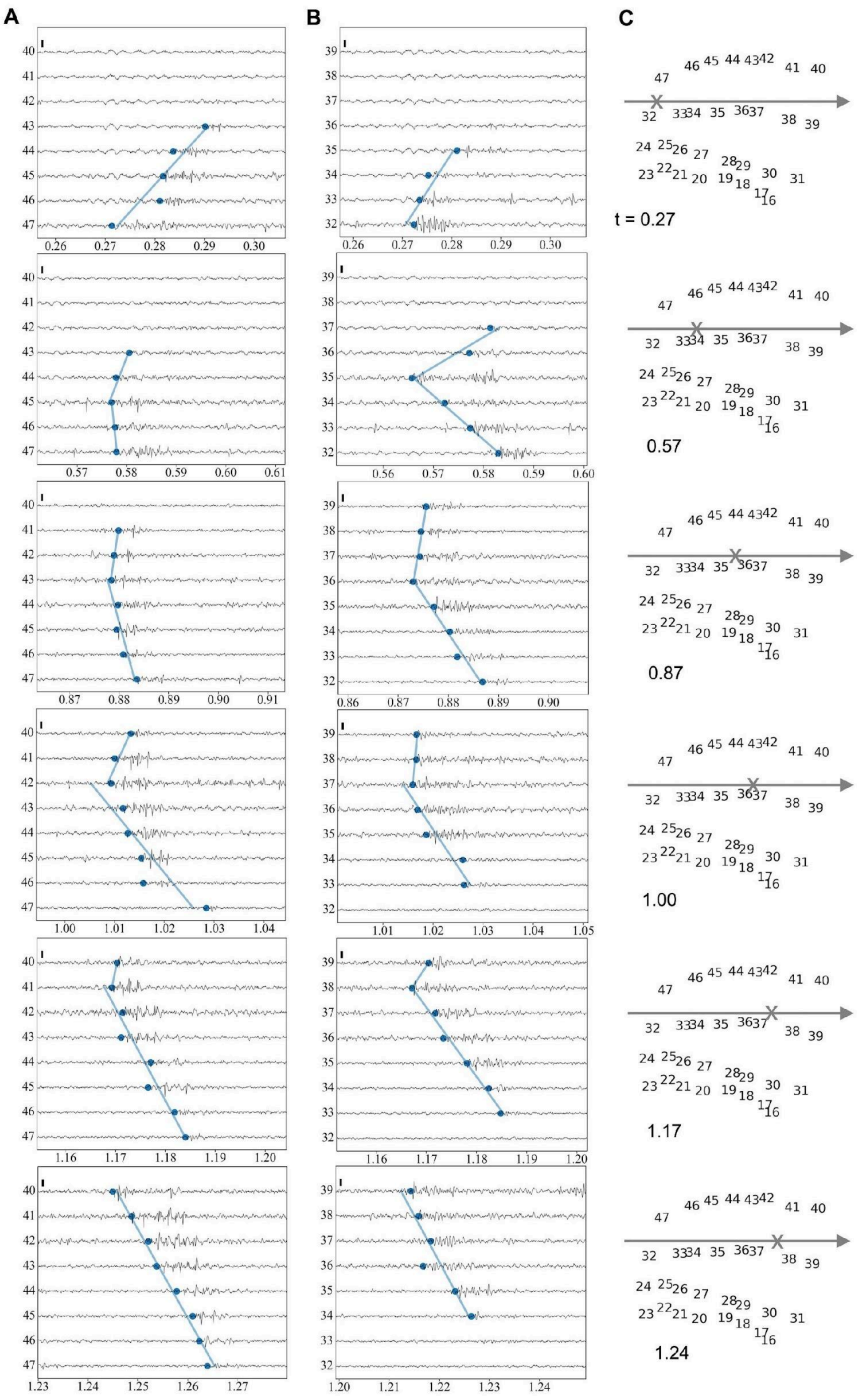

A,B, From top to bottom, 50 ms recording expansions of the six burst-waves marked with asterisks in Figure 3; **A**, corresponds to recordings of electrode row 47 to 40 and **B** to electrode row 32 to 39. Blue dots on each burst mark its beginning; lines correspond to the linear regression of position vs time of the marked dots using the shortest latency point as the first point. **C,** RF center configuration of the electrode array in coordinates of visual space showing the stimulus trajectory (arrow), position (X) and time (in sec, from beginning of motion). Note that as the stimulus moves to the right, the electrode recording the shortest latency burst in each row also shifts to the right, and the increasing time lags for neighboring electrodes reveal burst-waves expanding linearly from a source, in forward and backward directions. Calibration bar: 100 μV.

Figure S3. The burst-wave sources elicited during two-stimulus competition form two clusters around each stimulus

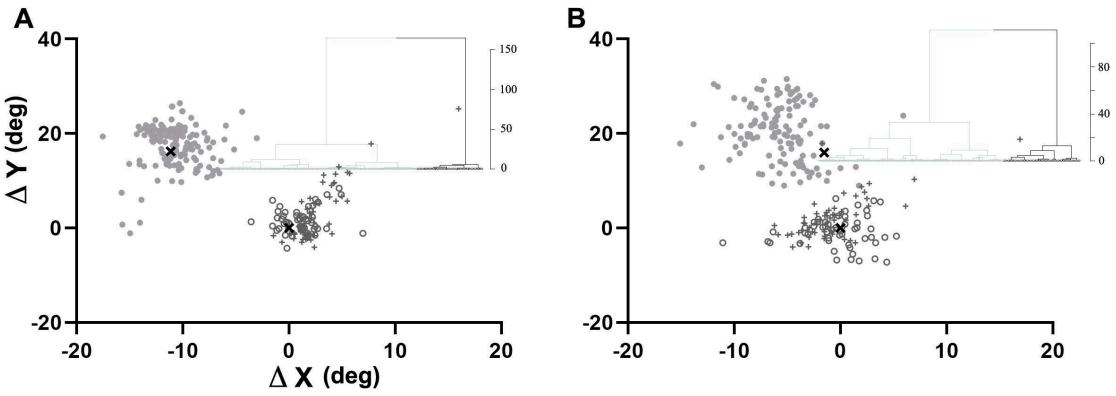

A,**B,** Scatter plots representing the relative source positions with respect to the stimulus position (using the inferior stimulus as a zero reference) for data presented in figures (**5A)** and (**5B),** respectively. The hierarchical clustering analysis for sources appearing during competition, represented in the respective dendrograms (**Insets**), separates the points based on their Euclidian distance (Jaccard index > 0.9) and divides the sources in two main clusters, each one around the respective stimulus position. Gray dots: sources assigned to the superior stimulus; empty dots: sources assigned to the inferior stimulus; dark crosses: stimulus positions. Discriminant analysis indicated that over 86 % of the sources appearing when only the inferior stimulus was present (light crosses) belonged to the same cluster assigned to this stimulus during stimulus competition. See also Table S1.

Figure S4. Steps of the burst detection procedure.

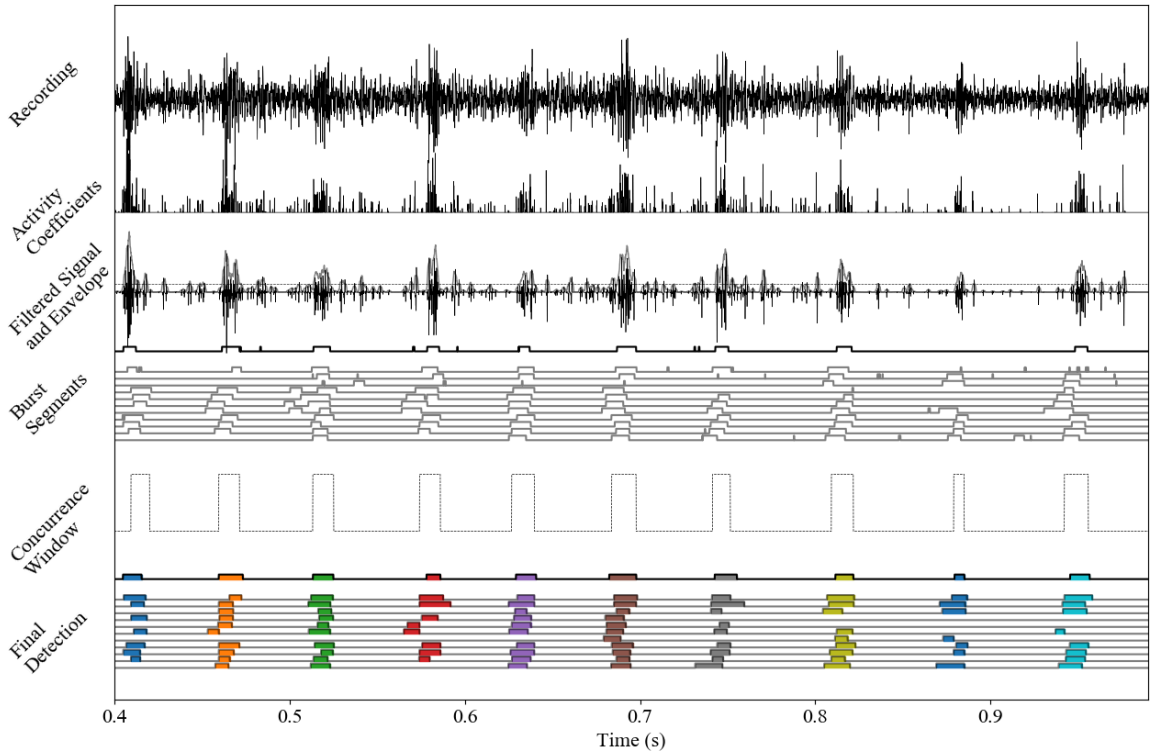

From top to bottom: **Recording:** the original recording after initial high-pass filtering. The bursting responses are mixed with noise and other neural activity. **Activity Coefficients:** They indicate the amplitude of the template components, as extracted by the SSNMF from the filtered recording. **Filtered Signal:** The reconstructed signal after the SSNMF decomposition, displaying bursts with a higher signal-to-noise ratio. To detect burst segments, the signal is rectified and smoothed (continuous line), and then thresholded to their 90th percentile value (dotted line). **Burst Segments:** Thresholded segments are shown for the recording channel (dark trace) and for other channels (light traces). **Concurrence Window:** Signals from a local set of 5 electrodes are pooled and a concurrence window is derived. **Final detection:** Single channel windows intersecting

with the concurrence window are selected and assigned to a burst-wave (different colors).

Star Methods

Resource availability

Lead contact

Further information and requests for resources and reagents should be directed to and will be fulfilled by the lead contact, Gonzalo J. Marin (gmarin@uchile.cl)

Materials availability

This study did not generate new unique materials

Data and code availability

The data reported in this paper has been deposited and is publicly available on line at https://data.mendeley.com/datasets/z9d9mpm2sk/2

This paper does not report original code. All scripts/functions were executed using Python v3.8.10 with the modules Numpy v1.17.4, Scipy v1.3.3 and Scikit-learn v0.20.2

Any additional information required to reanalyze the data reported in this paper is available from the lead contact upon request

Experimental model and subject details

Experiments were conducted on 9 adult, feral pigeons (*Columba livia*, 300-350 g) of both sexes, obtained from a local dealer and maintained in an institutional facility. Seven pigeons were recorded in anesthesia ant two were recorded in awake conditions. All pigeons had full access to food and water. All procedures were approved by the Ethics Committee of the Science Faculty of the University of Chile and the Institutional

Committee for the Care and Use of Animals on research of the University of Chile, and conformed to the guidelines of the NIH on the use of animals in experimental research.

Method details

Surgery and electrophysiological recording procedures in anesthetized animals

7 pigeons were anesthetized by intramuscular injection of ketamine (75 mg/kg) and xylazine (5 mg/kg) and placed in the standard stereotaxic position[91] in a custom-made stereotaxic frame that did not interfere with the animal's visual field. Anesthesia was maintained during surgery and throughout the recording process by infusing 15 % of the initial dose every 90 min via an intramuscular cannula. During the experiment, the body temperature of the animal was kept between 38–42 °C by means of a thermo-regulated blanket (FHC Inc., Bowdoin, ME). A small window was opened on the right side of the skull, exposing the dorsal-lateral part of the tectum. The dura overlying these structures was removed and the exposed surface covered with cotton threads embedded in 0.85 % saline solution. Extracellular recordings were performed using two arrays of regularly spaced tungsten microelectrodes (4x4 and 4x8, 1-2 MOhms, 125 μm thick, 250-300 μm electrode tip separation (Microprobes, Gaithersburg, MD)) and a RHD2000-EVAL multi-channel amplifier (Intan Technologies, Los Angeles, CA). Each array was inserted at approximate 500 μm depth in the tectum (Figure 1B) using independent micromanipulators (Narishige, East Meadow, NY). A silver wire was implanted in the bone in contact with the saline as a reference electrode. Neural signals were amplified, band-passed between 10 Hz and 10 KHz, digitized at 20 KHz and fed into a personal computer. Individual channels were simultaneously displayed on the computer screen and selectively played on an audio monitor. Acquisition, display and analysis of neural

data and presentation of visual stimuli were controlled by custom software written in Python v3.8.10 with the modules Numpy v1.17.4, Scipy v1.3.3 and Scikit-learn v0.20.2.

Surgical procedures for electrophysiological recordings in awake animals

Two out of nine pigeons were recorded in awake conditions. To that end, the dorsal-lateral part of the tectum was exposed following the same surgical procedure described above. Over this bone window, a small recording chamber was crafted using dental acrylic such that no bone remained exposed. The dura was removed and the chamber was sealed using silicone elastomer (Kwik Sil (WPI, Sarasota, FL)). During the same procedure, small holes were drilled in the porous temporal bone and infiltrated with dental acrylic to provide a solid base attached to the skull. Then, two small, stainless steel bolts were cemented, head down to this base, which were then used to hold the head to a small metal plate attached to the stereotaxic frame. After a three-day recovery period the pigeon body was wrapped in a soft bag and its head attached to the stereotaxic frame. Under gaseous anesthesia (2% isoflurane in O2 at 1 lt/min), the silicone elastomer was removed, and the surface of the tectum cleaned with saline and antibiotics, (chloramphenicol). Then, a single Microprobe array of 16 electrodes was inserted around the same tectal location chosen in the anesthetized experiments. Then the anesthesia was removed, and after a 20 min recovery period the recording session was initiated. For visual stimulation the eyelid of the stimulated eye was kept opened with a piece of tape. During the recording sessions, eye displacements were recorded using an infrared eye-tracker system (Arrington Research, Scottsdale, AZ). Eye saccades in birds are the combination of large amplitude oscillatory rotations, of about 25 Hz, combined with a small (usually less than 20 deg.) sustained shift in eye position. Because calibration of an eye-tracker system is very time-consuming in untrained

animals, we used this system only to discard recordings in which the eyes manifestly moved during the recording samples. To avoid excessive discomfort to the animal, recordings were limited to three recording sessions during one week, each lasting no longer than four hours.

Visual stimulation

Visual stimuli were presented on a 19-inch LED monitor (Samsung, operating at 60 or 120 Hz refresh rate) placed 20 to 40 cm from the pigeon's eye, using the software Presentation (Neurobehavioral Systems Inc, Berkeley, CA). Stimuli consisted of stationary or moving white spots and bars presented over a dark background. Looming stimulation was simulated by a white spot increasing in size from 2 to 30 deg in 1 sec. A photodiode placed on the monitor corner was used to synchronize the neural recordings with the visual stimulus; this diminished the uncertainty of stimulus time presentation to 5 ms.

Determination of the receptive fields (RFs) of the bursting responses and of visually-evoked local field potential (LFP) recorded by each electrode

At the beginning of the recording session, a hand-held laser pointer was used to rapidly locate the visual local field potential (LFP) recorded by each electrode on the screen. This LFP is recorded in the first 500 microns from the tectal surface and represents the retino-tectal synaptic volley elicited by a transient stimulus; its slow negative-going deflection is distinctly recognized by a low frequency sound in the audio monitor. This first mapping permitted to re-locate the monitor to present all visual stimuli in and around the visual field sector sampled by the electrodes. Then, to obtain a detailed RF mapping of both the burst RF and the LFP RF recorded by each electrode, a small bright spot (0.5-1.5 deg, 16 to 32 ms ON, 1.5 sec duty cycle) was flashed at pseudo

random positions in a square virtual grid of 20 px node separation. After burst detection during offline analysis, the burst RFs were outlined by mapping the strength of burst responses, defined as the added duration of bursts elicited by the stimulus, at each stimulus position. This 2 D distribution was smoothed using a Gaussian kernel (σ = 40 px) and displayed as a heat map. The contour of the RFs was defined as 20% of the peak response and the RF center as the center of mass of the area above the 60 % contour level. The LFP RF recorded by each electrode was determined in a similar way. The recording trace was centered to zero by subtracting its average amplitude. Then the trace was filtered between 3 and 300 Hz, using a fifth order Butterworth filter, and smoothed by a running average procedure, which replaced each point value with the average value of neighboring points in a 20 ms window. The peak LFP value between the 50 and 100 ms after the visual stimulus was mapped at different stimulus positions. Then, the RF was smoothed with the same Gaussian kernel used above and the center of mass of the 60 % contour level was defined as the RF center of the retinal response. The position of both centers closely matched (Figure S1A), and the burst RF center was used as representing the electrode position in visual space (Figures 2A and 2B).

Detection of bursting responses and burst-waves

A major finding of this work was that bursting responses from the Ipc propagate in all directions from a source point located at or near the stimulated tectal locus. Bursts were considered to be part of a wave when they were recorded within the same timeframe in neighboring electrodes. As bursts usually appear in bouts, assigning a group of bursts to a single wave was a simple task, which could be performed manually by visual inspection of the records. However, to detect the bursting responses and the burst-waves in the whole data set, we designed a multi-step algorithm, which first

reduced the noise, then parsed the recordings into window segments containing the bursts, and finally evaluated the bursts across multiple electrodes to group them together by their co-occurrence (Figure S4).

Briefly, to separate the bursts from noise and other neural activity present in the recordings, we followed the method of Le Roux (2008) and applied a shift-invariant semi non-negative matrix factorization on the individual recordings (SSNMF)[92]. This is a template matching technique in which the templates are directly learnt from the recording. This procedure decomposes the signal in two matrices: S=AB in which A contains the activity coefficients, which mark the time of occurrence and magnitude of events, and B contains the waveform of these events, namely, the component templates. We obtained the templates by averaging the resulting B matrix of 20 decompositions with randomized initial conditions. After testing different parameters, we found that single templates of 1.25 ms duration were enough to reconstruct most of the signal. As the burst profile among electrodes varied, the obtained templates were specific for each electrode. The obtained templates remained constant under different stimulation protocols and, in most cases, followed the stereotypical pattern of triphasic, extracellularly recorded action potentials.

We then reconstructed the signal S = AB, which contained enhanced burst signals and reduced noise. This signal was then rectified and smoothed over 2 ms, and then thresholded to its p90 values. Thresholded segments were further filtered using either one of two criteria: the segment was at least 5 ms long, or more than one segment was detected within a millisecond, in which case they were fused, as was frequent with some bursts which contained very demarcated spikes.

These segments provided a good indicator of the presence of bursts; however, as

bursts co-occurred in neighboring electrodes, we used this property to further refine the burst selection by defining concurrence windows. These windows are periods in which at least the majority of a set of 5 neighboring electrodes detected bursting responses simultaneously. Gaps smaller than 4 ms were filled, and windows shorter than 3 ms were removed. Concurrence windows were then used to further filter and refine the initial segments by selecting segments intersecting with the concurrence window and lowering the threshold of detection. This procedure improved the recognition of the bursts' onset.

Finally the result of this automatic procedure was visually inspected to correct errors in the detection of the bursts and their assignment to burst-waves. Note that although we used the concurrence of bursts recorded by neighboring electrodes as a criterion to both select the bursts themselves and group them in "burst-waves", the reported characteristics of these signals (e.g. their appearance from a single source, their radial propagation, blinking nature, and source dynamics) were not part of the detection algorithm.

Determination of burst-waves sources

After burst responses recorded by neighboring electrodes were assigned to a burst-wave, the position of the burst-wave source was determined by two methods. One method defined the source as the center of mass of the position of the three electrodes recording the earliest burst responses among all the electrodes recording the burst-wave. This simple procedure was used to define the burst-wave sources for data obtained with static visual stimulation and provided confidence that the model of burst-waves was accurate. Nevertheless, this method is limited to finding sources within the convex hull of the electrode set. Thus, for moving visual stimuli, which usually

included motion trajectories outside the recording array, the source was searched for within a space consisting of a rectangular grid 15 deg larger than the electrode distribution borders, at 0.3 deg resolution. The source was determined by the intercept of the linear regression giving the best fit (R2), among all possible source positions giving regressions with a p value < 0.05. The same procedure was repeated using a fixed regression slope obtained from the average slopes calculated in the first procedure. If both procedures did not agree within 5 deg, the data was discarded.

Determination of burst-wave velocity

The expansion of burst-waves elicited by static stimuli was represented by plotting the latencies of the bursts comprising each wave vs the distance of the electrodes recording that wave (Fig. 2G). We then used the slope of the linear regression that fitted a straight line to the points as an estimation of the expansion rate of each wave. In the case of moving stimuli, we tested whether burst-wave expansion was similar in forward and backward directions. To do this, we selected 8 electrodes that were collinear with the direction of motion. Then, for each burst-wave, electrodes were assigned to the left or right of the burst source. The latency vs distance relation was separately plotted for each direction, and the expansion rate was determined by the slope of the linear regression (Fig. 3C).

Quantification and statistical analysis

All statistical analysis was done in R studio. In general, data was not normally distributed so we used non-parametric tests. In one linear model analysis, we assumed normality because it involved a large statistical sample (Figure 3C). Statistical significance was set at $p < 0.05$.

To determine whether the velocity of the burst-wave propagation of moving stimuli (Figure 3C) was affected by some of the factors used in this investigation (pigeons, type of visual stimulation), we made a general linear model (GLM) in which the dependent variable was the burst-wave velocity determined for each burst-wave: Burst-wave velocity = A+B x Pigeons + C x (stimulus direction). The sample size range was between 95 and 137.

To determine if the median of a variable was different from zero (Figures 2I, 4C, 4F and 5E) or from one (Figures 4C and 4F), we used the Wilcoxon Test. To compare the dispersion of variables (burst positions, Figures 4B and 4E) for each pigeon and visual stimulation, we used the Fligner-Killeen Test. Outliers were defined as values greater than the third quartile + 1.5 times the interquartile range and less than the first quartile -1.5 times the interquartile range. The sample size range for Figure 2I was between 42 and 68, for figure 4B between 123 and 223, for Figure 4C between 9 and 13, for Figure 4E between 47 and 225, for Figure 4F between 6 and 10.

In the case of stimulus competition, to determine which stimulus each response belonged to, we performed a hierarchical clustering analysis using the Euclidian distance to calculate the matrix of distances between points. The clusters were defined using an application of Ward's method in R. Then we used a bootstrapping technique to test cluster adequacy. We considered clusters with an average Jaccard index greater than 0.6. In addition, we performed a Discriminant analysis to associate relative source position values before competition to one of the clusters defined during competition. The Discriminant model was created using the 60% of the previously classified data during competition, and then tested with the remaining 40% of the data. This model proved to be 100 % effective in this data classification.

To determine if inter-source intervals (ISI) were affected by the type of the stimulus we compared the median of each distribution using a Pairwise Wilcoxon test with Bonferroni correction (Figure 5G). The ISI sample size ranges for each type of visual stimulus were the following: Static spot, between 56 and 80; Moving spot, between 133 and 190; Moving bar, between 154 and 194; Looming, between 199 and 313; Competition, between 340 and 449.

References

1. Gilbert, C.D., and Li, W. (2013). Top-down influences on visual processing. Nat Rev Neurosci *14*, 350-363. 10.1038/nrn3476.

2. Sillito, A.M., Cudeiro, J., and Jones, H.E. (2006). Always returning: feedback and sensory processing in visual cortex and thalamus. Trends Neurosci *29*, 307-316. 10.1016/j.tins.2006.05.001.

3. Roelfsema, P.R., and de Lange, F.P. (2016). Early Visual Cortex as a Multiscale Cognitive Blackboard. Annu Rev Vis Sci *2*, 131-151. 10.1146/annurev-vision-111815-114443.

4. Markov, N.T., Vezoli, J., Chameau, P., Falchier, A., Quilodran, R., Huissoud, C., Lamy, C., Misery, P., Giroud, P., Ullman, S., et al. (2014). Anatomy of hierarchy: feedforward and feedback pathways in macaque visual cortex. J Comp Neurol *522*, 225-259. 10.1002/cne.23458.

5. Pennartz, C.M.A., Dora, S., Muckli, L., and Lorteije, J.A.M. (2019). Towards a Unified View on Pathways and Functions of Neural Recurrent Processing. Trends Neurosci *42*, 589-603. 10.1016/j.tins.2019.07.005.

6. Marques, T., Nguyen, J., Fioreze, G., and Petreanu, L. (2018). The functional organization of cortical feedback inputs to primary visual cortex. Nat Neurosci *21*, 757-764. 10.1038/s41593-018-0135-z.

7. Edelman, G.M., and Gally, J.A. (2013). Reentry: a key mechanism for integration of brain function. Frontiers in integrative neuroscience *7*, 63. 10.3389/fnint.2013.00063.

8. Larriva-Sahd, J.A. (2014). Some predictions of Rafael Lorente de No 80 years later. Frontiers in neuroanatomy *8*, 147. 10.3389/fnana.2014.00147.

9. Lorente-de-Nó, R. (1949). Cerebral cortex: architecture, intracortical connections, motor projections. In Physiology of the Nervous System, J.F. Fulton, ed. (Oxford University Press), pp. 288-312.

10. Shipp, S. (2017). The functional logic of corticostriatal connections. Brain structure & function *222*, 669-706. 10.1007/s00429-016-1250-9.

11. Hasse, J.M., and Briggs, F. (2017). Corticogeniculate feedback sharpens the temporal precision and spatial resolution of visual signals in the ferret. Proc Natl Acad Sci U S A *114*, E6222-E6230. 10.1073/pnas.1704524114.

12. Redgrave, P., Vautrelle, N., and Reynolds, J.N. (2011). Functional properties of the basal ganglia's re-entrant loop architecture: selection and reinforcement. Neuroscience *198*, 138-151. 10.1016/j.neuroscience.2011.07.060.

13. Luo, L. (2021). Architectures of neuronal circuits. Science *373*, eabg7285. 10.1126/science.abg7285.

14. Romei, V., Chiappini, E., Hibbard, P.B., and Avenanti, A. (2016). Empowering Reentrant Projections from V5 to V1 Boosts Sensitivity to Motion. Curr Biol *26*, 2155-2160. 10.1016/j.cub.2016.06.009.

15. Angelucci, A., Bijanzadeh, M., Nurminen, L., Federer, F., Merlin, S., and Bressloff, P.C. (2017). Circuits and Mechanisms for Surround Modulation in Visual Cortex. Annual review of neuroscience *40*, 425-451. 10.1146/annurev-neuro-072116-031418.

16. Keller, A.J., Roth, M.M., and Scanziani, M. (2020). Feedback generates a second receptive field in neurons of the visual cortex. Nature *582*, 545-549. 10.1038/s41586-020-2319-4.

17. Wang, Y., Luksch, H., Brecha, N.C., and Karten, H.J. (2006). Columnar projections from the cholinergic nucleus isthmi to the optic tectum in chicks (Gallus gallus): A possible substrate for synchronizing tectal channels. J Comp Neurol *494*, 7-35. Doi 10.1002/Cne.20821.

18. Wang, Y., Major, D.E., and Karten, H.J. (2004). Morphology and connections of nucleus isthmi pars magnocellularis in chicks (Gallus gallus). J Comp Neurol *469*, 275-297. 10.1002/cne.11007.

19. Marin, G., Mpodozis, J., Sentis, E., Ossandon, T., and Letelier, J.C. (2005). Oscillatory bursts in the optic tectum of birds represent re-entrant signals from the nucleus isthmi pars parvocellularis. J Neurosci *25*, 7081-7089. 10.1523/JNEUROSCI.1379-05.2005.

20. Marin, G., Salas, C., Sentis, E., Rojas, X., Letelier, J.C., and Mpodozis, J. (2007). A cholinergic gating mechanism controlled by competitive interactions in the optic tectum of the pigeon. J Neurosci *27*, 8112-8121. 10.1523/JNEUROSCI.1420-07.2007.

21. Asadollahi, A., Mysore, S.P., and Knudsen, E.I. (2010). Stimulus-driven competition in a cholinergic midbrain nucleus. Nat Neurosci *13*, 889-895. 10.1038/nn.2573.

22. Asadollahi, A., Mysore, S.P., and Knudsen, E.I. (2011). Rules of competitive stimulus selection in a cholinergic isthmic nucleus of the owl midbrain. J Neurosci *31*, 6088-6097. 10.1523/JNEUROSCI.0023-11.2011.

23. Mysore, S.P., and Knudsen, E.I. (2011). The role of a midbrain network in competitive stimulus selection. Curr Opin Neurobiol *21*, 653-660. 10.1016/j.conb.2011.05.024.

24. Knudsen, E.I. (2011). Control from below: the role of a midbrain network in spatial attention. Eur J Neurosci *33*, 1961-1972. 10.1111/j.1460-9568.2011.07696.x.

25. Knudsen, E.I. (2018). Neural Circuits That Mediate Selective Attention: A Comparative Perspective. Trends Neurosci *41*, 789-805. 10.1016/j.tins.2018.06.006.

26. Gunturkun, O., and Remy, M. (1990). The topographical projection of the nucleus isthmi pars parvocellularis (Ipc) onto the tectum opticum in the pigeon. Neurosci Lett *111*, 18-22.

27. Garrido-Charad, F., Vega-Zuniga, T., Gutierrez-Ibanez, C., Fernandez, P., Lopez-Jury, L., Gonzalez-Cabrera, C., Karten, H.J., Luksch, H., and Marin, G.J. (2018). "Shepherd's crook" neurons drive and synchronize the enhancing and suppressive mechanisms of the midbrain stimulus selection network. Proceedings of the National Academy of Sciences of the United States of America *115*, E7615-E7623. 10.1073/pnas.1804517115.

28. Marin, G.J., Duran, E., Morales, C., Gonzalez-Cabrera, C., Sentis, E., Mpodozis, J., and Letelier, J.C. (2012). Attentional capture? Synchronized feedback signals from the isthmi boost retinal signals to higher visual areas. J Neurosci *32*, 1110-1122. 10.1523/JNEUROSCI.4151-11.2012.

29. Mysore, S.P., and Knudsen, E.I. (2012). Reciprocal inhibition of inhibition: a circuit motif for flexible categorization in stimulus selection. Neuron *73*, 193-205. 10.1016/j.neuron.2011.10.037.

30. Mysore, S.P., and Knudsen, E.I. (2013). A shared inhibitory circuit for both exogenous and endogenous control of stimulus selection. Nat Neurosci *16*, 473-478. 10.1038/nn.3352.

31. Mysore, S.P., and Knudsen, E.I. (2014). Descending control of neural bias and selectivity in a spatial attention network: rules and mechanisms. Neuron *84*, 214-226. 10.1016/j.neuron.2014.08.019.

32. Goddard, C.A., Sridharan, D., Huguenard, J.R., and Knudsen, E.I. (2012). Gamma oscillations are generated locally in an attention-related midbrain network. Neuron *73*, 567-580. 10.1016/j.neuron.2011.11.028.

33. Letelier, J.C., Marin, G., Sentis, E., Tenreiro, A., Fredes, F., and Mpodozis, J. (2004). The mapping of the visual field onto the dorso-lateral tectum of the pigeon (Columba livia) and its relations with retinal specializations. J Neurosci Methods *132*, 161-168.

34. Clarke, P.G., and Whitteridge, D. (1976). The projection of the retina, including the 'red area' on to the optic tectum of the pigeon. Q J Exp Physiol Cogn Med Sci *61*, 351-358. 10.1113/expphysiol.1976.sp002366.

35. Gonzalez-Cabrera, C., Garrido-Charad, F., Mpodozis, J., Bolam, J.P., and Marin, G.J. (2016). Axon terminals from the nucleus isthmi pars parvocellularis control the ascending retinotectofugal output through direct synaptic contact with tectal ganglion cell dendrites. J Comp Neurol *524*, 362-379. 10.1002/cne.23860.

36. Hellmann, B., and Gunturkun, O. (2001). Structural organization of parallel information processing within the tectofugal visual system of the pigeon. J Comp Neurol *429*, 94-112.

37. Luksch, H., Cox, K., and Karten, H.J. (1998). Bottlebrush dendritic endings and large dendritic fields: motion-detecting neurons in the tectofugal pathway. J Comp Neurol *396*, 399-414.

38. Luksch, H., Karten, H.J., Kleinfeld, D., and Wessel, R. (2001). Chattering and differential signal processing in identified motion-sensitive neurons of parallel visual pathways in the chick tectum. J Neurosci *21*, 6440-6446.

39. Marin, G., Letelier, J.C., Henny, P., Sentis, E., Farfan, G., Fredes, F., Pohl, N., Karten, H., and Mpodozis, J. (2003). Spatial organization of the pigeon tectorotundal pathway: an interdigitating topographic arrangement. J Comp Neurol *458*, 361-380. 10.1002/cne.10591.

40. Gale, S.D., and Murphy, G.J. (2016). Active Dendritic Properties and Local Inhibitory Input Enable Selectivity for Object Motion in Mouse Superior Colliculus Neurons. J Neurosci *36*, 9111-9123. 10.1523/Jneurosci.0645-16.2016.

41. Luksch, H., Khanbabaie, R., and Wessel, R. (2004). Synaptic dynamics mediate sensitivity to motion independent of stimulus details. Nat Neurosci *7*, 380-388. 10.1038/nn1204.

42. Tombol, T., Eyre, M., Zayats, N., and Nemeth, A. (2003). The ramifications and terminals of optic fibres in layers 2 and 3 of the avian optic tectum: a golgi and light and electron microscopic anterograde tracer study. Cells Tissues Organs *175*, 202-222. 10.1159/000074942.

43. Fernandez, M., Morales, C., Duran, E., Fernandez-Colleman, S., Sentis, E., Mpodozis, J., Karten, H.J., and Marin, G.J. (2019). Parallel organization of the avian sensorimotor arcopallium: Tectofugal visual Pathway in the pigeon (Columba livia). J Comp Neurol. 10.1002/cne.24775.

44. Reiner, A., Brecha, N.C., and Karten, H.J. (1982). Basal ganglia pathways to the tectum: the afferent and efferent connections of the lateral spiriform nucleus of pigeon. J Comp Neurol *208*, 16-36. 10.1002/cne.902080103.

45. Mysore, S.P., Asadollahi, A., and Knudsen, E.I. (2010). Global inhibition and stimulus competition in the owl optic tectum. J Neurosci *30*, 1727-1738. 10.1523/JNEUROSCI.3740-09.2010.

46. Sereno, M.I., and Ulinski, P.S. (1987). Caudal topographic nucleus isthmi and the rostral nontopographic nucleus isthmi in the turtle, Pseudemys scripta. J Comp Neurol *261*, 319-346. 10.1002/cne.902610302.

47. Mahajan, N.R., and Mysore, S.P. (2022). Donut-like organization of inhibition underlies categorical neural responses in the midbrain. Nat Commun *13*, 1680. 10.1038/s41467-022-29318-0.

48. Krauzlis, R.J., Bogadhi, A.R., Herman, J.P., and Bollimunta, A. (2017). Selective attention without a neocortex. Cortex; a journal devoted to the study of the nervous system and behavior *102*, 161-175. 10.1016/j.cortex.2017.08.026.

49. Krauzlis, R.J., Lovejoy, L.P., and Zenon, A. (2013). Superior colliculus and visual spatial attention. Annual review of neuroscience *36*, 165-182. 10.1146/annurev-neuro-062012-170249.

50. Basso, M.A., Bickford, M.E., and Cang, J. (2021). Unraveling circuits of visual perception and cognition through the superior colliculus. Neuron *109*, 918-937. 10.1016/j.neuron.2021.01.013.

51. Isa, T., Marquez-Legorreta, E., Grillner, S., and Scott, E.K. (2021). The tectum/superior colliculus as the vertebrate solution for spatial sensory integration and action. Curr Biol *31*, R741-R762. 10.1016/j.cub.2021.04.001.

52. Basso, M.A., and May, P.J. (2017). Circuits for Action and Cognition: A View from the Superior Colliculus. Annu Rev Vis Sci *3*, 197-226. 10.1146/annurev-vision-102016-061234.

53. Dean, P., Redgrave, P., and Westby, G.W. (1989). Event or emergency? Two response systems in the mammalian superior colliculus. Trends Neurosci *12*, 137-147. 10.1016/0166-2236(89)90052-0.

54. May, P.J. (2006). The mammalian superior colliculus: laminar structure and connections. Progress in brain research *151*, 321-378. 10.1016/S0079-6123(05)51011-2.

55. Ingle, D. (1973). Two visual systems in the frog. Science *181*, 1053-1055.

56. Gruberg, E., Dudkin, E., Wang, Y., Marin, G., Salas, C., Sentis, E., Letelier, J., Mpodozis, J., Malpeli, J., Cui, H., et al. (2006). Influencing and interpreting visual input: the role of a visual feedback system. J Neurosci *26*, 10368-10371. 10.1523/JNEUROSCI.3288-06.2006.

57. Major, D.E., Luksch, H., and Karten, H.J. (2000). Bottlebrush dendritic endings and large dendritic fields: motion-detecting neurons in the mammalian tectum. J Comp Neurol *423*, 243-260.

58. Deichler, A., Carrasco, D., Lopez-Jury, L., Vega-Zuniga, T., Marquez, N., Mpodozis, J., and Marin, G.J. (2020). A specialized reciprocal connectivity suggests a link between the mechanisms by which the superior colliculus and parabigeminal nucleus produce defensive behaviors in rodents. Scientific reports *10*, 16220. 10.1038/s41598-020-72848-0.

59. Liang, F.X., Xiong, X.R.R., Zingg, B., Ji, X.Y., Zhang, L.I., and Tao, H.Z.W. (2015). Sensory Cortical Control of a Visually Induced Arrest Behavior via Corticotectal Projections. Neuron *86*, 755-767. 10.1016/j.neuron.2015.03.048.

60. Masterson, S.P., Zhou, N., Akers, B.K., Dang, W., and Bickford, M.E. (2018). Ultrastructural and optogenetic dissection of V1 corticotectal terminal synaptic properties. J Comp Neurol. 10.1002/cne.24538.

61. Zhao, X.Y., Liu, M.N., and Cang, J.H. (2014). Visual Cortex Modulates the Magnitude but Not the Selectivity of Looming-Evoked Responses in the Superior Colliculus of Awake Mice. Neuron *84*, 202-213. 10.1016/j.neuron.2014.08.037.

62. Zingg, B., Chou, X.L., Zhang, Z.G., Mesik, L., Liang, F.X., Tao, H.W., and Zhang, L.I. (2017). AAV-Mediated Anterograde Transsynaptic Tagging: Mapping Corticocollicular Input-Defined Neural Pathways for Defense Behaviors. Neuron *93*, 33-47. 10.1016/j.neuron.2016.11.045.

63. Bennett, C., Gale, S.D., Garrett, M.E., Newton, M.L., Callaway, E.M., Murphy, G.J., and Olsen, S.R. (2019). Higher-Order Thalamic Circuits Channel Parallel Streams of Visual Information in Mice. Neuron *102*, 477-492 e475. 10.1016/j.neuron.2019.02.010.

64. Beltramo, R., and Scanziani, M. (2019). A collicular visual cortex: Neocortical space for an ancient midbrain visual structure. Science *363*, 64-69. 10.1126/science.aau7052.

65. Baldwin, M.K., Wong, P., Reed, J.L., and Kaas, J.H. (2011). Superior colliculus connections with visual thalamus in gray squirrels (Sciurus carolinensis): evidence for four subdivisions within the pulvinar complex. J Comp Neurol *519*, 1071-1094. 10.1002/cne.22552.

66. Fredes, F., Vega-Zuniga, T., Karten, H., and Mpodozis, J. (2012). Bilateral and ipsilateral ascending tectopulvinar pathways in mammals: a study in the squirrel (Spermophilus beecheyi). J Comp Neurol *520*, 1800-1818. 10.1002/cne.23014.

67. Robson, J.A., and Hall, W.C. (1977). The organization of the pulvinar in the grey squirrel (Sciurus carolinensis). I. Cytoarchitecture and connections. J Comp Neurol *173*, 355-388. 10.1002/cne.901730210.

68. Zhou, N.A., Maire, P.S., Masterson, S.P., and Bickford, M.E. (2017). The mouse pulvinar nucleus: Organization of the tectorecipient zones. Vis Neurosci *34*, E011. 10.1017/S0952523817000050.

69. Hoy, J.L., Bishop, H.I., and Niell, C.M. (2019). Defined Cell Types in Superior Colliculus Make Distinct Contributions to Prey Capture Behavior in the Mouse. Curr Biol *29*, 4130-4138 e4135. 10.1016/j.cub.2019.10.017.

70. Eriksen, C.W., and St James, J.D. (1986). Visual attention within and around the field of focal attention: a zoom lens model. Percept Psychophys *40*, 225-240. 10.3758/bf03211502.

71. Treisman, A.M., and Gelade, G. (1980). A feature-integration theory of attention. Cogn Psychol *12*, 97-136. 10.1016/0010-0285(80)90005-5.

72. Itti, L., and Koch, C. (2000). A saliency-based search mechanism for overt and covert shifts of visual attention. Vision research *40*, 1489-1506.

73. Posner, M.I., Snyder, C.R., and Davidson, B.J. (1980). Attention and the detection of signals. J Exp Psychol *109*, 160-174.

74. Crick, F. (1984). Function of the thalamic reticular complex: the searchlight hypothesis. Proc Natl Acad Sci U S A *81*, 4586-4590. 10.1073/pnas.81.14.4586.

75. Fiebelkorn, I.C., and Kastner, S. (2019). A Rhythmic Theory of Attention. Trends in cognitive sciences *23*, 87-101. 10.1016/j.tics.2018.11.009.

76. Helfrich, R.F., Fiebelkorn, I.C., Szczepanski, S.M., Lin, J.J., Parvizi, J., Knight, R.T., and Kastner, S. (2018). Neural Mechanisms of Sustained Attention Are Rhythmic. Neuron *99*, 854-865 e855. 10.1016/j.neuron.2018.07.032.

77. VanRullen, R., Carlson, T., and Cavanagh, P. (2007). The blinking spotlight of attention. Proc Natl Acad Sci U S A *104*, 19204-19209. 10.1073/pnas.0707316104.

78. Fiebelkorn, I.C., Saalmann, Y.B., and Kastner, S. (2013). Rhythmic sampling within and between objects despite sustained attention at a cued location. Curr Biol *23*, 2553-2558. 10.1016/j.cub.2013.10.063.

79. Landau, A.N., and Fries, P. (2012). Attention samples stimuli rhythmically. Curr Biol *22*, 1000-1004. 10.1016/j.cub.2012.03.054.

80. VanRullen, R. (2016). Perceptual Cycles. Trends in cognitive sciences *20*, 723-735. 10.1016/j.tics.2016.07.006.

81. Maunsell, J.H.R. (2015). Neuronal Mechanisms of Visual Attention. Annu Rev Vis Sc *1*, 373-391. 10.1146/annurev-vision-082114-035431.

82. Moore, T., Armstrong, K.M., and Fallah, M. (2003). Visuomotor origins of covert spatial attention. Neuron *40*, 671-683. 10.1016/s0896-6273(03)00716-5.

83. Kastner, S., and Ungerleider, L.G. (2000). Mechanisms of visual attention in the human cortex. Annual review of neuroscience *23*, 315-341. 10.1146/annurev.neuro.23.1.315.

84. Szczepanski, S.M., Konen, C.S., and Kastner, S. (2010). Mechanisms of spatial attention control in frontal and parietal cortex. J Neurosci *30*, 148-160. 10.1523/JNEUROSCI.3862-09.2010.

85. Buschman, T.J., and Miller, E.K. (2009). Serial, covert shifts of attention during visual search are reflected by the frontal eye fields and correlated with population oscillations. Neuron *63*, 386-396. 10.1016/j.neuron.2009.06.020.

86. Dugue, L., Beck, A.A., Marque, P., and VanRullen, R. (2019). Contribution of FEF to Attentional Periodicity during Visual Search: A TMS Study. eNeuro *6*. 10.1523/ENEURO.0357-18.2019.

87. Dugue, L., Roberts, M., and Carrasco, M. (2016). Attention Reorients Periodically. Curr Biol *26*, 1595-1601. 10.1016/j.cub.2016.04.046.

88. Huh, C.Y.L., Peach, J.P., Bennett, C., Vega, R.M., and Hestrin, S. (2018). Feature-Specific Organization of Feedback Pathways in Mouse Visual Cortex. Curr Biol *28*, 114-120 e115. 10.1016/j.cub.2017.11.056.

89. Fiebelkorn, I.C., Pinsk, M.A., and Kastner, S. (2018). A Dynamic Interplay within the Frontoparietal Network Underlies Rhythmic Spatial Attention. Neuron *99*, 842-853 e848. 10.1016/j.neuron.2018.07.038.

90. Fiebelkorn, I.C., and Kastner, S. (2019). Functional Specialization in the Attention Network. Annu Rev Psychol *71*, 221-249. 10.1146/annurev-psych-010418-103429.

91. Karten, H.J., and Hodos, W. (1966). A stereotaxic atlas of the brain of the pigeon (Columba livia) (The Johns Hopkins Press).

92. Le Roux, J., De Cheveigné, A., and Parra, L. (2008). Adaptive Template Matching with Shift-Invariant Semi-NMF. In Advances in Neural Information Processing Systems 21, D. Koller, D. Schuurmans, Y. Bengio, and L. Bottou, eds. pp. 921-92

Conclusions

In this thesis, we made a significant contribution to the understanding of a proposed stimulus selection mechanism by conducting multi-electrode recordings in the optic tectum of pigeons. This enabled us to explore the spatio-temporal patterns of the Ipc feedback to TeO in unprecedented detail by giving us access to the neural activity landscape of the tectum. Our findings revealed a previously indiscernible geometric arrangement of the Ipc re-entrant response, characterized by a seemingly blinking spotlight of Ipc bursting activity. In particular, we recorded radially expanding waves of bursting activity (burst-waves) that invade the tectum horizontally. Our results provide a glimpse of the neurodynamics supporting a stimulus selection filter in the tectum that seems to be based on the selective enhancement of neural excitability. These findings provide evidence for the winner-takes-all model previously proposed for stimulus selection in the tectum, and further advance our understanding of the neural mechanisms underlying visual processing.

Oscillatory Bursts

Our study focused on the oscillatory bursts, which constitute the main response recorded in the optic tectum in response to visual stimuli[13]. This response is known to originate in the Ipc neurons innervating the tectum in topographical correspondence, and it travels to the tectum through the paintbrush axons. Using the SSNMF algorithm, we were able to isolate the fundamental components of oscillatory bursts, which turned out to be conventional extracellular action potentials. Once we recovered the detailed extracellular potential waveform from all of the analyzed recordings, we were able to successfully reconstruct and denoise the original signal using this waveform alone.

Thus, our findings provide evidence that the oscillatory bursts are mainly composed of the superposition of stereotypical extracellular action potentials. The morphology of the PB offers some clues on which elements are superposed at a single recording site. First, one must consider that the dense ramifications of the PB provide an enormous membrane surface leading to large currents being mobilized[4]. It follows that APs traveling through PBs can be recorded from a distance larger than normal spikes, and so a single electrode might be detecting the activity of multiple axons despite their mosaic-like organization. More specifically related to the PB, APs traveling through it might decohere through their branches, and even richer phenomena can occur in both branching points and en-passant buttons, such as intermittent transmission failure. All factors considered, the synchronized firing of Ipc neurons would probably give rise to multiple APs being detected at different phases once they arrive at the tectal layers.

Our novel understanding of the oscillatory burst waveform, together with the use of SSNMF, enabled us to automate the analysis and sift through the large volumes of data analyzed in this thesis, which would have been otherwise an insurmountable task. This allowed for a more efficient and thorough investigation of the tectal dynamics triggered by visual stimuli.

Tectal burst-waves

The study of the temporal progression of activity in the tectum led us to describe waves of bursting activity which originate from a source point and expand horizontally through the tectum. After employing a time-of-flight approximation to source location, we were able to pinpoint the origin of most burst-waves detected. We characterized the speed and reach of these waves and correlated the source-point's positions in the tectum to

the location of the stimulus representation. Our analysis showed that even though the activity starts at the site mapped to the stimulus, the response radially invades adjacent regions of the tectum, well beyond the limits of the stimulated region. Usually, after a burst-wave concludes, another one follows, with each subsequent wave having a larger radius than its predecessor, up to a limit of 20 degrees. The positions of the ensuing source-points were determined by the characteristics of the stimulation. For example, when the stimulus consisted of a moving point, the source-points tended to follow the tectal representation of the stimulus trajectory. When the stimulus was elongated and narrow, the vertical dispersion of source-points increased, but the horizontal dispersion remained the same as for a point stimulus. Our experiments allowed us to demonstrate the existence of a single unique burst-wave traveling through the observed portion of the tectum at any given time.

When burst-waves are considered in the context of the neurons generating this activity, it is apparent that the horizontal transport in the tectum points to the existence of a corresponding wave of activations in the Ipc. The progressive increase in the reach of the burst-waves is probably the result of recurrent excitation between the tectum and the Ipc, and the expansion of the projection areas in the reciprocal mappings: Both Ipc neurons and tectal Shepherd's Crook neurons innervate larger tissue than that represented by the incoming retinal input, thus recurrent activity progressively invades neighboring loops[13]. Moreover, the establishment, development and resolution of a burst-wave must be due to the complex interplay between reciprocal excitatory synapses and the wide-field inhibitory effect of the Imc, suggesting a rich panorama of neural excitability modulation. The same must be true for the fact that there is a single burst-wave source on the tectum at any given time. It is likely the Imc inhibits most of the tectal surface while the Ipc is firing, both events synchronized by their common input

from the Shcs neurons. Moreover, since the Imc also innervates the complementary Ipc regions, the effect is reinforced. We did not search for a footprint of the Imc activity in our recordings and none was immediately evident, but it is likely that one can be found when looking for long range, synchronized signals.

A blinking Spotlight

As previously mentioned, the burst-waves generated by oscillatory bursts are the landmark of the Ipc cell activity on the tectum[13]. The axons of these cells positively modulate the transference of activity between the retina and the rotundus nucleus in the thalamus, to an extent that they are considered as exerting a gating or boosting effect[6,15]. It is thus expected that the radial waves demarcate the tectal region in the open configuration of the filter, while any inputs received by the rest of the tectum would not be relayed further. It is possible then to draw an analogy between the burst-waves and a spotlight which enhances the saliency of certain portions of the visual environment while the remaining scene fades into the background. Just like a spotlight focuses on a specific area of the stage and highlights it, burst-waves in the tectum boost specific areas of the tectal representation of the visual environment. This raises the question of what determines the dynamics of the spotlight. As already mentioned, we have observed that the source-points position is tightly coupled with the presence of stimuli; i.e. source-points have a very strong tendency to manifest inside the visually stimulated tectal regions. When challenged with two stimuli, the spotlight does not split, multiply or transport from one position to another, it rather blinks alternating between both stimuli. It is likely that the receiving neural circuitry upstream requires input from a single TeO region for its adequate operation. The field-to-locus topography of the tectal

projections over the Rt suggest that if multiple regions of the visual input were forwarded simultaneously to the Rt, then this nucleus would receive activity representing a superposition or mix of the retinal input in which distant loci would converge to the same Rt neurons[11]. The gating mediated by the Ipc neurons is likely parceling the visual scene into pieces that can be readily processed by the Rt avoiding confusion. In this fashion, burst-waves would select a parcel of a single stimulus at a time avoiding the convergence of distant inputs on the Rt. This fragmented view of the environment stipulates that re-assembly of the visual scene into a complete landscape would require both a short term memory of the parcels along with an efferent copy of the Ipc activity or similar which would contain the information of the spatial relations between these parcels. Whether these parcels would be anatomical or functional, dynamical or fixed, or even clearly defined is an interesting question, but surely their existence can be supported by the rich recurrent excitatory-inhibitory interactions taking place in the tectum.

Additionally, it is noteworthy that a transient spot triggers not a single wave, but a series of waves, with source-points appearing around the stimulus location at higher frequencies than for moving stimuli. In the case of moving stimuli, the source-points appeared as an orderly sequence that tracked the trajectory of the stimulus at a lower pace. This indicates that far from being the sequential addition of transiently elicited responses, the dynamics of the spotlight are presumably shaped by substantial interactions between the sensory inputs activating tectal sites, top-down control from other parts of the brain or the isthmotectal circuit internal mechanism dictated by its anatomy and physiology[16–19].

Biological Significance

Our findings on the spotlight of neuronal excitability in the isthmotectal circuit have significant biological relevance. The optic tectum is homologous to the superior colliculus of mammals, a structure that plays a vital role in the control of spatial attention[7,20–23]. In all vertebrates, the TeO contributes to the development of orienting behaviors, either towards the stimulus, for example during prey catching maneuvers, or away from stimuli, in predator avoidance[24–26]. Stimulus selection is crucial for both behaviors, and a spotlight mechanism implementing such selection may have co-evolved with the tectal control of spatial attention. The isthmotectal system is highly conserved in sauropsids, and the characteristics described in the pigeon are presumably accurate for turtles, lizards and crocodiles[27]. TGC neurons, exhibiting identical morphology, physiological properties and central projections are also highly conserved, resembling neurons found in the superficial layers of the superior colliculus of mammals[28]. Although it remains unknown whether the mammalian TGCs receive the synapses from parabigeminal axons, the presumed homologue of the Ipc[29], the conservation of the isthmotectal system and TGC neurons supports the evolutionary importance of this mechanism.

Visual Attention

Our discovery might provide insights into how attention operates in the brain. The spotlight of neuronal excitability that we have described in the tectum is highly evocative of the phenomenon of visual attention[30–36]. Some aspects of visual attention are supported by the brain selectively processing certain aspects of the visual scene while

ignoring others. Several studies have developed the idea that spatial attention is comparable to a perceptual spotlight that scans internal representations of the visual scene. To our knowledge, a genuine neural correlate of a blinking spotlight such as the one we describe in the avian tectum has never been reported in other brain areas in any vertebrate species, making our finding a significant contribution to the field. The operation of the isthmotectal circuit is part of a larger scheme that entails perception: As the Ipc re-entry gates/boosts the tectofugal transmission, the link between the blinking spotlight, the thalamo-telencephalic rhythms recorded in this pathway, and the parsing of perception is straightforward. The blinking burst-waves would transmit the incoming visual image in a sequential and piecemeal fashion to higher tectofugal areas, which lack a clear retinotopic organization. The induced rhythm might drive the propagation of the selected activity promoting the large-scale neural interactions underlying an organized behavioral response, and/or the long-range synchrony underpinning sensory integration and multimodal perception[12,14,30,37–39]. The existence of a singular blinking spotlight scanning within the limits of a moving object, without visiting a competing one, would help feature binding and the initial segmentation of the visual scene, which could be refined by top-down interactions directed by the executed behavior and the animal's previous experience. Notably, this evidence shows that the distributed thalamic and pallial rhythms are closely associated with a highly structured recurrent process operating at a sub-pallial level.

Considering the previous paragraph, the neural substrate of visual attention is thus believed to involve a set of brain regions that act as a filter for incoming sensory information, allowing only the most behaviorally relevant information to reach higher processing stages.

The properties of the spotlight of neuronal excitability provided by the focal Ipc feedback in the tectum are highly consistent with the properties of a visual attention filter, which is characterized by the following properties:

- The fact that there is a single locus that is attended to.
- Attention spreads to nearby regions.
- The "spotlight" of attention scans regions with salient stimuli.
- The "spotlight" blinks rather than operating continuously, even when attending to a single, sustained stimulus.

Moreover, the fact that the Ipc axons exert a gating effect on the tectofugal transmission by making synaptic contacts upon the bottlebrush dendritic specializations of the TGCs, which project to the nucleus rotundus in the thalamus, suggests that the isthmotectal further strengthen the link between the properties of the Ipc spotlight and visual attention. Therefore, the spotlight of neuronal excitability in the tectum provides a compelling candidate for the neural substrate of visual attention, at least in birds, and may shed light on the mechanisms underlying this fundamental cognitive process in other vertebrate species as well.

Nevertheless, further investigation is required to determine whether the dynamics of this focal, recurrent activation is part of a stimulus selection mechanism and the parsing of perception, or it is indeed linked to how attention is deployed. Ideally, it should be examined in behaving animals in a controlled environment, allowing the understanding of both, the internal influences, such as top-down control of attention, and the external drivers, such as salient stimuli. Our current findings were facilitated by both the clear signature of the Ipc re-entrant signals, which permitted their selective recording, and the topographic organization of the reciprocal projections in the isthmotectal circuit, which

exposed the stereotyped spatiotemporal pattern of burst-waves. The well-defined structure of the isthmotectal circuit makes it an ideal system for such investigations. It is likely that analogous recursive patterns might be hidden in less bi-dimensionally-organized topographies.

In summary, our discovery of the spotlight of neuronal excitability in the isthmotectal circuit provides the first candidate for a neural substrate of visual attention and sheds light on how the brain processes and selects visual information in a specific and precise manner, with significant implications for our understanding of attention across vertebrates. This finding will undoubtedly serve as a foundation for future studies exploring the mechanisms underlying attention in other brain regions and circuits. The fact that this circuit has such a neat and well-defined structure makes it an ideal system for further investigation, potentially leading to a better understanding of the cellular and molecular mechanisms underlying visual attention.

What the pigeon’s tectum tells the pigeon’s brain

How do pigeons see the world? This is of course a rhetorical question, as seeing is an experience and experiences are inaccessible to observers and arguably even incomprehensible to observers of a different species. Yet, certainly something can be said about the existing mechanisms that enable the pigeon’s visual experience. We can theorize on what is available through the biological machinery and also derive hypotheses about the inner workings of the system by observing its inputs and outputs; that is, the correlation between the sensory landscape and the behavior of pigeons. Again, because we will be discussing a different species, we must draw some bridges

through analogies which take the role of metaphors rather than direct comparisons. What follows is then my best effort to explain how pigeons see the world as understood by humans, in the language of human experiences.

Most animals stabilize the image on the retina by means of the vestibulo-ocular and optokinetic reflexes. Animals which have high visual acuity distributed on a broad retinal area, such as pigeons, favor head and neck movements over eye movements, since the former strategy allows compensating for translations, whereas rotational eye movements would induce a parallax distortion when trying to balance a translation. This is the behavior behind the characteristic head bobbing observed in walking or perched pigeons[40]. For our purposes then, we can consider the visual field fixated, which is relevant since it implies that any movement on the image formed on the retina corresponds to actual movement of objects and not that of the observing subject. In other words, fixating the image allows discounting irrelevant stimuli due to self-movement.

The retina, on the other hand, is not an homogeneous surface; apart from the fovea, there are blindspots (e.g. caused by the pecten), an heterogeneous density distribution of receptors and a differential content in the oil droplets in the receptors, which change the spectral transmittance of the optic path to the cells[41]. All the output from the retina comes from the ganglion cells, which have been less studied in birds compared to mammals. Yet, already at this level, multiple transformations have been described to occur in terms of visual processing: ganglion cells have broad, overlapping receptive fields which respond selectively to direction, convexity, contrast, horizontal and vertical edges, and more[42]. It follows that the stimulation pattern received by the tectum is not a low fidelity copy of the neural activity elicited on the receptors by the visual flow field,

but a much more complicated, but likely more behaviorally attuned, encoding of it. The language in which the visual landscape is captured or internalized is not immediately obvious, but for sure the retina is not acting as a passive, camera-like surface. Whilst this means the retina is not sending an exact reproduction of the sensory input, it does not mean at all that relevant visual information is lost.

The main target of the retinal efferents is the tectum, in which again diverse response characteristics have been found, including ON and OFF receptive fields, motion and direction sensitivity, and even center-surround operations, some of these being inherited directly from the retinal input while some others must arise from the tectal circuitry. These responses have been described in different tectal layers, which for the most part preserve the topographic ordering; separate subgroups of retinal ganglion cells target different subgroups of tectal cells, giving rise to parallel visual channels[43]. At this point it is difficult to describe the net transformation resulting from the composition of the previous stages, but at least the spatial relationships of the emerging objects or percepts is maintained, albeit visual features are propagated separately[44]. That is, the image has been decomposed into multiple superimposed maps each encoding a distinct, operationally relevant feature which travels in what has been proposed as parallel streams or channels. Our next target in the tectofugal system is the rotundus thalamic nucleus, but retinal input is filtered by the isthmotectal circuit before it is relayed upstream.

The burst waves that we describe in this work provide a signature to understand the spatiotemporal properties of the isthmotectal filter. A single compact region in the tectum is selected and the input from that region is forwarded to the rotundus as a periodic series of visual parcels[5,6]. The result is akin to looking through a small aperture

while blinking rapidly, observing only a small fragment of the visual field each time. The temporal pace of the gating matches that of the burst waves, as evidenced by the synchrony between the tectal burst and the responses in the rotundus and the entopallium[5]. The durations of the burst waves and the interval between their occurrence indicate that almost as one wave dampens, the following starts, which might dictate an almost continuous flow to the rotundus. In any case, the gating mechanism imposes a rhythm on the rotundus and parses the visual input into temporal windows which impacts the encoding, as it probably defines semantic units, as a syntaxis would. For a successful integration upstream, it is likely that features that must be processed together, must be forwarded together.

The different rotundus nucleus subdivisions receive the gated input from the tectum. Although the topographic arrangement of the whole field is lost at this stage, as we described earlier, it might still be the case that locality is preserved, since the rotundus will not receive inputs from the whole tectum at once, but only from a small region of it. Little is known about the transformations that occur in this nucleus, as the topography still remains cryptic, but given this nucleus segmentation into subregions, we can assume that no final assembly, integration or association has yet happened. The visual flow still may consist of parallel streams of features, although now they are constrained to a small region of the visual field.

The entopallium is a nucleus in the telencephalon which receives extensive efferent projections from the rotundus. Less is known about the receptive fields of this area, but evidence suggests different subregions of the rotundus project to separate regions of the entopallium[45]. Finally, integration seems to happen at the next processing stage, the

mesopallium ventrolaterale layer where there is evidence of advanced object feature recognition[46,47].

The original question lingers. How, then, can we bring in concordance a continuous experience of vision with such a fragmented transmission of visual activity? Final object reconstruction requires persistence of the previous parcels along with the knowledge of how that piece fits in the puzzle; i.e. which tectal region was selected. The reconstruction, if it ever happens in this visual pathway, must occur quickly, before the pigeon changes the position of its retina relative to the visual field and a new sensory landscape is presented to its eyes, or, the reconstruction mechanism must take this additional factor into account. But is this reconstruction even necessary?

It might be worthwhile at this point to take a step back and ponder that pigeons do not necessarily experience their *Umwelt* in a similar fashion to ours. It might very well be the case that pigeons can get by as long as they are able to recognize sources of food, predators, obstacles and potential mates. These tasks do not require a concerted, continuous and complex perception of the world, but only one that understands its most immediate features. In other words, if we embark on the search for the neuronal circuitry that allows pigeons to recognize or formulate the idea of say trees, lakes and clouds, we might never find it for it might not exist at all. Pigeons, and animals in general do not *require* such notions; their behavior can be explained by reducing or abstracting their experience to matching the right nervous activity patterns to trigger adequate responses, such as pecking, avoidance, etc… As long as animals are able to tag their experiences with operationally relevant distinctions; that should suffice. This thesis started with a statement that animals must react to a complex, dynamical environment.

But the function of the nervous system in this context could be to abstract that complexity away. The aforementioned transformations in the retina, and the visual filter we described in this work are potential mechanisms which simplify/incorporate the environment. Moreover, attentional circuits and related structures might be playing the role of simplifying, translating and routing the initial nervous activity from the senses into a semiotic/semantic system in congruence with the story of interactions between the organism and its medium. In this sense, circuits like the one described in this work would support the development of adapted behavior and thus act as cornerstones for the emergence of a language, as simple or as complex as need be.

Returning to the argument of how might be the total experience synthesized in the tectofugal system, one must consider that this pathway is associated with the generation of escape and perhaps food capture behaviors, which do not necessarily require a global view of the environment; the "representation" of just the relevant object parcels would be enough to determine the adequate response. The tectum and upstream structures do have neurons with receptive fields responding mainly to movement and looming and this might be enough to accurately deploy a behavioral response. This distinction between local and global processing has been pointed out before, along with the suggestion that indeed the tectofugal pathway is a local processor whereas the thalamofugal pathway is the global processor, where scene reconstruction, rather than individual object processing might take place[47,48]. This idea is supported by recent experiments which indicate that birds do not generate emergent Gestalts, but seem to rather see the whole as a simple addition of parts[49]. Although an alternative explanation might be that their visual operations are different enough from

those found in primates, so that previous experiments have failed to trigger the emergence of objects. This last point is supported by Brooks et al., (2022)[50].

To conclude, understanding how pigeons *see* is a complex endeavor, which might first require answering how pigeons see behaviourally relevant visual configurations, then how they perceive objects and finally how pigeons see the world. These three questions might find separate, different answers.

Future Work

This work provides important insights into the neural mechanisms underlying visual attention; specifically in the case of the isthmotectal circuit. The homology of this circuit in different vertebrate species suggests that it may be a fundamental building block for attentional control. By understanding the workings of this circuit, we may gain new insights into how the brain selectively processes and filters sensory information to support adaptive behavior. Future research may investigate how the spotlight of excitability relates to other neural systems involved in attention, and how it can be modulated by situation and experience. Of particular interest would be performing recordings in awake, behaving animals. Another aspect that needs further proving is the role of the different isthmic nuclei and the tectum; simultaneous, in register, recordings of the Ipc, Imc, TeO and Rt would provide a trove of data to understand the isthmotectal circuit even further. Alternatively, imaging studies could provide a more complete picture of the neural activity in the tectum.

References

1. Folta, K., Diekamp, B. & Güntürkün, O. 2004. Asymmetrical Modes of Visual Bottom-Up and Top-Down Integration in the Thalamic Nucleus Rotundus of Pigeons. J. Neurosci. Off. J. Soc. Neurosci. 24: 9475–9485
2. Luksch, H. 2003. Cytoarchitecture of the Avian Optic Tectum: Neuronal Substrate for Cellular Computation. Rev. Neurosci. 14: 85–106
3. Wylie, D., Gutiérrez-Ibáñez, C., Pakan, J. & Iwaniuk, A. 2009. The optic tectum of birds: Mapping our way to understanding visual processing. Can. J. Exp. Psychol. Rev. Can. Psychol. Expérimentale 63: 328–338
4. Wang, Y., Major, D. & Karten, H. 2004. Morphology and Connections of Nucleus Isthmi Pars Magnocellularis in Chicks (Gallus gallus). J. Comp. Neurol. 469: 275–297
5. Marín, G.J., Durán, E., Morales, C., González-Cabrera, C., Sentis, E., Mpodozis, J. & Letelier, J.C. 2012. Attentional Capture? Synchronized Feedback Signals from the Isthmi Boost Retinal Signals to Higher Visual Areas. J. Neurosci. Off. J. Soc. Neurosci. 32: 1110–1122
6. Garrido-Charad, F., Vega-Zuniga, T., Gutiérrez-Ibáñez, C., Fernandez, P., López-Jury, L., González-Cabrera, C., Karten, H.J., Luksch, H. & Marín, G.J. 2018. “Shepherd’s crook” neurons drive and synchronize the enhancing and suppressive mechanisms of the midbrain stimulus selection network. Proc. Natl. Acad. Sci. 115: 7615–7623
7. Basso, M. & May, P. 2017. Circuits for Action and Cognition: A View from the Superior Colliculus. Annu. Rev. Vis. Sci. 3: 197–226
8. Lee, K., Tran, A., Turan, Z. & Meister, M. 2020. The sifting of visual information in the superior colliculus. eLife 9

9. Dutta, A. & Gutfreund, Y. 2014. Saliency mapping in the optic tectum and its relationship to habituation. Front. Integr. Neurosci. 8

10. Knudsen, E. 2011. Control from below: The role of a midbrain network in spatial attention. Eur. J. Neurosci. 33: 1961–1972

11. Marín, G., Letelier, J.C., Henny, P., Sentis, E., Farfán, G., Fredes, F., Pohl, N., Karten, H. & Mpodozis, J. 2003. Spatial organization of the pigeon tectorotundal pathway: An interdigitating topographic arrangement. J. Comp. Neurol. 458: 361–380

12. Sridharan, D., Boahen, K. & Knudsen, E. 2011. Space coding by gamma oscillations in the barn owl optic tectum. J. Neurophysiol. 105: 2005–2017

13. Marín, G., Mpdozis, J., Sentis, E., Ossandón, T. & Letelier, J.C. 2005. Oscillatory Bursts in the Optic Tectum of Birds Represent Re-Entrant Signals from the Nucleus Isthmi Pars Parvocellularis. J. Neurosci. 25: 7081–7089

14. Goddard, C., Sridharan, D., Huguenard, J. & Knudsen, E. 2012. Gamma Oscillations Are Generated Locally in an Attention-Related Midbrain Network. Neuron 73: 567–580

15. González-Cabrera, C., Garrido Charad, F., Mpodozis, J., Bolam, J. & Marín, G. 2015. Axon terminals from the nucleus isthmi pars parvocellularis control the ascending retinotectofugal output through direct synaptic contact with tectal ganglion cell dendrites. J. Comp. Neurol. 524: 362–379

16. Fernández, M., Morales, C., Durán, E., Fernández-Colleman, S., Sentis, E., Mpodozis, J., Karten, H.J. & Marín, G. J. 2019. Parallel organization of the avian sensorimotor arcopallium: Tectofugal visual Pathway in the pigeon (Columba livia). J. Comp. Neurol. 528: 597–623

17. Reiner, A., Brecha, N. & Karten, H. 1982. Basal ganglia pathways to the tectum The afferent and connections of the lateral spiriform nucleus of pigeon. J. Comp.

Neurol. 208: 16–36

18. Mysore, S. & Knudsen, E. 2013. A shared inhibitory circuit for both exogenous and endogenous control of stimulus selection. Nat. Neurosci. 16: 473–478

19. Asadollahi, A., Mysore, S. & Knudsen, E. 2010. Stimulus-driven competition in a cholinergic midbrain nucleus. Nat. Neurosci. 13: 889–895

20. Isa, T., Marquez-Legorreta, E., Grillner, S. & Scott, E. 2021. The tectum/superior colliculus as the vertebrate solution for spatial sensory integration and action. Curr. Biol. 31: 741–762

21. Basso, M., Bickford, M. & Cang, J. 2021. Unraveling circuits of visual perception and cognition through the superior colliculus. Neuron 109: 918–937

22. Krauzlis, R., Bogadhi, A., Herman, J. & Bollimunta, A. 2017. Selective attention without a neocortex. Cortex 102: 161–175

23. Krauzlis, R., Lovejoy, L. & Zenon, A. 2013. Superior Colliculus and Visual Spatial Attention. Annu. Rev. Neurosci. 36: 165–182

24. Dean, P., Redgrave, P. & Westby, G. 1989. Event or emergency? Two response systems in the mammalian superior colliculus. Trends Neurosci. 12: 137–147

25. May, P. 2005. The mammalian superior colliculus: Laminar structure and connections. Prog. Brain Res. 151: 321–378

26. Ingle, D. 1973. Two Visual Systems in the Frog. Science 181: 1053–1055

27. Sereno, M. & Ulinski, P. 1987. Caudal topographic nucleus Isthmi and the rostral nontopographic nucleus isthmi in the turtle, Pseudemys scripta. J. Comp. Neurol. 261: 319–346

28. Major, D., Luksch, H. & Karten, H. 2000. Bottlebrush dendritic endings and large dendritic fields: Motion-detecting neurons in the mammalian tectum. J. Comp. Neurol. 423: 243–260

29. Gruberg, E., Dudkin, E., Wang, Y., Marín, G., Salas, C., Sentis, E., Letelier, J., Mpodozis, J., Malpeli, J., Cui, H., Ma, R., Northmore, D. & Udin, S. 2006. Influencing and Interpreting Visual Input: The Role of a Visual Feedback System. J. Neurosci. 26: 10368–10371

30. Fiebelkorn, I. & Kastner, S. 2018. A Rhythmic Theory of Attention. Trends Cogn. Sci. 23: 87–101

31. VanRullen, R., Carlson, T. & Cavanagh, P. 2008. The blinking spotlight of attention. Proc. Natl. Acad. Sci. U. S. A. 104: 19204–19209

32. Eriksen, C. & James, J. 1986. Visual attention within and around the field of focal attention: A zoom lens model. Percept. Psychophys. 40: 225–240

33. Itti, L. & Koch, C. 2000. A saliency-based mechanism for overt and covert shifts of visual attention. Vision Res. 40, 1489-1506. Vision Res. 40: 1489–1506

34. Crick, F. 1984. Function of the thalamic reticular complex: The searchlight hypothesis. Proc. Natl. Acad. Sci. USA 81, 4586-4590. Proc. Natl. Acad. Sci. U. S. A. 81: 4586–4590

35. Helfrich, R.F., Fiebelkorn, I.C., Szczepanski, S.M., Lin, J.J., Parvizi, J., Knight, R.T. & Kastner S. 2018. Neural Mechanisms of Sustained Attention Are Rhythmic. Neuron 99: 854-865

36. Fiebelkorn, I., Saalmann, Y. & Kastner, S. 2013. Rhythmic Sampling within and between Objects despite Sustained Attention at a Cued Location. Curr. Biol. CB 23

37. VanRullen, R. 2015. Perceptual Cycles. J. Vis. 15, 1401

38. Fiebelkorn, I., Pinsk, M. & Kastner, S. 2018. A Dynamic Interplay within the Frontoparietal Network Underlies Rhythmic Spatial Attention. Neuron 99: 842-853

39. Fiebelkorn, I. & Kastner, S. 2019. Functional Specialization in the Attention Network. Annu. Rev. Psychol. 71: 1–29

40. Theunissen, L. & Troje, N. 2017. Head Stabilization in the Pigeon: Role of Vision to Correct for Translational and Rotational Disturbances. Front. Neurosci. 11: 551

41. Hayes, B. P. 1982. The structural organization of the pigeon retina. Prog. Retin. Res. 1: 197–226

42. Maturana, H. & Frenk, S. 1963. Directional Movement and Horizontal Edge Detectors in the Pigeon Retina. Science 142: 977–979

43. Reinhard, K., Li, C., Do, Q., Burke, E.G., Heynderickx, S. & Farrow, K. 2019. A projection specific logic to sampling visual inputs in mouse superior colliculus. eLife 8: e50697

44. Donovan, W. 1978. Structure and function of the pigeon visual system. Physiol. Psychol. 6: 403–437

45. Fredes, F., Tapia Pino, S., Letelier, J., Marín, G. & Mpodozis, J. 2010. Topographic Arrangement of the Rotundo-entopallial Projection in the Pigeon (Columba livia). J. Comp. Neurol. 518: 4342–61

46. Clark, W., Chilcott, M., Azizi, A., Pusch, R., Perry, K. & Colombo, M. 2022. Neurons in the pigeon visual network discriminate between faces, scrambled faces, and sine grating images. Sci. Rep. 12

47. Clark, W. & Colombo, M. 2022. Seeing the Forest for the Trees, and the Ground Below My Beak: Global and Local Processing in the Pigeon's Visual System. Front. Psychol. 13

48. Shimp, C. & Friedrich, F. 1993. Behavioral and Computational Models of Spatial Attention. J. Exp. Psychol. Anim. Behav. Process. 19: 26–37

49. Goto, K. & Watanabe, S. 2020. The whole is equal to the sum of its parts: Pigeons (Columba livia) and crows (Corvus macrorhynchos) do not perceive emergent configurations. Learn. Behav. 48: 53–65

50. Brooks, D., Cook, R. & Goto, K. 2022. Perceptual grouping and detection of trial-unique emergent structures by pigeons. Anim. Cogn. 25: 1–13